PRACTICAL ISSUES IN FORMATION CONTROL OF MULTI-ROBOT SYSTEMS

A Dissertation

by

JUNJIE ZHANG

Submitted to the Office of Graduate Studies of
Texas A&M University
in partial fulfillment of the requirements for the degree of

DOCTOR OF PHILOSOPHY

May 2010

Major Subject: Mechanical Engineering

PRACTICAL ISSUES IN FORMATION CONTROL OF MULTI-ROBOT SYSTEMS

A Dissertation

by

JUNJIE ZHANG

Submitted to the Office of Graduate Studies of
Texas A&M University
in partial fulfillment of the requirements for the degree of

DOCTOR OF PHILOSOPHY

Approved by:

Chair of Committee,	Suhada Jayasuriya
Committee Members,	Alan Palazzolo
	Won-Jong Kim
	Dezhen Song
Head of Department,	Dennis O'Neal

May 2010

Major Subject: Mechanical Engineering

ABSTRACT

Practical Issues in Formation Control of Multi-Robot Systems. (May 2010)

Junjie Zhang, B.S., Dalian University of Technology;

M.S., University of Michigan-Ann Arbor

Chair of Advisory Committee: Dr. Suhada Jayasuriya

Considered in this research is a framework for effective formation control of multi-robot systems in dynamic environments. The basic formation control involves two important considerations: (1) Real-time trajectory generation algorithms for distributed control based on nominal agent models, and (2) robust tracking of reference trajectories under model uncertainties.

Proposed is a two-layer hierarchical architecture for collective motion control of multi-robot nonholonomic systems. It endows robotic systems with the ability to simultaneously deal with multiple tasks and achieve typical complex formation missions, such as collision-free maneuvers in dynamic environments, tracking certain desired trajectories, forming suitable patterns or geometrical shapes, and/or varying the pattern when necessary.

The study also addresses real-time formation tracking of reference trajectories under the presence of model uncertainties and proposes robust control laws such that over each time interval any tracking errors due to system uncertainties are driven down to zero prior to the commencement of the subsequent computation segment. By considering a class of nonlinear systems with favorable finite-time convergence characteristics, sufficient conditions for exponential finite-time stability are established and then applied to distributed formation tracking controls. This manifests in the settling time of the controlled system being finite and no longer than the predefined reference trajectory segment computing time interval, thus making tracking errors go to zero by the end of the time horizon over which a segment of the reference trajectory is generated. This way the next segment of the reference trajec-

tory is properly initialized to go into the trajectory computation algorithm. Consequently this could lead to a guarantee of desired multi-robot motion evolution in spite of system uncertainties.

To facilitate practical implementation, communication among multi-agent systems is considered to enable the construction of distributed formation control. Instead of requiring global communication among all robots, a distributed communication algorithm is employed to eliminate redundant data propagation, thus reducing energy consumption and improving network efficiency while maintaining connectivity to ensure the convergence of formation control.

ACKNOWLEDGMENTS

The following is my heartfelt appreciation to all those who gave me inspiration, insight, advice and direction to begin, conduct and complete this dissertation.

First of all, my greatest appreciation goes to my academic advisor and also my mentor, Dr. Suhada Jayasuriya, for his motivation, guidance, support and patience, without which these pages would not have been written. I am blessed and honored to be his student. As a Chinese proverb says: Even if someone is your teacher for only one day, you should regard him as your father for the rest of your life. From him I not only learned how to do academic research but also how to be a good man, which will definitely continue being of great benefit to me for the years to come...

I would specially thank Dr. Jingang Yi at Rutgeers. It was a great experience to work closely with him. I very much appreciate his advice, support and also personal help.

With great pleasure, I extend my gratitude to Dr. Alan Palazzolo, Dr. Won-Jong Kim and Dr. Dezhen Song, who willingly agreed to serve on my Ph.D. committee and sit at the preliminary and final examination in spite of their very busy schedules. Particularly I would like to thank Dr. Dezhen Song for the opportunity to work in his NetBot Laboratory at Texas A&M University.

I would like to extend my deepest gratitude and appreciation to my parents and my elder brother for their relentless encouragement, unselfish support and love. I owe special thanks to Mei for accompanying me on this journey. I also would like to take this opportunity to thank all of my friends here at Texas A&M University and back home for their support all these years. Thanks especially to my buddy, Asanka, for the many enlightening discussions and for being my role model, and also Xiaolong for his kind ”c++ support”.

NOMENCLATURE

OXY	inertial coordinate system ($\overrightarrow{I_E}, \overrightarrow{J_E}, \overrightarrow{K_E}$)
ox_by_b	body-fixed coordinate system ($\overrightarrow{i_b}, \overrightarrow{j_b}, \overrightarrow{k_b}$)
m_i	mass of the robot platform ($i = r$) and driving wheel ($i = w$)
d_i	diameter of the circular robot platform ($i = r$) and driving wheel ($i = w$)
l	distance between platform geometric center and center of mass
I_r	moment of inertia of the robot platform about the $\overrightarrow{k_b}$ axis
I_p	polar moment of inertia about the wheel axis
I_d	diametral moment of inertia about diameter of the driving wheel
X_g/Y_g	X/Y coordinate of center of mass in frame OXY
ψ	orientation angle of the platform in frame OXY
$\theta_i/\dot{\theta}_i$	angle/angular velocity of the right and left ($i = R, L$) driving wheels

TABLE OF CONTENTS

LIST OF TABLES

LIST OF FIGURES

FIGURE Page

CHAPTER I

INTRODUCTION

Cooperating multi-robot systems have received considerable attention in recent years due to technological advancements, and a wide range of potential applications. For example, as claimed by Technology Development Committee on Army Unmanned Ground Vehicles (UGVs), National Research Council: The urgent need to transform the current heavy armor and firepower army into a lighter, more responsive objective force both to increase combat effectiveness and to reduce the number of soldiers placed in danger has made development of practical UGV systems a necessity for future. Moreover, both the air force and NASA have identified autonomous formations of Unmanned Air Vehicles (UAVs) as key technological milestones for the 21st century [1, 2]. Not limited to military field, the applications of multi-robotic systems can be expanded to include housework assistance, patient rehabilitation, industrial automation, automated highways, geophysical mapping, facility monitoring and detection, disaster relief, and space exploration.

In all the aforementioned applications, multiple robots are expected to work cooperatively. Hence, establishing methodologies that can fully integrate and effectively organize many possible behaviors is imperative. In this regard formation keeping and formation reconfiguration become vitally important. Moreover, the degree of errors in formation depends not only on the accuracy of the reference trajectory calculations that are based on nominal models, but also on the realization of effective tracking controllers. In [3], a distributed and scalable algorithm proposed for real-time computation of individual agent reference trajectories for formation tracking under realistic dynamic and actuator constraints

---

The journal model is IEEE Transactions on Automatic Control.

shows remarkable formation keeping and formation reconfiguration capability. In that approach the ultimate zero formation errors were achieved by assuming no model uncertainties. However, there always exist uncertainties in postulated models of actual physical systems, and it is likely that during each time step of a local path planning for cooperative motion control, the online incrementally generated reference motion trajectories may not be exactly tracked in real time. If not carefully done tracking errors can accumulate over each time segment over which reference trajectories are computed leading to the ultimate formation to be significantly different from the desired one. Thus to guarantee desired formation control goals in spite of the ever present uncertainties, it is desirable and almost necessary to achieve zero tracking errors by the end of the time interval.

Furthermore, besides the indispensable plant model uncertainties, in practice it is almost impossible to have noise and latency free data channels. For instance, it is probable that data transmission between agents could be delayed one or more sampling periods, interrupted for extended intervals, or even randomized. In addition, in many works on formation control, synchronized and global communication is required for practical implementation. Therefore in essence each robot needs to communicate with all the others in a multi-robot system. From an energy consumption viewpoint, global communication schemes are not cost-effective since they use the maximal transmission power at all times. It can interfere and reduce the communication capacity and efficiency of the communication network. It is also observed that more communication does not necessarily lead to faster formation control convergence and may in fact even result in loss of convergence [4].

A. Review of the State of the Art

Because multi-robot systems have many issues that must be overcome over a single robot, such as scalability, flexibility, fault-tolerance and cost-effectiveness, we have witnessed a

significant growth in research on formation control or cooperative control. One fundamental question in formation control is how to prescribe desired global behaviors for a multi-agent system using only local interactions [5–7]. The major ideas in the state of the art of formation control are outlined as follows. There is a considerable amount of literature that addresses the formation control problem by utilizing the leader-follower idea, for example, [8, 9]. In such an approach, a group leader is designated in advance with a prescribed reference trajectory to achieve desired behaviors. The leader-follower method however has a pitfall that if the leader fails, then the entire robot network is paralyzed instantaneously. Another widely used approach is the real-time reactive concept, such as the artificial potential method, wherein a robot's motion is controlled by an artificial force resulting from virtual potential profiles [10, 11]. Since the artificial potential technique is easy to realize, it has been often applied to robot navigation. One drawback there is that local potential minima may result in the inability to conduct expected tasks. In [12], the authors considered a strategy through which formation behavior is integrated with other navigational behaviors for various types of formations. There the relative importance of each behavior has to be weighted in advance to get the final control. In [13] the authors presented an algorithm for geometric pattern formation of multiple autonomous robots and characterized the class of geometric patterns that the robots can form in terms of their initial configurations. Issues on controller development and stability analysis were discussed in [14–17]. Among them in [14, 15] proposed was a method that used feedback linearization techniques for controller design to exponentially stabilize the inter-agent distances. Similar results were also obtained in [17], where formation constraints and control Lyapunov functions were employed to develop formation control strategies and stability of the formation was discussed as well. Recently, dynamic model-based formation control has been studied by integrating backstepping control system design for asymptotic tracking with the potential function approach for collision avoidance [18].

It is well-known that in addition to performance degradation, the manifestation of time-delays in a system can also cause extra disturbances and even deteriorate the stability of the closed-loop control systems. In the problem of formation control the occurrence of control time-delays is primarily due to inherent information flow delays when robots are sensing and/or communicating with spatially separated neighboring robots. Sufficient and necessary conditions were given in [19] for reaching an average-consensus in presence of communication time-delays. By using delayed output feedback, Qu and Wang *et al.* in [20] proposed a sampled-data predictive cooperative control strategy for a general class of dynamic systems that can be input-output feedback linearizable to a given canonical form. Formation control of multi-vehicle systems under intermittent and delayed state data was demonstrated in [21] by utilizing an abbreviated zero order hold scheme in conjunction with the potential function method. However, it targeted only linear and holonomic systems. In [22,23] the problem of finite-time consensus control of multi-agent networks was studied based on a finite-time Lyapunov stability theorem in [24].

Not until recently have communication issues of wireless sensor networks attracted much attention, especially in the computer science community. Its key idea is that, instead of transmitting at maximal power, agents collaboratively construct a communication network topology by forming proper neighborhood relations under certain criteria to reduce energy consumption and improve network efficiency while preserving network connectivity [25, 26]. Several connectivity-preserving communication algorithms have been proposed in formation control [27–30].

B. Problem Statement

As discussed above, without addressing the key practically meaningful issues, it is inconceivable that theoretical developments in formation control can be satisfactorily imple-

mented and executed on real robotic systems. Consequently, this research is focused on the key issues alluded to earlier that must be addressed in the study of formation control. Namely,

(i) To develop a framework for formation control of multi-robot nonholonomic systems capable of handling multiple tasks

(ii) To construct decentralized real-time robust controllers to ensure satisfactory collective motion of multiple robots subject to inevitable system uncertainties

(iii) To relieve global communication requirement in formation control with a local dynamic communication algorithm

C. Dissertation Outline

The rest of the dissertation is organized as follows. Chapter II presents a framework for multi-task formation control of nonholonomic robotic systems. The problem of stabilizing uncertain time-delay multi-robot systems with saturated actuators is investigated in Chapter III. Finite-time settling real-time formation tracking controls under uncertainties are considered in Chapter IV. In Chapter V by incorporating a local dynamic communication algorithm, formation control of multi-robot systems subject to interconnection time-delays is discussed. Chapter VI concludes the work with a summary of contributions and a discussion of future work.

CHAPTER II

A FRAMEWORK FOR MULTI-TASK FORMATION CONTROL OF MULTI-ROBOT SYSTEMS

In this chapter, a formation control methodology for a class of nonholonomic dynamic systems is presented. First, the nonholonomic system is transformed into a non-constrained format that is favorable for control design. Tracking control is then realized by employing input-output feedback linearization. Additionally, the integration of a two-stage formation control framework is proposed to simultaneously deal with several tasks, such as collision prevention, obstacle avoidance, trajectory tracking and pattern formation. The trajectory planner at the top layer generates desired trajectories for the tracking controller at the bottom layer. The trajectory planner is based on defined task objective functions and a null-space-based multi-task fusion methodology [31, 32]. An optimization method is employed for each decomposed task. The effectiveness of the proposed two-layer framework is illustrated and validated through the successful fulfillment of a series of desired multi-robot behaviors.

A. Dynamic Model-based Tracking Control

1. Dynamic Model

Figure 1 is a schematic of the robot platform considered, which has two differentially driven wheels powered by DC motors and one caster wheel (not shown in the figure). The kine-

matics for this system can be expressed as:

$$\dot{X}_g cos\psi + \dot{Y}_g sin\psi + \dot{\psi}\frac{d_r}{2} - \dot{\theta}_r \frac{d_w}{2} = V_G, \tag{2.1}$$

$$\dot{X}_g cos\psi + \dot{Y}_g sin\psi - \dot{\psi}\frac{d_r}{2} - \dot{\theta}_l \frac{d_w}{2} = V_H, \tag{2.2}$$

$$\dot{Y}_g cos\psi - \dot{X}_g sin\psi - \dot{\psi} l - \dot{P}_g \cdot \overrightarrow{j_b} = 0, \tag{2.3}$$

where P_g is the position vector of the center of mass $P_g \triangleq [X_g \;\; Y_g]^T$, and V_G and V_H are the velocities of the contact points of the right and left wheels, respectively.

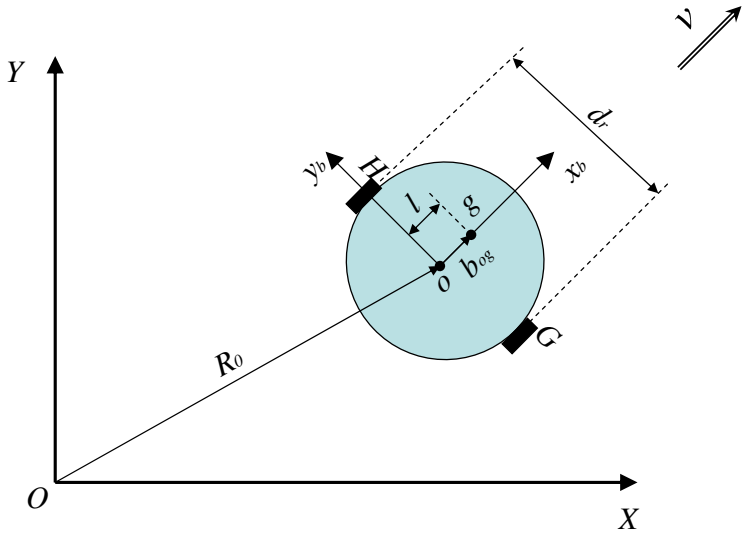

Fig. 1. Sketch of the robot platform

Unlike skid-steered mobile robots [33], nonholonomic constraint of zero lateral velocity is normally considered for differentially driven mobile robots. Thus for this two-wheel robot prototype, we assume it has negligible lateral velocity (or lateral skid) and longitudinal slip, and obtain the following nonholonomic kinematic constraints in the matrix

form:

$$C(q)\dot{q} = 0, \tag{2.4}$$

where $q \triangleq [X_g\ Y_g\ \psi\ \theta_R\ \theta_L]^T$ and

$$C(q) \triangleq \begin{bmatrix} cos\psi & sin\psi & \frac{d_r}{2} & -\frac{d_w}{2} & 0 \\ cos\psi & sin\psi & -\frac{d_r}{2} & 0 & -\frac{d_w}{2} \\ -sin\psi & cos\psi & -l & 0 & 0 \end{bmatrix}.$$

The kinetic energy is derived as

$$\begin{aligned} T =& \frac{m_r}{2}|\dot{R}_0|^2 + m_r\dot{R}_0 \cdot (\omega \times b_{og}) + \frac{1}{2}\omega^T\hat{I}\omega \\ =& \frac{m_r}{2}(\dot{X_g}^2 + \dot{Y_g}^2) + m_r\dot{\psi}l(\dot{Y}_g cos\psi - \dot{X}_g sin\psi) \\ &+ \frac{1}{2}(I_p\dot{\theta}_R^2 + I_p\dot{\theta}_L^2) + \Big[I_d + m_w\big(\frac{d_r}{2}\big)^2 + \frac{I_r}{2}\Big]\dot{\psi}^2, \end{aligned} \tag{2.5}$$

where

$$\begin{aligned} \dot{R}_0 &= \dot{X}_g\overrightarrow{I_E} + \dot{Y}_g\overrightarrow{J_E} \\ &= \dot{X}_g(cos\psi\,\overrightarrow{i_b} - sin\psi\,\overrightarrow{j_b}) + \dot{Y}_g(sin\psi\,\overrightarrow{i_b} + cos\psi\,\overrightarrow{j_b}) \\ &= (\dot{X}_g cos\psi + \dot{Y}_g sin\psi)\,\overrightarrow{i_b} + (\dot{Y}_g cos\psi - \dot{X}_g sin\psi)\,\overrightarrow{j_b}, \\ \omega &= (\dot{\theta}_R + \dot{\theta}_L)\,\overrightarrow{j_b} + \dot{\psi}\overrightarrow{k_b},\ b_{og} = l\,\overrightarrow{i_b} \text{ and} \\ \hat{I} &= 2\begin{bmatrix} I_d + m_w\big(\frac{d_r}{2}\big)^2 & 0 & 0 \\ 0 & I_p & 0 \\ 0 & 0 & I_d + m_w\big(\frac{d_r}{2}\big)^2 + \frac{I_r}{2} \end{bmatrix}. \end{aligned}$$

Then *Lagrangian Principle* yields the following dynamic equations of motion for this type of wheeled mobile robotic system:

$$M(q)\ddot{q} + A(q,\dot{q}) = C(q)^T\lambda + B\tau, \tag{2.6}$$

where

$$M(q) \triangleq \begin{bmatrix} m_r & 0 & -m_w l sin\psi & 0 & 0 \\ 0 & m_r & m_w l cos\psi & 0 & 0 \\ -m_w l sin\psi & m_w l cos\psi & 2\Big[I_d + m_w\big(\frac{d_r}{2}\big)^2 + \frac{I_r}{2}\Big] & 0 & 0 \\ 0 & 0 & 0 & I_p & 0 \\ 0 & 0 & 0 & 0 & I_p \end{bmatrix},$$

$$A(q,\dot{q}) \triangleq \begin{bmatrix} -m_w l\dot{\psi}^2 cos\psi \\ -m_w l\dot{\psi}^2 sin\psi \\ 0 \\ 0 \\ 0 \end{bmatrix}, \; B \triangleq \begin{bmatrix} O_{3\times 2} \\ I_{2\times 2} \end{bmatrix},$$

τ denotes the control input torques, λ is the *Lagrange Multiplier*, and O, I denotes zero and identity matrix, respectively.

In [34], quasi-velocities $\vartheta \triangleq [\dot{\theta}_R \quad \dot{\theta}_L]$ are introduced and its differentials are *Pfaffian* forms in terms of q and t:

$$\dot{q} = E(q)\vartheta \Rightarrow \ddot{q} = \dot{E}(q)\vartheta + E(q)\dot{\vartheta}. \tag{2.7}$$

As shown in [35], it is always possible to find a matrix $E(q) \in \mathbb{R}^{n\times(n-m)}$ in the *null space* of $C(q)$, namely,

$$C(q)E(q) = 0. \tag{2.8}$$

One way to construct this $E(q)$ matrix is

$$E(q) \triangleq \begin{bmatrix} -{C_1}^{-1}(q)C_2(q) \\ I_{(n-m)\times(n-m)} \end{bmatrix}, \tag{2.9}$$

where $C_1(q) \in \mathbb{R}^{m\times m}$ and $C_2(q) \in \mathbb{R}^{m\times(n-m)}$ are sub-matrices of $C(q)$, that is, $C(q) =$

$[C_1(q) \quad C_2(q)]$. Note that the existence of ${C_1}^{-1}(q)$ is guaranteed by the fact that $C(q)$ is full rank: $r(C(q)) = 3$. Therefore, for this type of robotic system,

$$E(q) = \begin{bmatrix} d_w\left(\frac{cos\psi}{4} - \frac{lsin\psi}{2d_r}\right) & d_w\left(\frac{cos\psi}{4} + \frac{lsin\psi}{2d_r}\right) \\ d_w\left(\frac{sin\psi}{4} + \frac{lcos\psi}{2d_r}\right) & d_w\left(\frac{sin\psi}{4} - \frac{lcos\psi}{2d_r}\right) \\ \frac{d_w}{2d_r} & -\frac{d_w}{2d_r} \\ 1 & 0 \\ 0 & 1 \end{bmatrix}. \tag{2.10}$$

By augmenting the generalized coordinates q into $x \triangleq [q \quad \vartheta]^T$, and using the following input transformation

$$u \triangleq -\left[E^T(q)M(q)E(q)\right]^{-1}\left[E^T(q)M(q)\dot{E}(q)\vartheta + E^T(q)A(q,\dot{q}) - E^T(q)B\tau\right], \tag{2.11}$$

the nonholonomic system (2.6) can be put into a state space format [36]:

$$\dot{x} = f(x) + g(x)u, \tag{2.12}$$

$$y = h(x), \tag{2.13}$$

where $x \in D \subset \mathbb{R}^7$, the mappings $f : D \to \mathbb{R}^7$ and $g : D \to \mathbb{R}^7$ are vector fields on D, and

$$f(x) \triangleq \begin{bmatrix} E(q)\vartheta \\ O_{2\times 1} \end{bmatrix} \text{ and } g(x) \triangleq \begin{bmatrix} O_{5\times 2} \\ I_{2\times 2} \end{bmatrix}.$$

2. Tracking Controller

Similar to [37], input-output linearization is applied to design controls for this class of mobile robots with nonholonomic constraints. With output $h(x) \triangleq [X_g \quad Y_g]^T$ used for

trajectory, the decoupling matrix $\Xi(q)$ becomes

$$\Xi(q) \triangleq L_E h(q) = \begin{bmatrix} d_w\left(\frac{cos\psi}{4} - \frac{lsin\psi}{2d_r}\right) & d_w\left(\frac{cos\psi}{4} + \frac{lsin\psi}{2d_r}\right) \\ d_w\left(\frac{sin\psi}{4} + \frac{lcos\psi}{2d_r}\right) & d_w\left(\frac{sin\psi}{4} - \frac{lcos\psi}{2d_r}\right) \end{bmatrix}, \tag{2.14}$$

where $L_{(.)}$ is the *Lie Derivative* along $(.)$. From [38] a necessary and sufficient condition for input-output linearization is that the decoupling matrix must be full rank, which is satisfied in this case, since rank $(\Xi) = 2$.

The nonlinear system (2.12)-(2.13) is transferred into a normal form via the new state transformation:

$$T(x) \triangleq \begin{bmatrix} s_1(x) \\ s_2(x) \\ s_3(x) \\ --- \\ h(x) \\ L_f h(x) \end{bmatrix} \triangleq \begin{bmatrix} \eta \\ --- \\ \zeta \end{bmatrix} = \begin{bmatrix} \eta \\ --- \\ P_g \\ \Xi\vartheta \end{bmatrix}, \tag{2.15}$$

where $\rho = 2$ is the relative degree of the nonlinear system (2.12)-(2.13); see Appendix A for calculation. $s_i(x)$, $i = 1, 2, 3$, are chosen such that $T(x)$ is a ***diffeomorphism**** on a domain $D_0 \subset D$ and $\frac{\partial s_i(x)}{\partial x} g(x) = 0$, $\forall\ x \in D_0$. The existence (at least locally) of $s_i(x)$ is captured by Theorem 13.1 in [39]. Using the above state transformation, the following normal form can be obtained

$$\dot{\eta} = f_0(\eta, \zeta), \tag{2.16}$$

$$\dot{\zeta} = \hat{A}\zeta + \hat{B}\beta(x)[u - \alpha(x)], \tag{2.17}$$

$$y = \hat{C}\zeta, \tag{2.18}$$

*Namely, both $T(.)$ and $T^{-1}(.)$ are continuously differentiable.

where $\zeta \in \mathbb{R}^4, \eta \in \mathbb{R}^3$, and $\alpha(x)$ and $\beta(x)$ are independent of the choice of $s_i(x)$:

$$\beta(x) = L_g L_f^{\rho-1} h(x) = L_g L_f h(x) = \Xi, \tag{2.19}$$

$$\alpha(x) = -\beta^{-1}(x) L_f^{\rho} h(x) = -\Xi^{-1} L_f(\Xi\vartheta) = -\Xi^{-1}\dot{\Xi}\vartheta, \tag{2.20}$$

where in the last step, we use a calculation similar to what is shown in Appendix A. Matrices $(\hat{A}, \hat{B}, \hat{C})$ are in canonical forms given by $\hat{A} \triangleq \begin{bmatrix} O_{2\times2} & I_{2\times2} \\ O_{2\times2} & O_{2\times2} \end{bmatrix}$, $\hat{B} \triangleq \begin{bmatrix} O_{2\times2} \\ I_{2\times2} \end{bmatrix}$ and $\hat{C} \triangleq \begin{bmatrix} I_{2\times2} & O_{2\times2} \end{bmatrix}$.

To achieve trajectory tracking, a state feedback control law is designed such that the output y asymptotically tracks a reference signal $r(t)$. The reference signal $r(t)$ with its higher derivatives is generated by the trajectory planner that will be discussed in the next section. Let

$$\mathcal{R} \triangleq \begin{bmatrix} r \\ \dot{r} \end{bmatrix} \triangleq \begin{bmatrix} P_g^d \\ \dot{P}_g^d \end{bmatrix} \text{ and } e \triangleq \zeta - \mathcal{R} \triangleq \begin{bmatrix} P_g - P_g^d \\ \Xi\vartheta - \dot{P}_g^d \end{bmatrix}$$

and we obtain

$$\dot{\eta} = f_0(\eta, e + \mathcal{R}), \tag{2.21}$$

$$\dot{e} = \hat{A}e + \hat{B}\{\beta(x)[u - \alpha(x)] - r^{(\rho)}\}. \tag{2.22}$$

The choice of state feedback control

$$u \triangleq \alpha(x) + \beta^{-1}(x)(v + r^{(\rho)}) \tag{2.23}$$

reduces the above normal form into the cascade system:

$$\dot{\eta} = f_0(\eta, e + \mathcal{R}), \tag{2.24}$$

$$\dot{e} = \hat{A}e + \hat{B}v. \tag{2.25}$$

With control $v = -Ke$, where the gain $K \in \mathbb{R}^{2\times 4}$ is selected such that $\hat{A} - \hat{B}K$ is *Hurwitz*, the control of (2.23) becomes

$$u = -\Xi^{-1}\dot{\Xi}\vartheta + \Xi^{-1}\left\{\ddot{P}_g - K\begin{bmatrix} P_g - P_g^d \\ \Xi\vartheta - \dot{P}_g^d \end{bmatrix}\right\}. \tag{2.26}$$

Substituting into Eq. (2.11) and noticing that $E^T(q)B = I_{2\times 2}$, the driving torque is then obtained as

$$\tau = \big[E^T(q)M(q)E(q)\big]u + E^T(q)M(q)\dot{E}(q)\vartheta + E^T(q)A(q,\dot{q}). \tag{2.27}$$

Besides, the internal dynamics is

$$\dot{\eta} = \frac{\partial \eta(x)}{\partial x} f(x) = FE\vartheta = FE\Xi^{-1}\zeta_2, \tag{2.28}$$

where $F \triangleq \frac{\partial \eta(x)}{\partial x}\begin{bmatrix} I_{5\times 5} \\ O_{2\times 5} \end{bmatrix}$. Therefore, the zero dynamics

$$\dot{\eta} \triangleq f_0(\eta, 0) = 0 \tag{2.29}$$

indicates that the internal dynamics is bounded for all $t \geqslant 0$.

B. Trajectory Planner

In this section, to accomplish desired behaviors of multi-robot systems, a null-space-based methodology [32, 40] is first summarized and then utilized to integrate and prioritize multiple specific tasks. These tasks are accounted for by defining a series of objective functions along with the desired behaviors in the task space. Note that in the rest of the chapter n denotes the number of robots in the multi-robot system.

1. Null-space Method

The objective function for a given task a is denoted as

$$J_a(t) \triangleq f(P_1(t), \dots P_i(t), \dots P_n(t)), \tag{2.30}$$

where $P_i(t)$ is the position vector of robot i, defined as $P_i(t) \triangleq [X_i(t)\ Y_i(t)\ Z_i(t)]^T \in \mathbb{R}^3$. Taking the derivative of Eq. (2.30) with respective to time t, we obtain

$$\dot{J}_a(t) = \sum_{i=1}^{n} \frac{\partial J_a(t)}{\partial P_i(t)} \dot{P}_i(t).$$

The desired velocity vector for task a can be obtained through

$$V_a^d(t) \triangleq \dot{P}_a^d(t) = \Phi_a^\dagger(t) \dot{J}_a^d(t) \triangleq \Phi_a^T(t) \big[\Phi_a(t) \Phi_a^T(t)\big]^{-1} \dot{J}_a^d(t),$$

where the superscript † denotes pseudo-inverse and $\Phi_a(t) \triangleq \left[\frac{\partial J_a(t)}{\partial P_1(t)} \dots \frac{\partial J_a(t)}{\partial P_i(t)} \dots \frac{\partial J_a(t)}{\partial P_n(t)}\right]$. Then the desired position vector $P_a^d(t)$ can be acquired by numerically integrating $V_a^d(t)$. To avoid numerical drift, $\dot{J}_a^d(t)$ is replaced by shifting with position error. This leads to the following discrete time version:

$$V_a^d(k+1) = \Phi_a^T(k+1) \big[\Phi_a(k+1) \Phi_a^T(k+1)\big]^{-1} \big[\dot{J}_a^d(k+1) + \Lambda_a J_{a,e}(k+1)\big],$$

where position error $J_{a,e}(k+1) \triangleq J_a^d(k+1) - J_a(k+1)$ and Λ_a is a gain matrix with appropriate dimension. This in turn leads to the desired velocity vector for multiple different tasks a, b, c, *etc.*[†]:

$$\begin{aligned} V^d(k+1) &= V_a^d(k+1) + \big[I - \Phi_a^\dagger(k+1)\Phi_a(k+1)\big] \\ &\times \Big\{ V_b^d(k+1) + \big[I - \Phi_b^\dagger(k+1)\Phi_b(k+1)\big] \big[V_c^d(k+1) + \dots\big] \Big\}. \end{aligned} \tag{2.31}$$

[†]Task priorities are a-priori. Task a is assumed to have the highest priority, then comes task b, which is followed by task c, *etc.*

Using *Simpson's rule* for smoother trajectory,

$$P^d(k) = \frac{1}{3}\Delta t\big[V^d(k-1) + 4V^d(k) + V^d(k+1)\big] + P^d(k-1), \tag{2.32}$$

where Δt is the integration time step.

The idea here is that the desired velocity vector for a lower priority task is projected onto the null space of the desired velocity of the immediately higher one to eliminate its interference with the higher priority task; see Appendix B for derivation. In this way, the highest priority task is always fully accomplished, while the immediately lower one is partially completed by keeping its velocity component perpendicular to the velocity of the highest priority one, instead of being completely shut down. If there are more tasks, then a hierarchical structure is enforced based on priorities.

2. Objective Functions

How expected tasks may be integrated and prioritized by the null-space-based approach are described through a series of objective functions that correspond to the desired behaviors in the task space in what follows. Some typical formation missions are highlighted.

a. Collision Prevention

In most work on rigid formation keeping, such as [41], a key point is that random initial conditions do not guarantee the avoidance of inter-agent collision during the transient phase before stabilizing into a formation pattern. A new collision prevention mechanism is introduced here to resolve this issue.

Define the following objective function of collision avoidance for robot i

$$J_{cp} = \sum_{\substack{j=1 \\ j\neq i}}^{n} \ln(\mu||P_j - P_i||^2), \tag{2.33}$$

where $||\ ||$ denotes *Euclidean norm*, and $\mu \in \mathbb{R}^+$ is used to adjust the internal distances between robots for a given desired objective function value $J_{cp}^d \triangleq d_{cp} \in \mathbb{R}^+$. We obtain

$$\Phi_{cp} = \left[\frac{\partial J_{cp}}{\partial X_1} \ \frac{\partial J_{cp}}{\partial Y_1} \cdots \frac{\partial J_{cp}}{\partial X_i} \ \frac{\partial J_{cp}}{\partial Y_i} \cdots \frac{\partial J_{cp}}{\partial X_n} \ \frac{\partial J_{cp}}{\partial Y_n} \right],$$

where

$$\frac{\partial J_{cp}}{\partial X_j} = \begin{cases} \frac{2(X_j - X_i)}{||P_j - P_i||^2} & \text{if } j \neq i, \\ -2 \sum_{\substack{k \neq i \\ k=1}}^{n} \frac{X_k - X_i}{||P_k - P_i||^2} & \text{otherwise}, \end{cases}$$

and

$$\frac{\partial J_{cp}}{\partial Y_j} = \begin{cases} \frac{2(Y_j - Y_i)}{||P_j - P_i||^2} & \text{if } j \neq i, \\ -2 \sum_{\substack{k \neq i \\ k=1}}^{n} \frac{Y_k - Y_i}{||P_k - P_i||^2} & \text{otherwise}. \end{cases}$$

The above proposed objective function is inspired by the logarithmic barrier approach, which was first proposed in [42] and further developed in [43, 44]. This method transforms the nonlinearly constrained optimization problem into an unconstrained one by constructing a sequence of logarithmic barrier functions. Notice here that the objective function, which one may label the logarithmic two-body potential, is built with regard to each robot by adding up all the distances between it and the other robots rather than distinguishing the internal distances between two robots one pair at a time. We know if any two robots occupy the same spot at the same time, then collision would occur and the objective function of collision avoidance J_{cp}, defined in (2.33), would go infinity. As illustrated in Section C as follows, a proper control gain for collision prevention, Λ_{cp}, can drive and confine J_{cp} to a given desired finite value d_{cp}. Thus this prevents robots from colliding each other. This treatment can also tremendously lower the computational burden, especially with a very large number of robots, and is favorable for real-time implementation. In most practical circumstances, the ultimate internal distances between each pair of robots are not required to be accurately constrained to be at certain fixed values to achieve rigid formation. The

above objective function secures the in-between distances to be non-zero and within a certain range to ensure that collisions would not happen. Meanwhile, the proposed objective function also guarantees that no robot would escape from the team so that they can work cooperatively as a whole to conduct given tasks effectively and efficiently.

b. Obstacle Avoidance

The objective function of robot i for obstacle avoidance is defined as the distance between it and the obstacle

$$J_{i,oa} = ||P_i - P_o||, \tag{2.34}$$

where P_o is the position vector of the obstacle. Then $\Phi_{oa} = {e_i}^T$ and $\Phi_{oa}^{\dagger} = e_i$, where $e_i \triangleq \frac{P_i - P_o}{J_{i,oa}}$. The desired objective function value is specified as ${J_i}^d_{,oa} \triangleq d_o \in \mathbb{R}^+$, which is both the desired objective function value and the threshold to activate the task to achieve obstacle avoidance.

Note that the objective function for obstacle avoidance is built individually for each robot and is not an objective function for the whole multi-robot system, and it is activated solely in the bounded sensing region of each individual robot. One of the attractive features of the above obstacle avoidance scheme is its ability to sufficiently avoid obstacles, as long as the obstacle is detected by any one of the robots.

c. Mean of Formation

The overall multi-robot system is taken into consideration here by defining the following mean of formation function

$$J_{cm} = \bar{P} \triangleq [\bar{X}\ \bar{Y}\ \bar{Z}]^T \triangleq \frac{1}{n}\sum_{i=1}^{n} P_i. \tag{2.35}$$

Accordingly, $\Phi_{cm} = \frac{1}{n}[I_1 \dots I_i \dots I_n]_{3\times 3n}$ where $\Phi_{cm}^{\dagger} = n\Phi_{cm}^{T}$ and I_i denotes identity matrix. $J_{cm}^{d} \triangleq \bar{P}^{d} \triangleq [\bar{X}^{d}\ \bar{Y}^{d}\ \bar{Z}^{d}]^{T}$ is the desired objective function value.

By defining the above objective function as the center of mass, the whole multi-robot system can be regulated to a target position or made to track a predefined trajectory. In other words, it lends itself to local control of the multi-robot system.

d. Variance of Formation

Define variance objective function, J_v, as

$$J_v = \frac{1}{n}\sum_{i=1}^{n}(P_i - \bar{P})^2. \tag{2.36}$$

Then, $\Phi_v = \frac{2}{n}\begin{bmatrix} S_1 \dots S_i \dots S_n \end{bmatrix}$,

$$\text{where } S_i \triangleq \begin{bmatrix} X_i - \bar{X} & 0 \\ 0 & Y_i - \bar{Y} \end{bmatrix}.$$

Also $\Phi_v^{\dagger} = \frac{2}{n}\begin{bmatrix} N_1 \dots N_i \dots N_n \end{bmatrix}^{T}$,

$$\text{where } N_i \triangleq \begin{bmatrix} \frac{X_i - \bar{X}}{\sum_{i=1}^{n}(X_i - \bar{X})^2} & 0 \\ 0 & \frac{Y_i - \bar{Y}}{\sum_{i=1}^{n}(Y_i - \bar{Y})^2} \end{bmatrix}.$$

By changing the desired objective function, $J_v^{d} \in \mathbb{R}^{2\times 1}$, the diffusion of the multi-robot system will vary accordingly, namely, how big is the formation or to what extent to deploy the multi-robot system.

e. Rigid Formation

Denote $P_r \triangleq [r_1 \dots r_i \dots r_n]^{T}$, where r_i is the position vector of robot i with respect to the center of mass of the multi-robot system. Then define the following objective function for

rigid formation task,

$$J_r \triangleq (P_r \begin{bmatrix}1\\0\\0\end{bmatrix}) \otimes \begin{bmatrix}1\\0\\0\end{bmatrix} + (P_r \begin{bmatrix}0\\1\\0\end{bmatrix}) \otimes \begin{bmatrix}0\\1\\0\end{bmatrix} + (P_r \begin{bmatrix}0\\0\\1\end{bmatrix}) \otimes \begin{bmatrix}0\\0\\1\end{bmatrix} - \bar{P} \otimes U_{3n\times 1}, \quad (2.37)$$

where $\otimes$ denotes *Kronecker product* and U is unit matrix.

In this case,

$$\Phi_r = \begin{bmatrix} M_{n\times n} & O_{n\times n} & O_{n\times n} \\ O_{n\times n} & M_{n\times n} & O_{n\times n} \\ O_{n\times n} & O_{n\times n} & M_{n\times n} \end{bmatrix}, \text{ where } M \triangleq I_{n\times n} - \frac{1}{n} U_{n\times n}.$$

The desired objective function is specified as $J_r^d \in \mathbb{R}^{3n\times 1}$. Then it is said that the multi-robot system converges to formation $J_r^d(t) \otimes \begin{bmatrix}1\\0\end{bmatrix}$, if $J_r(t) \otimes \begin{bmatrix}1\\0\end{bmatrix} + \frac{d}{dt}\Big\{ J_r(t) \otimes \begin{bmatrix}0\\1\end{bmatrix} \Big\} - J_r^d(t) \otimes \begin{bmatrix}1\\0\end{bmatrix} \to 0, \text{ as } t \to \infty.$

Additionally, through varying the desired objective function, formation reconfiguration can be thus accomplished.

f. Chasing

Chasing can be achieved by combining the following two sub-tasks.

(a) Circle Formation Define this objective function as an $n \times 1$ vector,

$$J_c = \Big[\ldots, \tfrac{1}{2}(P_i - P_c)^T (P_i - P_c), \ldots \Big]^T, \quad (2.38)$$

where P_c is the position vector of the center of the circle. Then, $\Phi_c = blockdiag(\ldots, (P_i - P_c)^T, \ldots)$ and $\Phi_c^\dagger = blockdiag(\ldots, \frac{P_i - P_c}{(P_i - P_c)^T (P_i - P_c)}, \ldots)$, which is $n \times 2n$ and $2n \times n$ diag-

onal matrix, respectively. The desired objective function is $J_c^d \triangleq \frac{\hat{r}^2}{2} U_{n\times 1}$, where $\hat{r} \in \mathbb{R}^+$ is the desired circle radius.

(b) Regular Polygon Formation Similarly, define the objective function as

$$J_{rp} = ||P_n - P_1||^2 + \sum_{i=1}^{n-1} ||P_{i+1} - P_i||^2. \tag{2.39}$$

Accordingly, Φ_{rp} is a $1 \times 2n$ row vector,

$$\Phi_{rp} = 2 \begin{bmatrix} (P_1 - P_2)^T + (P_1 - P_n)^T \\ (P_2 - P_1)^T + (P_2 - P_3)^T \\ \vdots \\ (P_i - P_{i-1})^T + (P_i - P_{i+1})^T \\ \vdots \\ (P_{n-1} - P_{n-2})^T + (P_{n-1} - P_n)^T \\ (P_n - P_{n-1})^T + (P_n - P_1)^T \end{bmatrix}^T .$$

The desired objective function is defined as $J_{rp}^d \triangleq n\big[2Rsin(\frac{\pi}{n})\big]^2$, where $R \in \mathbb{R}^+$ is the circumradius.

Consequently, by incorporating the above defined objective function, mean of formation, a moving target can be successfully chased and caught.

For formation control purposes, a two-layer hierarchical architecture is proposed; see Fig. 2. The tracking controller is the bottom layer, whereas the trajectory planner is the top layer. Based on the defined task objective functions and the multi-task fusion scheme, the trajectory planner generates motion reference inputs for the tracking controller. Thus, complex missions of a team of robots may be successfully achieved.

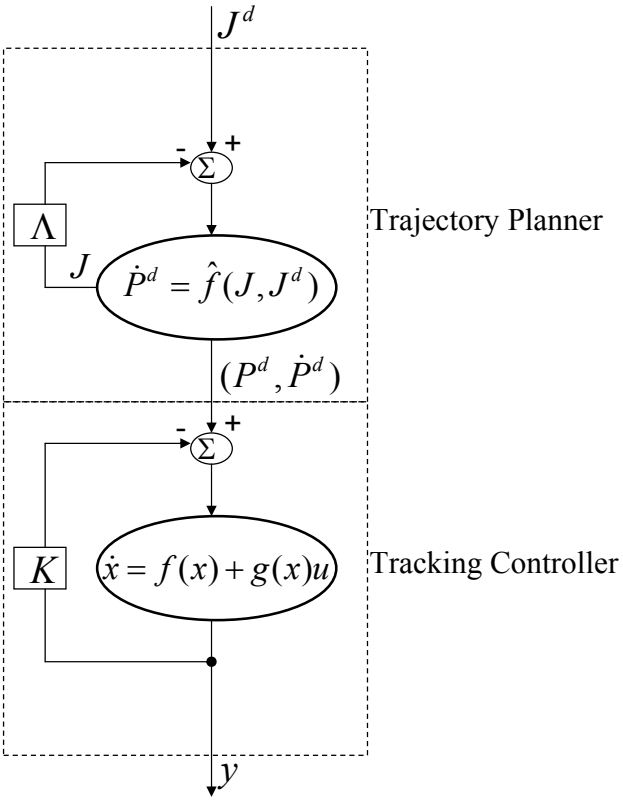

Fig. 2. A framework for formation control

C. Case Studies

In this section, as an immediate illustration and application of the proposed methodology, a series of realistic case studies are presented to verify the effectiveness of the introduced framework for formation control and also the incorporated dynamics modeling and tracking control design strategies. The parameters of the nonholonomic robotic system and also the selected control gains are listed in Tables I and II, respectively.

Table I. Parameters of the robotic system

m_r	32 kg
m_w	1 kg
d_r	1.5 m
d_w	0.3 m
l	0.6 m
I_r	15.625 kgm^2
I_p	0.005 kgm^2
I_d	0.0025 kgm^2

Case 1:

In this case study, from any initial distribution, multiple robots are required to arrange themselves into a desired regular polygon pattern and track a circular trajectory while avoiding both inter-agent collisions and obstacles in the environment.

Figure 3 shows three robots that are randomly posed around origin area (plus sign) successfully accomplish the tracking circle task (dashdot line) without any inter-agent collision, even during the transient phase before stabilizing into formation. Furthermore, an external obstacle (solidline) is avoided when it is present, and trajectory tracking is lowered from the 2nd to the 3rd priority. Collision avoidance is always assigned the highest priority. Figure 4 shows the internal distances between robots, which illustrates that the three robots, while tracking the circular reference trajectory, approximately form an equilateral

Table II. Selected control gains

K	$\begin{bmatrix} 810 & 0 & 12.6 & 0 \\ 0 & 810 & 0 & 12.6 \end{bmatrix}$
Collision Prevention, Λ_{cp}	10
Obstacle Avoidance, Λ_{oa}	10
Mean of Formation, Λ_{cm}	$I_{2\times 2}$
Variance of Formation, Λ_v	$0.2I_{2\times 2}$
Rigid Formation, Λ_r	$0.1I_{10\times 10}$
Circle Formation, Λ_c	$I_{3\times 3}$
Regular Polygon Formation, Λ_{rp}	1

triangle. Note that even when avoiding the obstacle the internal distances are bounded within a certain range: The lower bound prevents collision, and the upper bound constrains the formation to be in cohesion and guarantees no robot would escape from the team. This result demonstrates the effectiveness of the proposed collision-prevention approach. Smooth curves in Fig. 5 are the transients of the right and left control inputs of each robot. This satisfactory performance demonstrates the effectiveness of the above tracking control design.

The proposed framework is scalable. One simulation with ten robots in an obstacle-free environment is shown in Fig. 6. A change in the tasks gives a more interesting observation as shown in Fig. 7, where each robot travels along its own circle while simul-

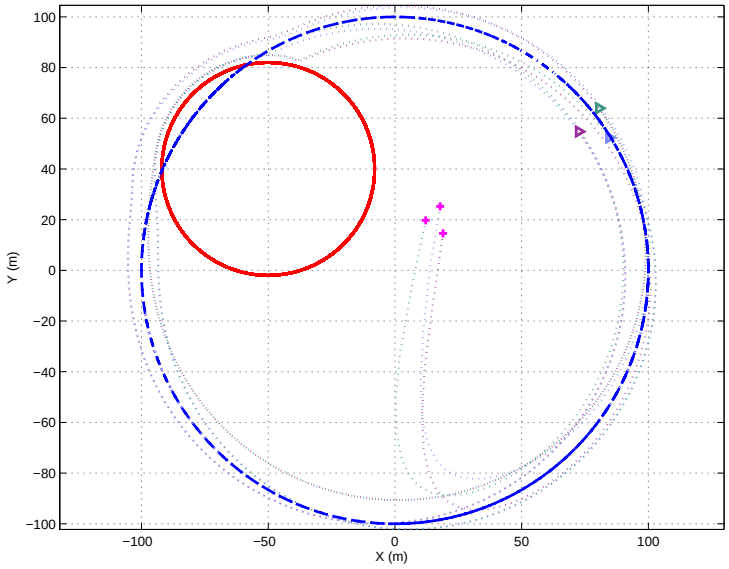

Fig. 3. Three robots track a circle avoiding inter-agent collision and external obstacle.

taneously forming a rigid circle formation (dashed line) whose center tracks the desired circular trajectory (dashdot line). Although it is desirable that multi-robot systems should self-organize themselves into fixed patterns, it is practically more beneficial to accommodate scenarios that some robots can loiter around their equilibrium states to acquire more sensor readings. Such enhanced sensor network capability can be achieved by averaging the measured data as they cover their local neighborhood multiple times.

Case 2:

Two snapshots (Fig. 8) give an appealing and practically meaningful case–chase a moving target. Three robots (solid circles) cooperatively and approvingly steer themselves such that their center of mass always falls onto the moving quarry (plus sign). At the same time

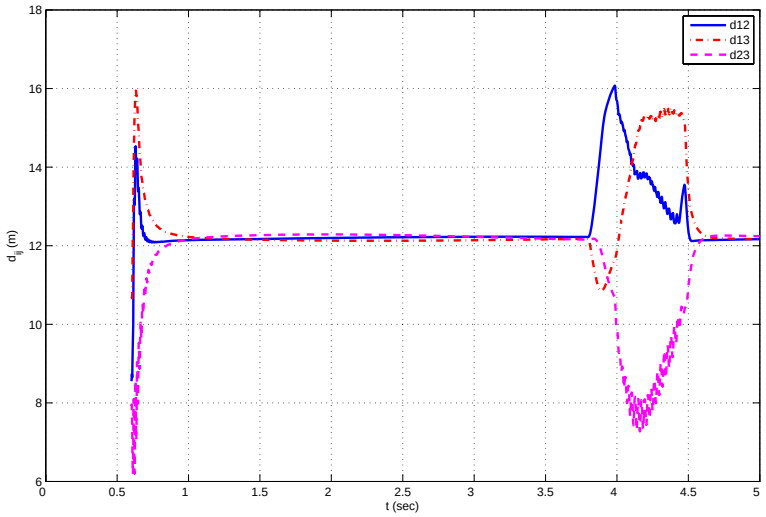

Fig. 4. Internal distances between robots

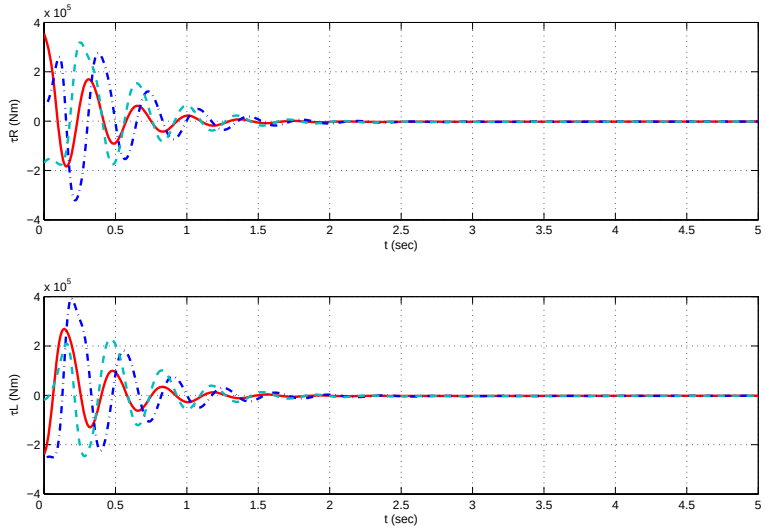

Fig. 5. Control input torques

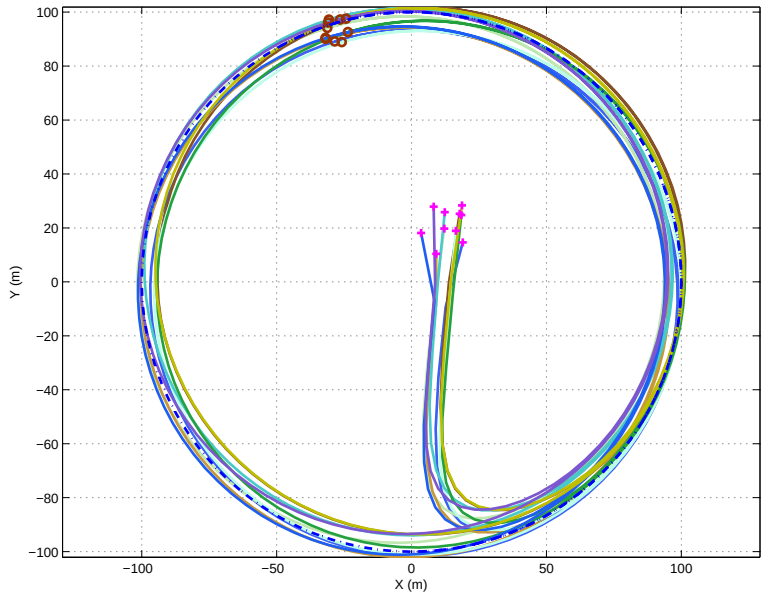

Fig. 6. Ten robots track a circle avoiding inter-agent collision ($d_{cp} = 10$ and $\mu = 0.1$).

the ”net”, the circle on which the three robots uniformly distribute, is gradually drawn in until the prey is captured.

In this case study, three of the above defined objective functions are applied: mean of formation, circle formation and regular polygon formation. The priorities are also assigned in this order.

Case 3:

In dynamic environments, especially when passing through certain areas, members of the robot team may need to change their relative positions in formation in order to avoid hazards, subsequently resuming the deployment pattern as needed. Such a scenario is illustrated in Fig. 9. A team of robots adaptively congregate themselves to tunnel through when

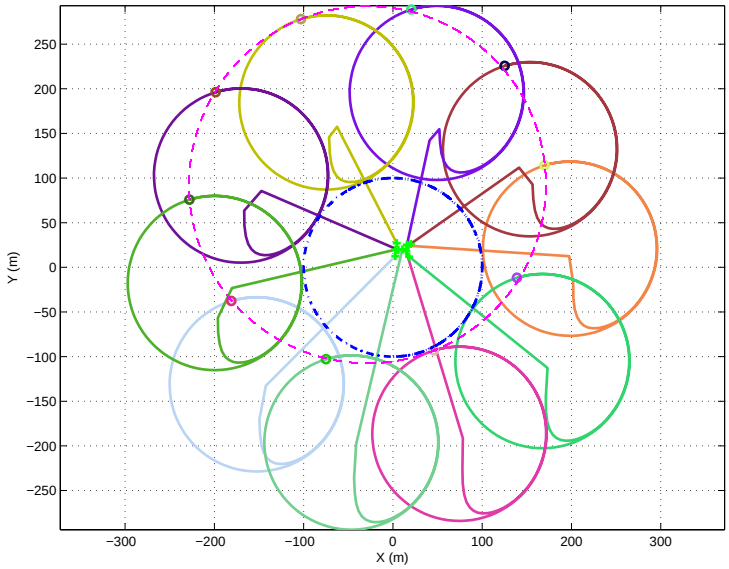

Fig. 7. Ten robots track a circle forming a rigid circle formation ($d_{cp} = 100$ and $\mu = 1$).

moving forward. Figure 10 shows the smooth gradual transient response of the objective function, J_v, relative to the desired one (solid line).

Case 4:

In this simulation, multiple robots are required to track pre-specified spatial paths while both reconfiguring inter-robot formation patterns and avoiding obstacles. Formation reconfiguration is demonstrated in the snapshots of five robots' motion evolvement (Fig. 11-Fig. 15). While their center of mass tracks a sinusoid curve, they start from point formation,

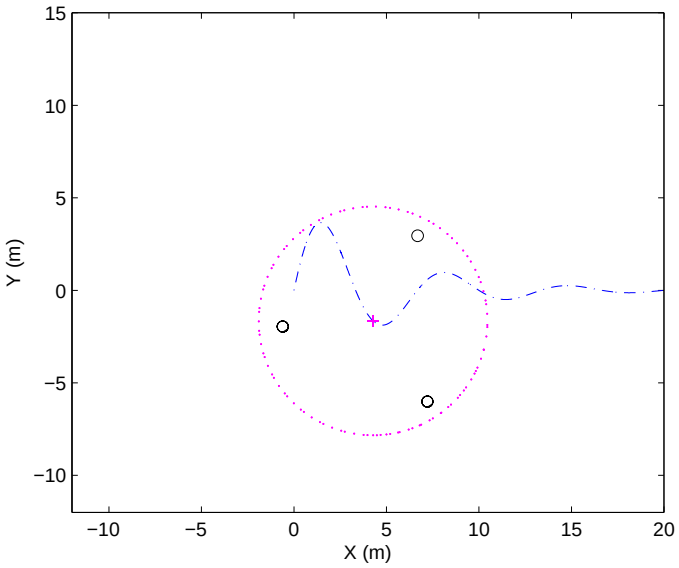

(a)

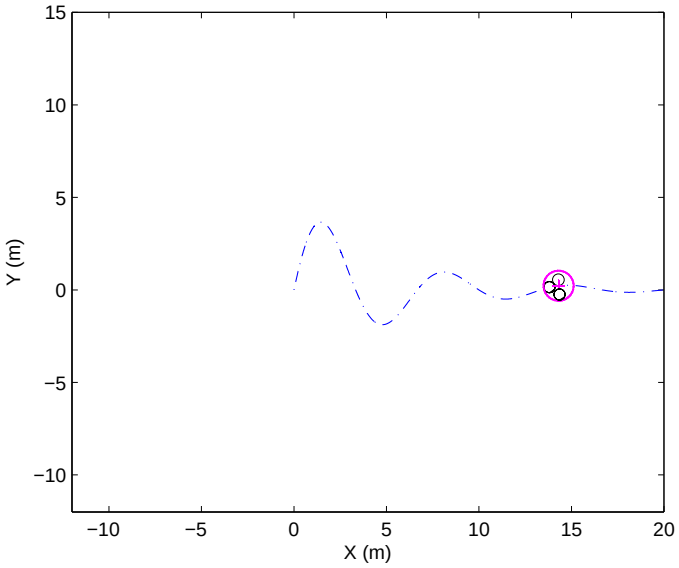

(b)

Fig. 8. Chasing a moving target: (a) t=5.15 sec, and (b) t=15.84 sec.

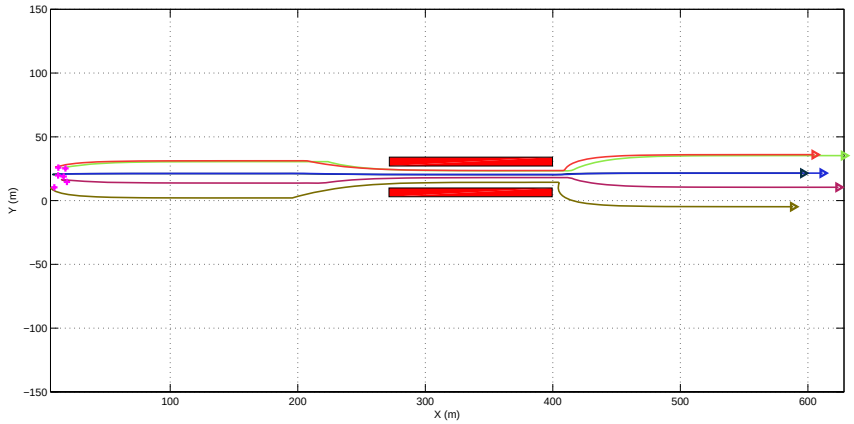

Fig. 9. Six robots pass a tunnel.

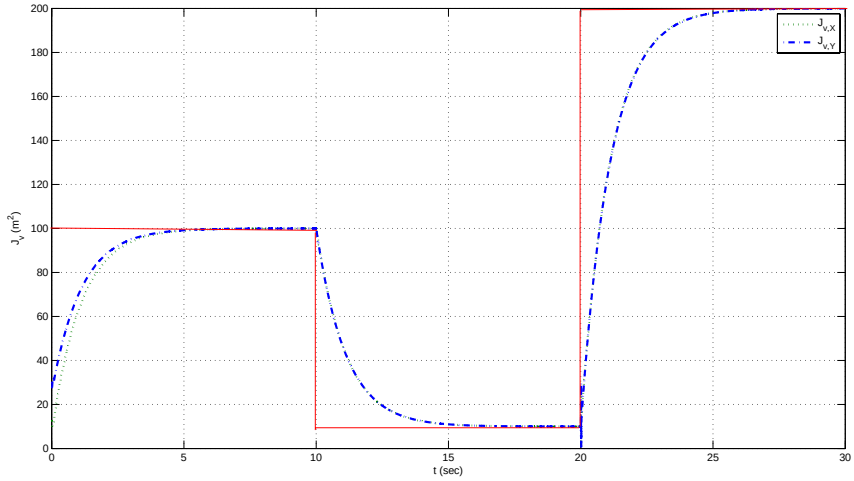

Fig. 10. Objective function of variance of formation

then change to wedge, followed by line and pentagon patterns[‡]. Furthermore, obstacles are properly avoided. In terms of task priority, obstacle avoidance is assigned the highest, then tracking, which is followed by formation reconfiguration.

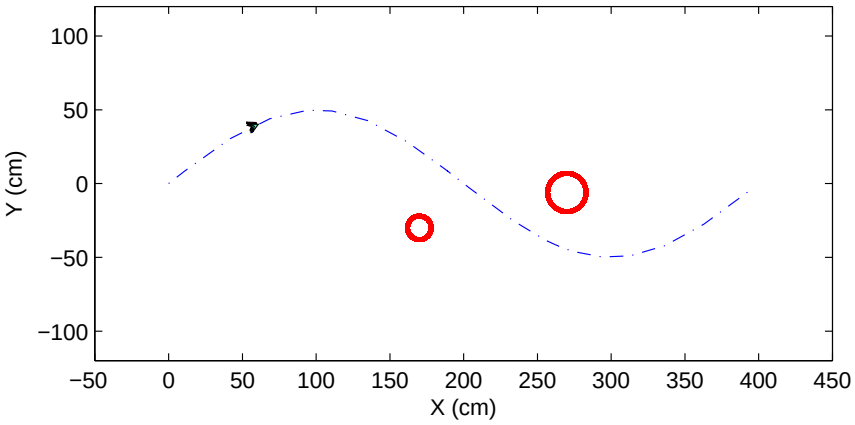

Fig. 11. Point formation (t=6 sec).

[‡]The desired formation pattern is predefined by expressing each robot's position vector relative to the center of mass.

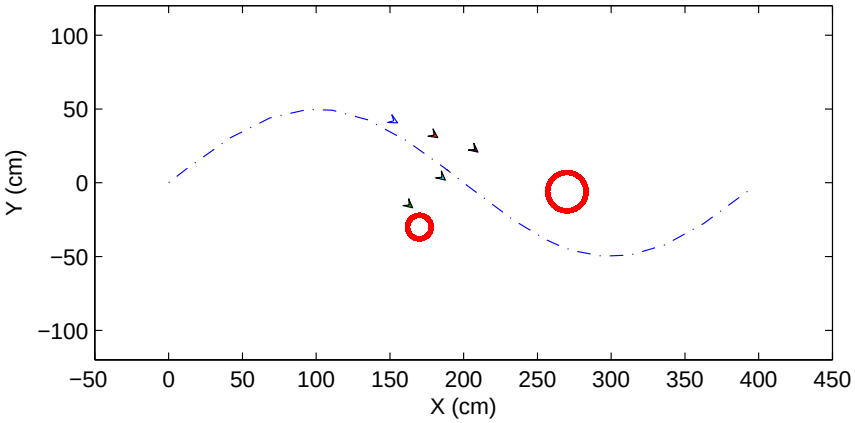

Fig. 12. Wedge formation (t=18 sec).

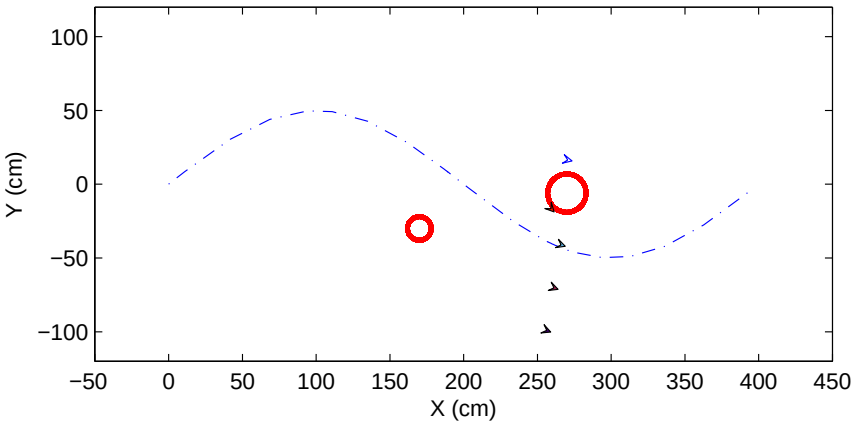

Fig. 13. Line formation before colliding with obstacle (t=26.57 sec).

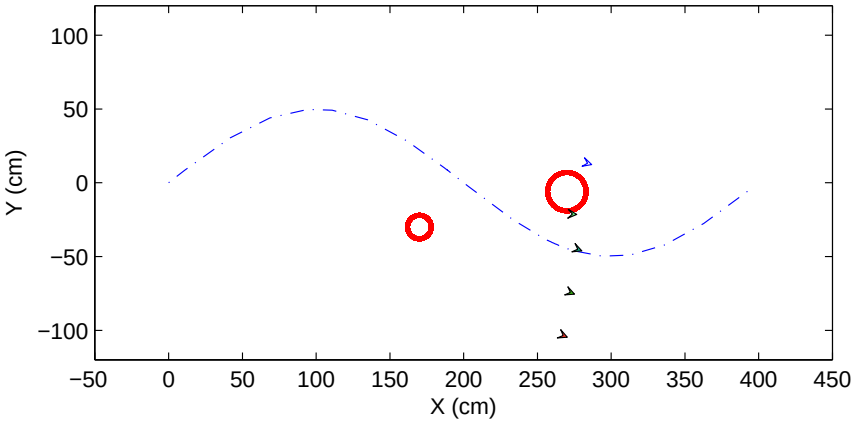

Fig. 14. Line formation after avoiding obstacle (t=27.76 sec).

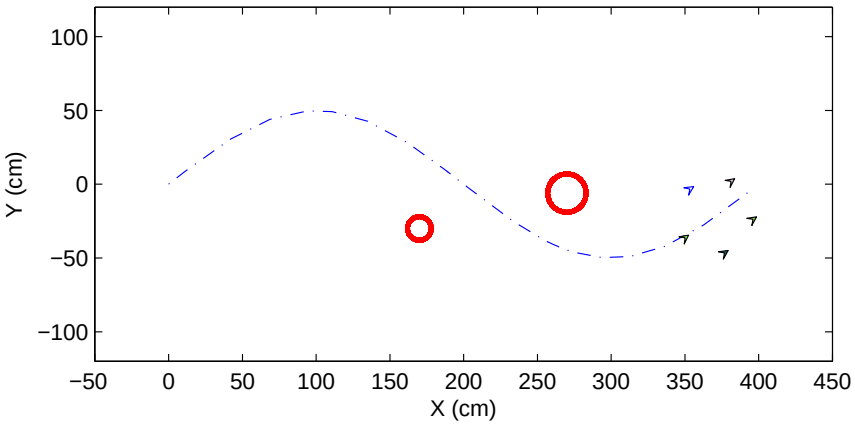

Fig. 15. Pentagon formation (t=37.4 sec).

CHAPTER III

MULTI-TASK FORMATION CONTROL OF MULTI-ROBOT SYSTEMS WITH DYNAMICS UNCERTAINTIES AND CONTROL TIME-DELAYS

For practical implementation of the formation control framework developed in the previous chapter, we propose in this chapter a systematic and provable design procedure for controlling collective motion of multi-robotic systems subject to dynamics modeling uncertainties and control input time-delays. First, modeling uncertainties and input time-delays are introduced into this class of time-varying nonlinear systems (2.12)-(2.13). After transforming into a perturbed system, a robust compensation tracking controller is proposed and justified based on Lyapunov stability theorem. The compensated system effectively suppresses the perturbation effects to guarantee robust stability with tracking errors exponentially converging to a bounded residual set.

A. Robust Tracking Control

To make the problem more realistic, during the following remodeling and robust control design, modeling uncertainties and control time-delays are brought into the previously treated nominal system (2.12)-(2.13):

$$\begin{aligned}\dot{x}(t) &= \big[f(x(t)) + \triangle\, f(x(t))\big] + \big[g(x(t)) + \triangle\, g(x(t))\big]u(t-\tau) \\ &\triangleq f(x(t)) + g(x(t))u(t-\tau) + \Sigma(x(t), u(t-\tau)), \qquad (3.1)\\ y(t) &= h(x(t)), \qquad (3.2)\end{aligned}$$

where $\Sigma(x(t), u(t-\tau)) \triangleq \triangle\ f(x(t)) + \triangle\ g(x(t))u(t-\tau)$ and $\tau$is time constant. This is similar in spirit to early work in [45], which investigated output tracking control of this class of nonlinear systems with mismatched uncertainties. But it did not consider input

time-delays.

First, the external dynamics are obtained as

$$\begin{aligned}\dot{\zeta}_1(t) =&\frac{\partial \delta_1}{\partial x}\frac{dx}{dt} = \frac{\partial h}{\partial x}\frac{dx}{dt}\\ =&L_f h(x(t)) = \delta_2(x(t)) = \zeta_2(t), \qquad (3.3)\\ &\vdots\\ \dot{\zeta}_{\rho-1}(t) =&\frac{\partial \delta_{\rho-1}}{\partial x}\frac{dx}{dt} = \frac{\partial L_f^{\rho-2} h}{\partial x}\frac{dx}{dt}\\ =&L_f^{\rho-1} h(x(t)) = \delta_\rho(x(t)) = \zeta_\rho(t), \qquad (3.4)\\ \dot{\zeta}_\rho(t) =&\frac{\partial \delta_\rho}{\partial x}\frac{dx}{dt} = \frac{\partial L_f^{\rho-1} h}{\partial x}\frac{dx}{dt}\\ =&L_f^{\rho} h(x(t)) + L_g L_f^{\rho-1} h(x(t))u(t). \qquad (3.5)\end{aligned}$$

The internal dynamics are as the following:

$$\begin{aligned}\dot{\eta}_j(t) =&\frac{\partial \delta_k}{\partial x}(f(x(t)) + g(x(t))u(t))\\ =&L_f \delta_j(x(t)) + L_g \delta_j(x(t))u(t)\\ =&L_f \delta_j(x(t)),\ j = \rho+1, \rho+2, \cdots, n. \qquad (3.6)\end{aligned}$$

Thus, the transformed nominal system has the following state space representation: Thus, combining equations (3.3)-(3.6) the transformed nominal system has the following state space representation:

$$\begin{aligned}\dot{\zeta}_i(t) =&\zeta_{i+1}(t),\ i = 1, 2, \cdots, \rho-1 \qquad (3.7)\\ \dot{\zeta}_\rho(t) =&L_f^{\rho} h(x(t)) + L_g L_f^{\rho-1} h(x(t))u(t), \qquad (3.8)\\ \dot{\eta}_j(t) =&L_f \delta_j(x(t)),\ j = \rho+1, \rho+2, \cdots, n \qquad (3.9)\\ y(t) =&\zeta_1(t), \qquad (3.10)\end{aligned}$$

where $\zeta(t) \in \mathbb{R}^{m\rho}$ and $\eta(t) \in \mathbb{R}^{n-m\rho}$. Note that m is the dimension of output $y(t)$.

Accordingly, the linearized nonlinear state feedback control law can be derived as

$$u(t) = \big[L_g L_f^{\rho-1} h(x(t))\big]^{-1}\big[- L_f^{\rho} h(x(t)) + \hat{v}(t)\big], \tag{3.11}$$

where $\hat{v}(t)$ is the newly introduced control to be designed for signal tracking. Applying the above transformation and control design to the perturbed system (3.1)-(3.2) yields

$$\dot{\zeta}_1(t) = \zeta_2(t) + \frac{\partial h(x(t))}{\partial x(t)}(\Sigma(x(t), u(t-\tau))) \tag{3.12}$$

$$\vdots$$

$$\dot{\zeta}_{\rho-1}(t) = \zeta_\rho(t) + \frac{\partial L_f^{\rho-2} h(x(t))}{\partial x(t)}(\Sigma(x(t), u(t-\tau))) \tag{3.13}$$

$$\begin{aligned}\dot{\zeta}_\rho(t) =& \hat{v}(t) + \frac{\partial L_f^{\rho-1} h(x(t))}{\partial x(t)}\big[\Sigma(x(t), u(t-\tau)) \\ &+ g(x(t))(u(t-\tau) - u(t))\big]\end{aligned} \tag{3.14}$$

$$\begin{aligned}\dot{\eta}_1(t) =& L_f \delta_1(x(t)) + \frac{\partial \delta_{\rho+1}}{\partial x(t)}(\Sigma(x(t), u(t-\tau))) \\ \triangleq& p_1(\zeta(t), \eta(t)) + \frac{\partial \delta_{\rho+1}}{\partial x(t)}(\Sigma(x(t), u(t-\tau)))\end{aligned} \tag{3.15}$$

$$\vdots$$

$$\begin{aligned}\dot{\eta}_{n-\rho}(t) =& L_f \delta_{n-\rho}(x(t)) + \frac{\partial \delta_n}{\partial x(t)}(\Sigma(x(t), u(t-\tau))) \\ \triangleq& p_{n-\rho}(\zeta(t), \eta(t)) + \frac{\partial \delta_n}{\partial x(t)}(\Sigma(x(t), u(t-\tau)))\end{aligned} \tag{3.16}$$

Namely,

$$\dot{\zeta} = \bar{A}\zeta + \bar{B}v + \triangle\ \Omega(x, u, u(t-\tau)), \tag{3.17}$$

$$\dot{\eta} = p(\zeta, \eta) + \triangle\ \Psi(x, u(t-\tau)), \tag{3.18}$$

$$y = \bar{C}\zeta, \tag{3.19}$$

where $\bar{B} = \begin{bmatrix} 0 & 0 \cdots 1 \end{bmatrix}^T \in \mathbb{R}^{\rho \times 1}$, $\bar{C} = \begin{bmatrix} 1 & 0 \cdots 0 \end{bmatrix} \in \mathbb{R}^{1 \times \rho}$,

$$\bar{A} = \begin{bmatrix} 0 & 1 & 0 & \cdots & 0 \\ 0 & 0 & 1 & \cdots & 0 \\ \vdots & \vdots & \vdots & \ddots & \vdots \\ 0 & 0 & 0 & \cdots & 1 \\ 0 & 0 & 0 & \cdots & 0 \end{bmatrix} \in \mathbb{R}^{\rho \times \rho}, \ \triangle \ \Psi = \begin{bmatrix} \frac{\partial \delta_{\rho+1}}{\partial x} \Sigma(x, u(t-\tau)) \\ \vdots \\ \frac{\partial \delta_n}{\partial x} \Sigma(x, u(t-\tau)) \end{bmatrix},$$

$$\triangle \ \Omega = \begin{bmatrix} \frac{\partial h(x)}{\partial x} \Sigma(x, u(t-\tau)) \\ \vdots \\ \frac{\partial L_f^{\rho-2} h(x)}{\partial x} \Sigma(x, u(t-\tau)) \\ \frac{\partial L_f^{\rho-1} h(x)}{\partial x} \big[\Sigma(x, u(t-\tau)) + g(x)(u(t-\tau) - u(t)) \big] \end{bmatrix}.$$

Note that $\triangle \ \Psi \in \mathbb{R}^{(n-\rho) \times 1}$ and $\triangle \ \Omega \in \mathbb{R}^{\rho \times 1}$.

For tracking control purpose, we define tracking errors as $e_i \triangleq \zeta_i - r^{(i-1)} \in \mathbb{R}^m$ where r is reference trajectory and $i = 1, 2, \cdots, \rho$. Then

$$\dot{e} = \bar{A}e + \bar{B}(\hat{v} - r^{(\rho)}) + \triangle \ \Omega, \tag{3.20}$$

$$\dot{\eta} = p(\zeta, \eta) + \triangle \ \Psi. \tag{3.21}$$

Control $\hat{v}(t)$ was postulated as follows

$$\hat{v} = r^{(\rho)} - c_1 e_1 - c_2 e_2 - \cdots - c_\rho e_\rho + u_a, \tag{3.22}$$

where $c_1, \cdots, c_\rho$ are chosen such that $s^\rho + c_\rho s^{\rho-1} + \cdots + c_2 s + c_1$ is a *Hurwitz* polynomial with the resulting closed system $(\bar{A}_c, \bar{B})$ controllable. Here s is the Laplace operator. Notice that in order to compensate perturbations, an additional robust control term $u_a(t)$ is brought in.

Hence, we obtain the closed-loop system as follows:

$$\dot{e} = \bar{A}_c e + \bar{B} u_a + \triangle\ \Omega(x, u, u(t-\tau)), \tag{3.23}$$

$$\dot{\eta} = p(\zeta, \eta) + \triangle\ \Psi(x, u(t-\tau)), \tag{3.24}$$

where

$$\bar{A}_c \triangleq \begin{bmatrix} 0 & 1 & \cdots & 0 \\ \vdots & \vdots & \ddots & \vdots \\ 0 & 0 & \cdots & 1 \\ -c_1 & -c_2 & \cdots & -c_\rho \end{bmatrix} \in \mathbb{R}^{\rho \times \rho}.$$

The robust control objective is to design a robust feedback control law such that despite the effects of perturbations resulting from system uncertainties and input time-delays, the desired output trajectories of the closed-loop system are still achieved while maintaining the boundedness of all signals. To this end, it is known that if $(\bar{A}_c, \bar{B})$ given in system (3.23) is controllable, then for any symmetric positive definite matrix (spdm) $Q \in \mathbb{R}^{m\rho \times m\rho}$ the algebraic Riccati equation

$$\bar{A}_c^T P + P \bar{A}_c + Q - \gamma P \bar{B} \bar{B}^T P = 0 \tag{3.25}$$

has a solution $P \in \mathbb{R}^{m\rho \times m\rho}$, which is also a spdm. Then this particular matrix is utilized to propose the following local state feedback controller:

$$u_a = -\bar{k} \gamma \bar{B}^T P e, \tag{3.26}$$

where the decentralized control gain $\bar{k}$ satisfies

$$\bar{k} = \frac{1}{2} + \sum_{i=1}^{3} \kappa_i \tag{3.27}$$

and depends on dynamics uncertainties, which will be addressed in the following.

Before stating the main theorem, the following conditions are given.

(C1): The trajectory planner guarantees the reference signal $r(t)$ and its first ρ derivatives are all uniformly bounded by $B_r \in \mathbb{R}^+$, namely, $||r^{(i)}(t)|| \leqslant B_r,$ for $i = 0, 1, \cdots, \rho$. Then

$$||\zeta_i|| \leqslant ||e_i|| + B_r. \tag{3.28}$$

(C2): As discussed above, the internal dynamics $\eta(t)$ in nominal system (2.12) is stable. Moreover, by Lyapunov converse theorem [39], assume there exists a Lyapunov function $V_i(t) : \mathbb{R}^{n-\rho} \to \mathbb{R}^+$ that for some $\chi_i > 0$ $(i = 1, ..., 4)$ satisfies

$$\chi_1||\eta(t)||^2 \leqslant V_i(\eta(t)) \leqslant \chi_2||\eta(t)||^2, \tag{3.29}$$

$$\frac{V_i(\eta(t))}{\eta(t)} p(0, \eta(t)) \leqslant \chi_3||\eta(t)||^2, \tag{3.30}$$

$$||\frac{V_i(\eta(t))}{\eta(t)}|| \leqslant \chi_4||\eta(t)||^2. \tag{3.31}$$

(C3): For uncertainty terms $\triangle\ \Omega$ and $\triangle\ \Psi$, unlike most work on control of time-delay systems where matched conditions are a prerequisite, here we only assume less conservative mismatched conditions. Suppose there exist κ_i, $\epsilon_i \in \mathbb{R}^+ (i = 1, 2, 3)$ such that

$$||2P \triangle\ \Omega(x, u, u(t-\tau))|| \leqslant \kappa_1||\zeta|| + \kappa_2||\eta|| + \kappa_3, \tag{3.32}$$

$$||\triangle\ \Psi(x, u(t-\tau))|| \leqslant \epsilon_1||\zeta|| + \epsilon_2||\eta|| + \epsilon_3, \tag{3.33}$$

where P is defined in (3.25). Moreover, if $p(\zeta(t), \eta(t))$ is *Lipschitz* in $\zeta(t)$, then it is known that the following holds:

$$||p(\zeta(t), \eta(t)) - p(0, \eta(t))|| \leqslant L||\zeta(t)||,\ \forall\ \eta(t) \in \mathbb{R}^{n-\rho}, \tag{3.34}$$

where $L \in \mathbb{R}^+$, a *Lipschitz* constant of $p(\zeta(t), \eta(t))$ with respective to $\zeta(t)$.

Theorem A.1. *For the uncertain nonlinear system (3.1)-(3.2) with control input time-delays satisfying conditions (C1)-(C3), under control law (3.22) and (3.25)-(3.27) there exist* ς^* *and* ϵ^* *for all* $0 < \frac{1}{2} + \kappa_1 \leqslant min(\frac{\lambda_{min}(Q)}{2}, \varsigma), \kappa_2 \in (0, \varsigma^*]$ *and* $\epsilon_2 \in (0, \epsilon_2^*]$ *such that*

the states of the closed loop system (3.23)-(3.24) are uniformly bounded. Furthermore, the output tracking error $e(t)$ *converges to a residual set*

$$\Gamma_e \triangleq \{e(t) \in \mathbb{R}^{m\rho} | V(e(t)) \leqslant k_e^{-1} b_e\}$$

$$\textit{where } k_e \triangleq \frac{\lambda_{min}(Q) - \kappa_1 - \frac{1}{2}}{\lambda_{max}(P)} \textit{ and } b_e \triangleq (\kappa_2 B_i)^2 + (\kappa_1 B_r + \kappa_3)^2.$$

Proof. See Appendix C. □

As a demonstration and verification of the presented remodeling and robust control schemes for the perturbed nonholonomic robotic system, the problem of coordinated trajectory tracking is reconsidered. We employ the previously developed two-stage hierarchical architecture for formation control and incorporate the above dynamics remodeling and robust tracking control design into the bottom tracking controller layer.

B. Case Study

The lumped nonlinear perturbation in system (3.1) is modeled as

$$\Sigma(x(t), u(t-\tau)) \triangleq \begin{bmatrix} \varpi_1 \\ \varpi_1 \\ \varpi_2 |1 - sin\psi| \\ \varpi_2(\dot{\theta}_R + \dot{\theta}_L) \\ \varpi_2(cos\psi\dot{\theta}_R + sin\psi\dot{\theta}_L) \\ u_R(t-\tau)\varpi_2 \\ u_L(t-\tau)|cos\psi| \end{bmatrix},$$

where ϖ_1 and ϖ_2 are uncertain parameters that randomly lie within [-0.03 0.03] and [-0.1 0.1], respectively. Sampling period is $\triangle\ t = 0.1$ sec and $\tau = 6\Delta t$. The selected control gains are listed in Table III.

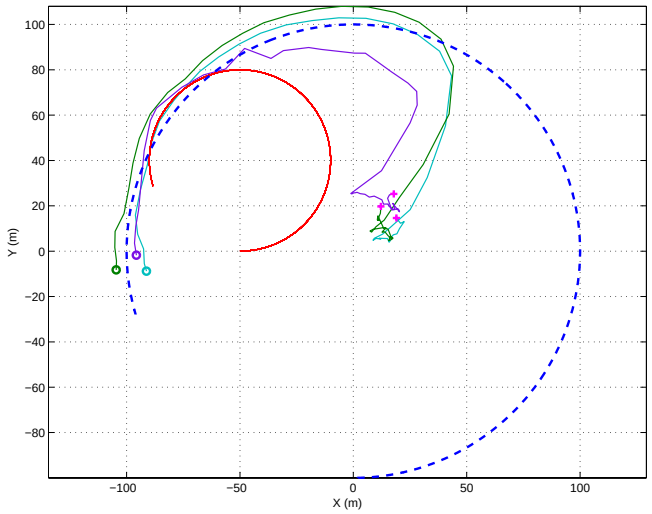

(a)

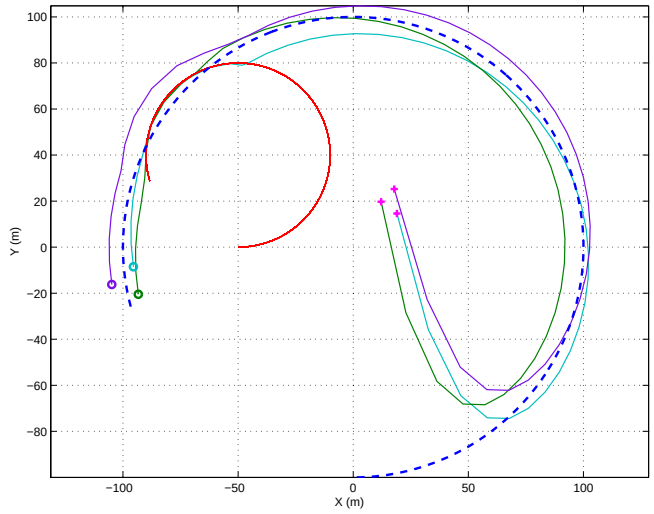

(b)

Fig. 16. Three robots track a circle avoiding inter-agent collision and external obstacle ($d_{cp} = 10$ and $\mu = 1$): (a) without robust control u_a, and (b) with u_a.

Table III. Selected control gains with time-delays

Q	$500I_{4\times4}$
γ	1000
c_1	2025
c_2	63

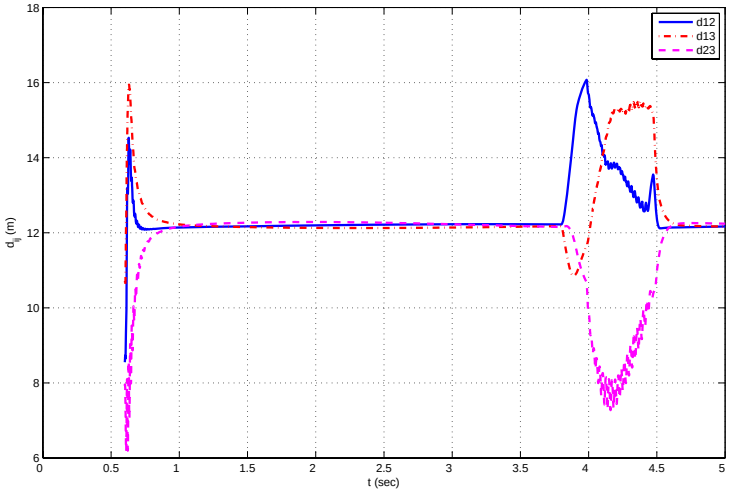

Fig. 17. Internal distances between robots

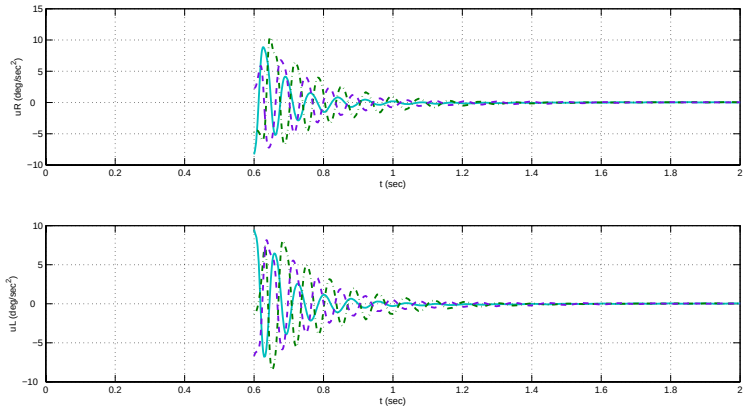

Fig. 18. Delayed control inputs

As indicated in Fig. 16(a), without augmented robust control u_a, the desired formation mission cannot be achieved. However, by including u_a, similar with the scenario of Case 1 in pervious chapter, figure 16(b) shows that in spite of the appearance of perturbations three robots that are randomly posed around origin area (plus sign) successfully accomplish the tracking circle task (dashdot line) without any inter-agent collision, even during the transient phase before stabilizing into formation. Furthermore, an external obstacle (solid line) is avoided when it is present, and trajectory tracking is lowered from the 2nd to the 3rd priority. Collision avoidance is always assigned the highest priority. Figure 17 shows the internal distances between robots, which illustrates that the three robots, while tracking the circular reference trajectory, approximately form an equilateral triangle, though the multi-robotic system is subject to dynamics modeling uncertainties and control input time-delays. Note that even when avoiding the obstacle the internal distances are bounded within a certain range: The lower bound prevents collision, and the upper bound constrains the formation to be in cohesion and guarantees no robot would escape from the

team. This result demonstrates the effectiveness of the proposed collision-prevention approach. Smooth curves in Fig. 18 are the transients of the right and left delayed control inputs of each robot. This satisfactory performance demonstrates the effectiveness of the Lyapunov-based local robust tracking control design.

C. An Afterthought: Actuator Saturation

Another issue possibly encountered when implementing the formation control algorithm on real robotic systems is control input saturation. Consequently, this research also considers an investigation of robust stabilization of a class of large-scale networked robotic systems subject to multiple time-varying state delays in the interconnections, parameter perturbation uncertainties and also saturated actuators. Decentralized memoryless state feedback control is studied mainly via the Lyapunov-Krasovskii functional concept. By checking the Hamiltonian matrix and solving an algebraic Riccati equation, control gain matrix can be obtained to achieve global asymptotical stability of this class of large-scale interconnected dynamical systems.

1. Problem Formulation

Consider a class of large-scale multi-robot systems S composed of N robotic subsystems S_i, $i = 1, \cdots, N$, described by the following perturbed linear differential-difference dynamic equations with saturated control inputs:

$$\begin{aligned}\dot{x}_i(t) =& A_i x_i(t) + \triangle f_i(x_i(t), t) + \sum_{j \in N_i} A_{ij} x_j(t - \tau_{ij}(t)) \\ &+ B_i sat(u_i(t)) + \triangle g_i(sat(u_i(t)), t),\end{aligned} \tag{3.35}$$

where $x_i(t) \triangleq [P_{iX}\ P_{iY}\ \dot{P}_{iX}\ \dot{P}_{iY}]^T \in R^4$; $u_i(t) \triangleq [u_{i1}(t)\ u_{i2}(t)]^T \in R^2$; $\triangle f_i(\cdot) : R^4 \times R \to R^4$ represents unknown parameter perturbation uncertainties, which can be constant,

linear, nonlinear, and/or time-varying, but is bounded as $|| \triangle f_i(x_i(t), t)|| \leqslant \alpha_i||x_i(t)||$, where $\alpha_i \in R^+$; $\tau_{ij}(t) \in R^+$ is unknown inconsistent state time-delays, occurring while robot i sensing or communicating with neighboring robot j in order to achieve desired formation; set N_i refers to the neighboring robots of robot i; $sat(u_i(t)) \in R^2$ symbolizes actuator saturation and $\triangle g_i(\cdot) : R^2 \times R \to R^2$ represents perturbed control inputs, which is bounded as $|| \triangle g_i(sat(u_i(t)), t)|| \leqslant \beta_i||sat(u_i(t))||$, where $\beta_i \in R^+$;

$A_i \triangleq \begin{bmatrix} 0 & 1 & 0 & 0 \\ 0 & a & 0 & 0 \\ 0 & 0 & 0 & 1 \\ 0 & 0 & 0 & b \end{bmatrix}$ and $B_i \triangleq \begin{bmatrix} 0 & 1 & 0 & 0 \\ 0 & 0 & 0 & 1 \end{bmatrix}^T$,

where $a, b \in R^*$; A_{ij} are constant matrices with appropriate dimensions.

Note that in the following analysis, the arguments of functions may be omitted when no confusion arises.

2. Control Design

The saturation function is defined as follows:

$$sat(u_i(t)) \triangleq \begin{cases} u_s & \text{if } u_s < u_i(t) \leqslant u_{max}, \\ u_i(t) & \text{if } -u_s \leqslant u_i(t) \leqslant u_s, \\ -u_s & \text{if } -u_{max} \leqslant u_i(t) < -u_s. \end{cases} \tag{3.36}$$

Most of the work considering saturated actuators in the literature simply assumes the nonlinear saturation is inside the sector $[0, 1]$, which leads to conservative results. Here we consider only a finite part of the actual system operation, *i.e.*, inside the sector $[a, 1]$, where

*Without loss of generality, here choose a=b=0 to have typical double integrators.

$0 \leqslant a \leqslant 1$, as illustrated in Fig. 19. Moreover , this implies

$$||sat(u_i(t)) - \frac{a+1}{2}u_i(t)|| \leqslant ||\frac{a-1}{2}u_i(t)||. \tag{3.37}$$

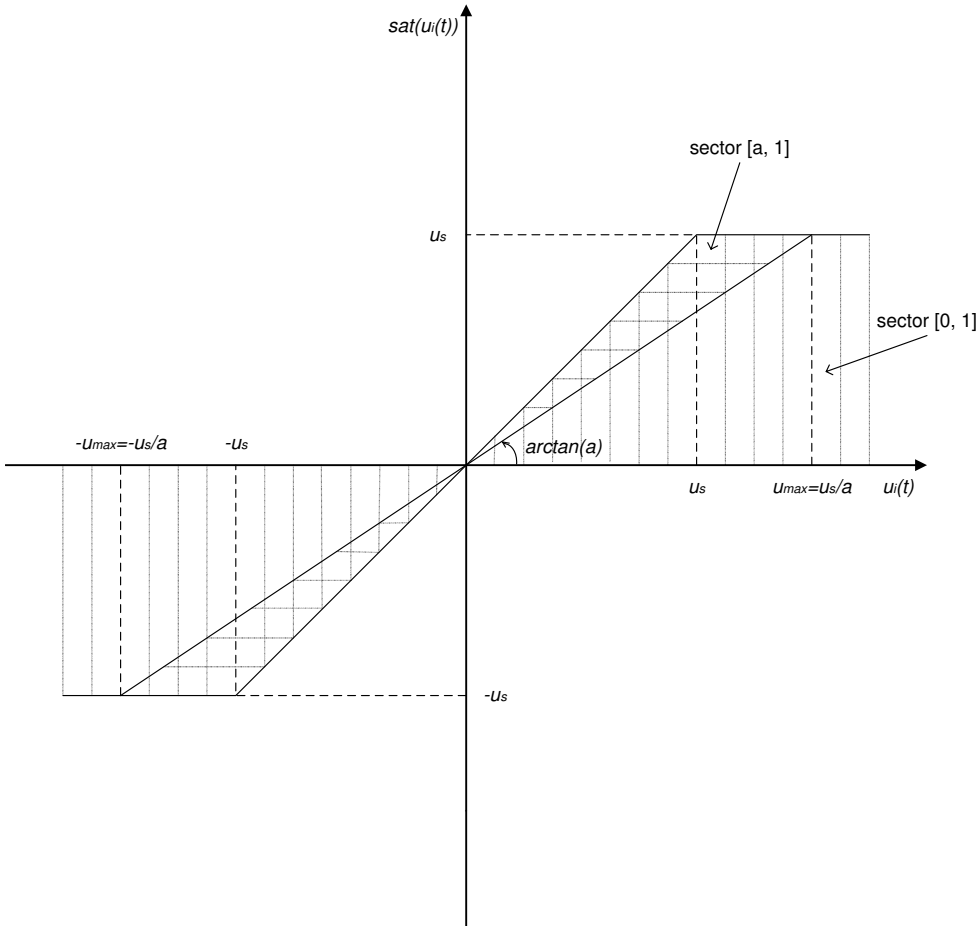

Fig. 19. Saturation function $sat(u_i(t))$

For this class of large-scale systems S including delayed states in the interconnections, the objective is to introduce a decentralized local memoryless state feedback controller $u_i = -K_i x_i$ for each subsystem S_i such that the overall system with parameter pertur-

bation uncertainties and saturated controls is globally stabilized. Note that the feedback controller only intends to utilize local delay-free states and does not include any delayed state information of neighboring robots, thus the requirement of the knowledge of time-delays is certainly released. Hence, we have the following closed-loop system:

$$\begin{aligned}\dot{x}_i(t) =&(A_i - \frac{a+1}{2}B_iK_i)x_i(t)+ \triangle\ f_i(x_i(t),t)\\ &+\sum_{j\in N_i} A_{ij}x_j(t-\tau_{ij}(t)) + B_i\big[sat(u_i(t))\\ &-\frac{a+1}{2}u_i(t)\big]+ \triangle\ g_i(sat(u_i(t)),t). \end{aligned} \tag{3.38}$$

The above equation can be further formulated into

$$\begin{aligned}\dot{x}_i(t) =&(A_i - \frac{a+1}{2}B_iK_i)x_i(t)+ \triangle\ f_i(x_i(t),t) + \sum_{j\in N_i} A_{ij}x_j(t)\\ &-\sum_{j\in N_i} A_{ij}\int_{t-\tau_{ij}(t)}^{t}\dot{x}_j(s)ds + B_i\big[sat(u_i(t)) - \frac{a+1}{2}u_i(t)\big]\\ &+ \triangle\ g_i(sat(u_i(t)),t)\\ =&(A_i - \frac{a+1}{2}B_iK_i)x_i(t)+ \triangle\ f_i(x_i(t),t) + \sum_{j\in N_i} A_{ij}x_j(t)\\ &-\sum_{j\in N_i} A_{ij}\int_{t-\tau_{ij}(t)}^{t}\Big\{(A_j - \frac{a+1}{2}B_jK_j)x_j(s)\\ &+ \triangle\ f_j(x_j(s),s) + \sum_{k\in N_j} A_{jk}x_k(s-\tau_{jk}(s)) + B_j\big[sat(u_j(s))\\ &-\frac{a+1}{2}u_j(s)\big]+ \triangle\ g_j(sat(u_j(s)),s)\Big\}ds + B_i\big[sat(u_i(t))\\ &-\frac{a+1}{2}u_i(t)\big]+ \triangle\ g_i(sat(u_i(t)),t). \end{aligned} \tag{3.39}$$

Before giving the main theorem, we need the following lemma.

Lemma [46]: Given the Hamiltonian matrix defined as

$$H \triangleq \begin{bmatrix} A & BB^T \\ -\gamma I & -A^T \end{bmatrix}, \text{where } \gamma > 0.$$

If

(i) A is *Hurwitz*, and

(ii) H has no purely imaginary eigenvalues,

then the algebraic Riccati equation

$$A^T P + PA^T + PBB^T P = -\gamma I \tag{3.40}$$

always has a symmetric positive definite solution P, where I denotes identity matrix.

Theorem C.1. *If the local state feedback gain matrix K_i is selected such that the above Lemma is satisfied, where*

$$A \triangleq [A_i - \frac{a+1}{2} B_i K_i] \tag{3.41}$$

and

$$BB^T \triangleq \sum_{j \in N_i} \Big[A_{ij}[A_j - \frac{a+1}{2} B_j K_j] \;\; \alpha_j A_{ij} \;\; \sqrt{|N_j|} A_{ij} \;\; \frac{1-a}{\sqrt{2}} ||K_j|| A_{ij} B_j \;\; \beta_i ||K_j|| A_{ij} \;\; \sqrt{|N_i|} I_{n \times n} \Big], \tag{3.42}$$

and

$$\gamma > 2\alpha_i ||P|| + (1-a)||PB_i|| ||K_i|| + 2\beta_i ||P|| ||K_i|| + \sum_{j \in N_i} \big[(4\tau_{ij}^2 + ||A_{ij}||^2) p_j + \sum_{k \in N_j} \tau_{ij}^2 p_j ||A_{jk}||^2 p_k \big], \tag{3.43}$$

then the class of large-scale multi-robot systems S, consisting of N subsystems (3.35), is globally asymptotically stable.

Before proceeding to give the proof of the above theorem, the following conditions

are needed.

(C1): According to the well-known Razumikhin Theorem [47], define $W(\cdot) \triangleq (\cdot)^T P(\cdot)$, where P is the solution to the algebraic Riccati equation (3.40), and the assumption that

$$W(x_j(t - \tau_{ij}(t))) < q^2 W(x_j(t)),$$

where $q > 1$, we obtain

$$||x_j(t - \tau_{ij}(t))|| < q\rho||x_j(t)||, \tag{3.44}$$

where $\rho \triangleq \sqrt{\frac{\lambda_{max}(P)}{\lambda_{min}(P)}}$ (See Appendix D for derivation). The above condition claims that if delay-free states are bounded, then the corresponding delayed ones are also bounded.

(C2): $\exists\ p_j, p_k \geqslant 1$, where $j \in N_i$ and $k \in N_j$, such that

$$||x_j(t)|| \leqslant p_j||x_i(t)||, \tag{3.45}$$

$$||x_k(t)|| \leqslant p_k||x_j(t)|| \leqslant p_k p_j||x_i(t)||. \tag{3.46}$$

Namely, neighboring robots perform similarly as a whole and do not have great disparity in motion behaviors.

Proof. To investigate the stability of each closed loop subsystem S_i, which contains multiple state time-delays in the interconnections, introduce a Lyapunov-Krasovskii function $v_i(t)$ of the form:

$$\begin{aligned} v_i(t) \triangleq & x_i^T(t) P x_i(t) + 4 \sum_{j \in N_i} \tau_{ij} \int_{-\tau_{ij}}^{0} \int_{t+r}^{t} x_j^T(s) x_j(s) ds dr \\ & + \sum_{j \in N_i} \sum_{k \in N_j} \tau_{ij} ||A_{jk}||^2 \int_{-\tau_{ij}-\tau_{jk}}^{-\tau_{jk}} \int_{t+r}^{t} x_k^T(s) x_k(s) ds dr, \end{aligned} \tag{3.47}$$

where P satisfies equation (3.40) and $r < 0$.

With the aid of formula

$$\frac{d}{dt}\Big(\int_{a(t)}^{b(t)} f(z,t)dz\Big) = \int_{a(t)}^{b(t)} \frac{\partial f(z,t)}{\partial t}dz + f(b(t),t)\frac{db(t)}{dt} - f(a(t),t)\frac{da(t)}{dt}, \quad (3.48)$$

differentiating v_i along the trajectory of closed system (3.39) yields

$$\begin{aligned}\dot{v}_i =& \dot{x}_i^T(t)Px_i(t) + x_i(t)P\dot{x}_i^T(t) + 4\sum_{j\in N_i}\tau_{ij}\big[\tau_{ij}x_j^T(t)x_j(t) - \int_{t-\tau_{ij}}^{t} x_j^T(s)x_j(s)ds\big] \\ &+ \sum_{j\in N_i}\sum_{k\in N_j}\tau_{ij}||A_{jk}||^2\big[\tau_{ij}x_k^T(t)x_k(t) - \int_{t-\tau_{ij}-\tau_{jk}}^{t-\tau_{jk}} x_k^T(s)x_k(s)ds\big], \end{aligned} \quad (3.49)$$

in which

$$\begin{aligned}&\dot{x}_i^T(t)Px_i(t) + x_i(t)P\dot{x}_i^T(t) \\ =&x_i^T\Big\{\big[A_i - \frac{(a+1)B_iK_i}{2}\big]^T P + P\big[A_i - \frac{(a+1)B_iK_i}{2}\big]\Big\}x_i \\ &- 2\sum_{j\in N_i} x_i^T PA_{ij}\int_{t-\tau_{ij}}^{t}\Big\{(A_j - \frac{a+1}{2}B_jK_j)x_j(s) \\ &+ \triangle f_j(x_j(s),s) + \sum_{k\in N_j} A_{jk}x_k(s-\tau_{jk}(s)) + B_j\big[sat(u_j(s)) \\ &- \frac{a+1}{2}u_j(s)\big] + \triangle g_j(sat(u_j(s)),s)\Big\}ds + 2\sum_{j\in N_i} x_i^T PA_{ij}x_j(t) \\ &+ 2x_i^T P\triangle f_i + 2x_i^T PB_i\big[sat(u_i) - \frac{a+1}{2}u_i\big] + 2x_i^T P\triangle g_i. \end{aligned} \quad (3.50)$$

Moreover, under assumptions $||\triangle f_i(x_i(t),t)|| \leqslant \alpha_i||x_i(t)||$ and $||\triangle g_i(sat(u_i(t)),t)|| \leqslant \beta_i||sat(u_i(t))||$, inequality (3.37), and also the inequality, $2ab \leqslant \frac{a^2}{c} + cb^2$, for any $a, b \in R$

and $c > 0$, one obtains

$$
\begin{aligned}
&2x_i^T P A_{ij} \int_{t-\tau_{ij}}^{t} (A_j - \frac{a+1}{2} B_j K_j) x_j(s) ds \\
&\leqslant 2 \int_{t-\tau_{ij}}^{t} ||x_i^T P A_{ij} (A_j - \frac{a+1}{2} B_j K_j)|| ||x_j(s)|| ds \\
&\leqslant x_i^T P A_{ij} \big[A_j - \frac{(a+1) B_j K_j}{2}\big] \big[A_j - \frac{(a+1) B_j K_j}{2}\big]^T A_{ij}^T P x_i \\
&\quad + \tau_{ij} \int_{t-\tau_{ij}}^{t} x_j^T(s) x_j(s) ds,
\end{aligned} \tag{3.51}
$$

$$
\begin{aligned}
&2x_i^T P A_{ij} \int_{t-\tau_{ij}}^{t} \triangle\ f_j(x_j(s), s) ds \\
&\leqslant 2 \int_{t-\tau_{ij}}^{t} \alpha_j ||x_i^T P A_{ij}|| ||x_j(s)|| ds \\
&\leqslant \alpha_j^2 x_i^T P A_{ij} A_{ij}^T P x_i + \tau_{ij} \int_{t-\tau_{ij}}^{t} x_j^T(s) x_j(s) ds,
\end{aligned} \tag{3.52}
$$

$$
\begin{aligned}
&2x_i^T P A_{ij} \int_{t-\tau_{ij}}^{t} \sum_{k \in N_j} A_{jk} x_k(s - \tau_{jk}(s)) ds \\
&\leqslant 2 \sum_{k \in N_j} ||x_i^T P A_{ij}|| \int_{t-\tau_{ij}}^{t} ||A_{jk}|| ||x_k(s - \tau_{jk}(s))|| ds \\
&\leqslant \sum_{k \in N_j} \Big[x_i^T P A_{ij} A_{ij}^T P x_i + \tau_{ij} ||A_{jk}||^2 \int_{t-\tau_{ij}-\tau_{jk}}^{t-\tau_{jk}} x_k^T(s) x_k(s) ds \Big] \\
&\leqslant |N_j| x_i^T P A_{ij} A_{ij}^T P x_i + \sum_{k \in N_j} \tau_{ij} ||A_{jk}||^2 \int_{t-\tau_{ij}-\tau_{jk}}^{t-\tau_{jk}} x_k^T(s) x_k(s) ds,
\end{aligned} \tag{3.53}
$$

where $|N_j|$ denotes the cardinality of the neighboring set N_j of robot j, *i.e.*, the number of

members of N_j, and the same goes for N_i, which will appear subsequently.

$$\begin{aligned}
&2x_i^T P A_{ij} \int_{t-\tau_{ij}}^{t} B_j \big[sat(u_j(s)) - \frac{a+1}{2} u_j(s)\big] ds \\
&\leqslant 2 \int_{t-\tau_{ij}}^{t} \frac{1-a}{2} ||K_j|| || x_i^T P A_{ij} B_j || || x_j(s) || ds \\
&\leqslant \big(\frac{1-a}{2}\big)^2 ||K_j||^2 x_i^T P A_{ij} B_j B_j^T A_{ij}^T P x_i + \tau_{ij} \int_{t-\tau_{ij}}^{t} x_j^T(s) x_j(s) ds,
\end{aligned} \tag{3.54}$$

$$\begin{aligned}
&2x_i^T P A_{ij} \int_{t-\tau_{ij}}^{t} \triangle\ g_j(sat(u_j(s)), s) ds \\
&\leqslant 2x_i^T P A_{ij} \int_{t-\tau_{ij}}^{t} \beta_i ||u_j(s)|| ds \\
&\leqslant 2 \int_{t-\tau_{ij}}^{t} \beta_i ||K_j|| || x_i^T P A_{ij} || || x_j(s) || ds \\
&\leqslant \beta_i^2 ||K_j||^2 x_i^T P A_{ij} A_{ij}^T P x_i + \tau_{ij} \int_{t-\tau_{ij}}^{t} x_j^T(s) x_j(s) ds,
\end{aligned} \tag{3.55}$$

$$\begin{aligned}
&2 \sum_{j \in N_i} x_i^T P A_{ij} x_j(t) \\
&\leqslant 2 \sum_{j \in N_i} ||x_i^T P A_{ij}|| || x_j(t) || \\
&\leqslant \sum_{j \in N_i} \big(x_i^T P P x_i + ||A_{ij}||^2 ||x_j(t)||^2 \big) \\
&= |N_i| x_i^T P P x_i + \sum_{j \in N_i} ||A_{ij}||^2 ||x_j(t)||^2,
\end{aligned} \tag{3.56}$$

$$2x_i^T P \triangle\ f_i \leqslant 2\alpha_i ||x_i^T P|| || x_i || \leqslant 2\alpha_i ||P|| || x_i ||^2, \tag{3.57}$$

$$\begin{aligned}
&2x_i^T P B_i \big[sat(u_i) - \frac{a+1}{2} u_i\big] \\
&\leqslant (1-a) ||x_i^T P B_i|| || K_i x_i || \leqslant (1-a) ||P B_i|| || K_i || || x_i ||^2,
\end{aligned} \tag{3.58}$$

$$2x_i^T P \triangle g_i \leqslant 2\beta_i||x_i^T P||||K_i x_i|| \leqslant 2\beta_i||P||||K_i||||x_i||^2. \tag{3.59}$$

Then,

$$\begin{aligned}\dot{v}_i \leqslant & x_i^T\Big\{\big[A_i - \frac{(a+1)B_iK_i}{2}\big]^T P + P\big[A_i - \frac{(a+1)B_iK_i}{2}\big]\Big\}x_i \\ & + \sum_{j\in N_i}\Big\{x_i^T P A_{ij}\big[A_j - \frac{(a+1)B_jK_j}{2}\big]\big[A_j - \frac{(a+1)B_jK_j}{2}\big]^T \\ & \times A_{ij}^T P x_i + \alpha_j^2 x_i^T P A_{ij} A_{ij}^T P x_i + |N_j| x_i^T P A_{ij} A_{ij}^T P x_i \\ & + \big(\frac{1-a}{2}\big)^2 ||K_j||^2 x_i^T P A_{ij} B_j B_j^T A_{ij}^T P x_i \\ & + \beta_i^2 ||K_j||^2 x_i^T P A_{ij} A_{ij}^T P x_i + (4\tau_{ij}^2 + ||A_{ij}||^2)||x_j(t)||^2 \\ & + \sum_{k\in N_j}\tau_{ij}^2 ||A_{jk}||^2 ||x_k||^2\Big\} + |N_i| x_i^T P P x_i \\ & + \big[2\alpha_i||P|| + (1-a)||PB_i||||K_i|| + 2\beta_i||P||||K_i||\big]||x_i||^2. \end{aligned}\tag{3.60}$$

Based on equations (3.40)-(3.42), it follows that

$$\begin{aligned}\dot{v}_i \leqslant & \sum_{j\in N_i}\big[(4\tau_{ij}^2 + ||A_{ij}||^2)||x_j||^2 + \sum_{k\in N_j}\tau_{ij}^2||A_{jk}||^2||x_k||^2\big] \\ & + \big[-\gamma + 2\alpha_i||P|| + (1-a)||PB_i||||K_i|| + 2\beta_i||P||||K_i||\big]||x_i||^2. \end{aligned}\tag{3.61}$$

(C2) implies

$$\dot{v}_i \leqslant -w||x_i||^2, \tag{3.62}$$

where

$$\begin{aligned} w \triangleq & \gamma - 2\alpha_i||P|| - (1-a)||PB_i||||K_i|| - 2\beta_i||P||||K_i|| \\ & - \sum_{j\in N_i}\big[(4\tau_{ij}^2 + ||A_{ij}||^2)p_j + \sum_{k\in N_j}\tau_{ij}^2 p_j ||A_{jk}||^2 p_k\big]. \end{aligned}\tag{3.63}$$

Accordingly, in light of Razumikhin Theorem [47], if (3.43) holds, then the global asymp-

totical stability of this class of large-scale dynamical systems S can be immediately follows from defining Lyapunov function $V(x,t) \triangleq \sum_{i=1}^{N} v_i$. This completes the proof. □

Feedback linearization techniques generally require accurate plant models to achieve exact linearization. However, there inevitably exist uncertainties in the constructed models of physical systems. Furthermore, in practice it is almost impossible to have noise and latency free data channels. To this end, as a further development of the previous chapter, a methodology for a class of nonholonomic nonlinear systems subject to dynamics modeling uncertainties and control input time-delays is presented. A robust compensation tracking controller is then developed and justified based on Lyapunov stability theorem. The compensated system effectively suppresses the perturbation effects to guarantee robust stability with tracking errors exponentially converging to a bounded residual set. The problem of robust stabilization of large-scale networked multi-robot systems subject to multiple state time-varying delays in the interconnections, saturated actuators and also parameter perturbation uncertainties is also investigated. Decentralized memoryless state feedback control is studied mainly via the Lyapunov-Krasovskii functional concept. By checking the Hamiltonian matrix and solving an algebraic Riccati equation, the control gain matrix can be obtained to achieve global asymptotical stability of this class of large-scale interconnected dynamical systems.

CHAPTER IV

FINITE-TIME SETTLING REAL-TIME FORMATION CONTROL OF MULTI-ROBOT SYSTEMS

Considered is the problem of formation keeping and reconfiguration under individual agent constraints and formation requirements. A motion planning algorithm which takes into account all constraints in real time computes appropriate reference trajectories to be followed by each agent over a small time interval. Piecing together such reference trajectory segments defines the trajectories over the entire time horizon. The accuracy of the reference trajectories computed in this manner depends on the requirement that the state of the system is accurately known at the beginning of each time step. Consequently, if such reference trajectory computations are to be utilized in real-time tracking then it is imperative that the tracking errors be zero at the end of the computation time segment. Since such computation time intervals are small the system controls should be such that the tracking errors are driven to zero within that short time interval. This necessarily calls for a very short settling time. This in turn calls for finite-time settling controllers which necessarily means that the control strategies must have nonlinear features. This requirement is fairly obvious because it is well-known that systems under linear control converge asymptotically*, that is, the closer to the target, the slower the convergence, and reach equilibria in infinite time. Thus when high precision (namely, system performance at equilibria) and stringent settling time are required, controllers enabling asymptotic stability may not perform adequately. Some nonlinear controls, *e.g.*, sliding mode control as the main mode of variable structure control resorting to discontinuous control laws have the ability to drive systems to steady state in finite time [48]. But one of the weaknesses of sliding mode control is the chatter-

*This also applies even for some nonlinear controls, *e.g.*, the tracking controller designed in Chapter II.

ing that occurs with the control input switching at high frequency when imperfections are present, and in certain applications this can be very detrimental [49]. Researchers in the control community have already realized these issues and have studied finite-time control, *e.g.*, [24, 50]. Very recently Nersesov, Haddad and Hui provided a general framework for finite-time stability analysis based on vector Lyapunov functions [51].

In Chapter II the tracking control design did not take the ever present model uncertainties into consideration. Thus, as alluded to above this chapter focuses on the problem of real-time formation tracking controls in a receding horizon setting for multiple robots under uncertainties and entails the study of designing robust control laws such that, over each time interval tracking errors are driven down to zero adequately fast in the presence of uncertainties. The key idea here is that if at the beginning of each time step the reference and actual trajectories are aligned, at the end of the time step they are again aligned. Even if they diverge in between, convergence to a desired formation can be anticipated. Consequently, we strive to make the settling time of the controlled system finite and not longer than the predefined reference trajectory segment computing time interval, while making tracking errors go to zero by the end of the segment. This way the next segment of the reference trajectory can be properly initialized to go into the trajectory computation algorithm. As a result, the desired motion evolution of multi-robot systems can still be ensured in spite of the ever present system uncertainties.

A. Preliminaries

In this section, inspired by work [52] finite-time settling control strategies are introduced to achieve zero formation tracking errors over each time interval for multi-robot systems under uncertainties by employing effective control laws with fractional powers as discussed below.

Consider the class of nonlinear systems,

$$\dot{x} = -\alpha sgn(x)|x|^{\frac{p}{q}}, x \in \mathbb{R}, \tag{4.1}$$

where $\alpha > 0$, $sgn(.)$ denotes signum function, and $p,\ q$ are rational numbers of the form

$$\frac{2m+1}{2n+1},\ \ m < n \text{ and } m, n \in \mathbb{Z}^+ \cup \{0\}. \tag{4.2}$$

It is apparent that, if $x(t_0) > 0$, $x(t)$ monotonically decreases until it becomes zero when time t reaches a certain value and remains zero value thereafter. On the other hand, if $x(t_0) < 0$, $x(t)$ monotonically increases until it settles at zero equilibrium after the same finite time. Obviously this is better than asymptotic behavior, which would never die out until infinite time. So we say that system (4.1) is finite-time stable, which is defined as follows [24, 53].

Definition 1. *Consider the system*

$$\dot{x} = f(x),\ \ \textit{with } f(0) = 0,\ \ x \in \mathbb{R}^n, \tag{4.3}$$

where $f : \mathcal{D} \to \mathbb{R}^n$ is continuous with respect to x in an open neighborhood $\mathcal{D} \subseteq \mathbb{R}^n$ of origin. $x(x_0, t)$ is a solution of system (4.3) with initial condition $x_0 \in \mathbb{R}$ at $t = t_0$. It is said that system (4.3) is finite-time stable if there exists a nonempty neighborhood of origin $\mathcal{N} \subseteq \mathcal{D}$ in $\mathbb{R}^n$ such that:

(i) there exists a function $T(x) : \mathcal{N}\backslash\{0\} \to \mathbb{R} \geqslant 0$ such that if $x_0 \in \mathcal{N}\backslash\{0\}$ then $x(x_0, t)$ is defined (and particularly unique) on $[t_0\ T(x_0)]$. Moreover, $x(x_0, t) \in \mathcal{N}\backslash\{0\}$ for all $t \in [t_0\ T(x_0)]$, $\lim_{t\to T(x_0)} x(x_0, t) = 0$, and $x(x_0, t) = 0$ for all $t \geqslant T(x_0)$. Thus T is called the settling-time function of system (4.3);

(ii) denote $\mathcal{B}^n$ as the open unit ball in $\mathbb{R}^n$, $\forall\ \epsilon > 0$, there exists $\delta(\epsilon) > 0$, for every $x_0 \in [\delta(\epsilon)\mathcal{B}^n\backslash\{0\}] \cap \mathcal{D}$, $x(x_0, t) \in \epsilon\mathcal{B}^n$ for all $t \in [t_0\ T(x_0)]$. In addition, the

system is said to be globally finite-time stable at origin if it is finite-time stable with $\mathcal{N} = \mathcal{D} = \mathbb{R}^n$.

Actually given every initial condition $\mathbb{R}\backslash\{0\}$, as shown in [50] nonlinear systems (4.1) has a unique solution and can be analytically solved as:

$$x(t) = \begin{cases} sgn(x(t_0))[x(t_0)^{\frac{q-p}{q}} - \alpha(1-\frac{p}{q})(t-t_0)]^{\frac{q}{q-p}} & \text{if } t_0 \leqslant t \leqslant t_0 + \frac{qx(t_0)^{\frac{q-p}{q}}}{\alpha(q-p)}, \\ 0 & \text{if } t > t_0 + \frac{qx(t_0)^{\frac{q-p}{q}}}{\alpha(q-p)}. \end{cases} \tag{4.4}$$

It is clear that according to the above definition system (4.1) is globally finite-time stable at the origin and the settling-time function is determined by

$$T(x) = t_0 + \frac{qx(t_0)^{\frac{q-p}{q}}}{\alpha(q-p)}. \tag{4.5}$$

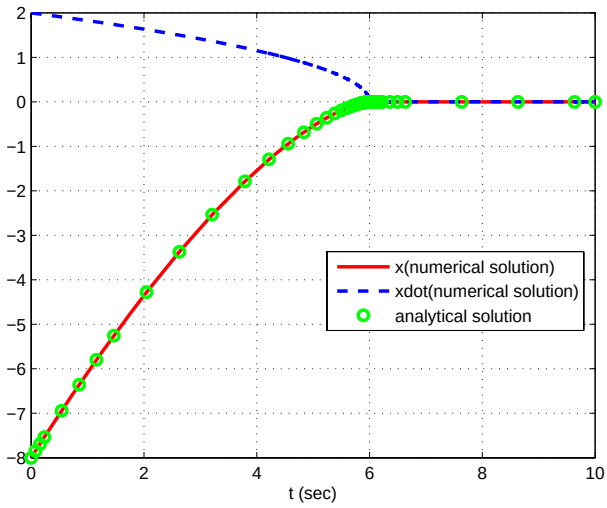

Fig. 20. Simulation of $\dot{x} = -sgn(x)|x|^{\frac{1}{3}}$ with initial condition $x(0) = -8$

Figure 20 shows a typical example of this class of nonlinear system and further verifies

this observation. One can see that the system is "locked" to zero at $T = 6$ sec and thereafter.

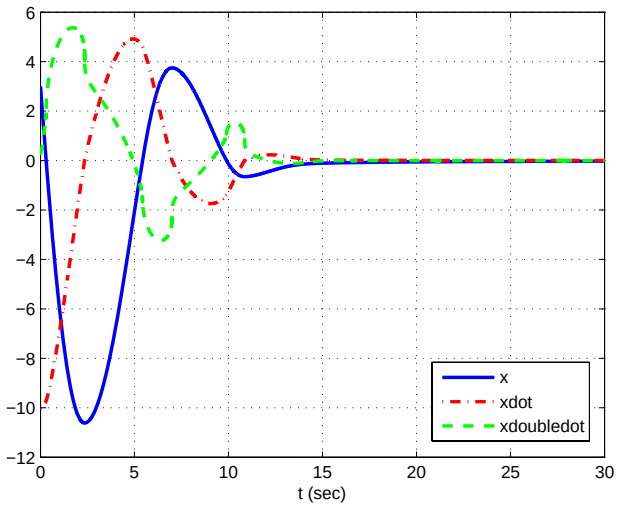

Fig. 21. Simulation of $\ddot{x} = -\dot{x}^{\frac{1}{3}} - x^{\frac{3}{5}}$ with initial conditions $x(0) = 3$ and $\dot{x}(0) = -10$

For a second order system, for example,

$$\ddot{x} = -\dot{x}^{\frac{1}{3}} - x^{\frac{3}{5}}, \tag{4.6}$$

indeed as shown in Fig. 21 it also settles down in finite time.

Furthermore, according to Theorem 4.2 of [24], it can also be asserted that this one dimensional system is finite-time stable through using Lyapunov function $V(x) = \frac{x^2}{2}$. Indeed, we have for all $x \in \mathbb{R}$,

$$\dot{V}(x) = x\dot{x} = -\alpha sgn(x)x|x|^{\frac{p}{q}} = -\alpha|x|^{\frac{q+p}{q}} = -\alpha 2^{\frac{q+p}{2q}} V(x)^{\frac{q+p}{2q}}, \text{ with } \frac{q+p}{2q} \in [0\ 1].$$

It should be noted that there is a close relationship between finite-time settling system (4.1) and time optimal control. As in [54] it is well established that the time optimal control

for the double integrator system

$$\dot{x}_1 = x_2, \;\; \dot{x}_2 = u, \;\; |u| \leqslant 1$$

can be designed as

$$u = sgn(\Xi(x))$$

where $x \triangleq [x_1 \; x_2]^T$ and

$$\Xi(x) = \begin{cases} \zeta(x) = x_1 + \frac{1}{2} x_2 |x_2| & \text{if } \zeta(x) \neq 0, \\ x_2 & \text{otherwise}, \end{cases}$$

where function $\zeta(x) = 0$ describes the arc on which the system trajectory will reach zero. If odd numbers p and q in (4.1) are very large such that $\frac{p}{q} \approx \frac{1}{2}$ and $\beta = 2^{\frac{p}{q}}$, replacing x with x_1 yields

$$\dot{x}_1 + 2^{\frac{p}{q}} {x_1}^{\frac{p}{q}} = 0,$$

which is equivalent to

$$x_2 + 2^{\frac{p}{q}} {x_1}^{\frac{p}{q}} = 0 \Rightarrow x_1 + \frac{1}{2} {x_2}^{\frac{q}{p}} \approx x_1 + \frac{1}{2} x_2 |x_2| = \zeta(x) = 0.$$

Hence, the finite-time settling system (4.1) can be used to approximate the time optimal arc for the double integrator system with any accuracy regardless of the sign of x_2.

Note that for p and q satisfying (4.2) and $x < 0$, $sgn(x)|x|^{\frac{p}{q}}$ is different from $x^{\frac{p}{q}}$. This is because the fractional power $\frac{p}{q}$ may lead to the term $x^{\frac{p}{q}} \notin \mathbb{R}$, which results in $\dot{x} \notin \mathbb{R}$. However, $sgn(x)|x|^{\frac{p}{q}}$ does not have this issue.

Consider the Jacobian of system (4.1) around the equilibrium $x = 0$, *i.e.*,

$$J = \frac{\partial \dot{x}}{\partial x} = -\frac{\alpha p}{q} \frac{1}{|x|^{\frac{q-p}{q}}} \rightarrow -\infty, \text{when } x \rightarrow 0,$$

which indicates that with such an infinitely large negative "slope" at origin the system tra-

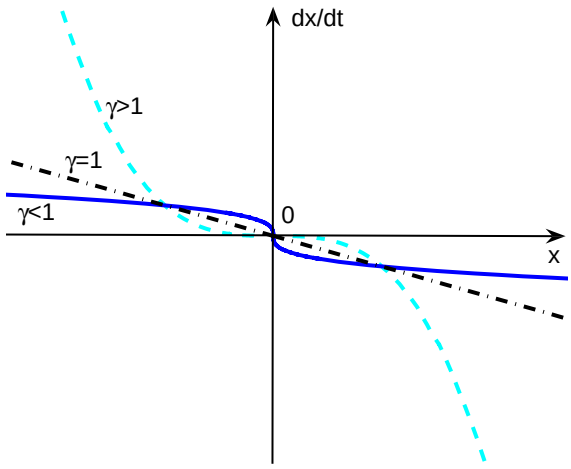

Fig. 22. Phase flows in the neighborhood of equilibrium for $\dot{x} = -\alpha sgn(x)|x|^{\gamma}$

jectory will converge to the equilibrium with an infinitely large speed. Namely, the closer to the equilibrium, the faster the convergence rate. The introduction of the nonlinear term $sgn(x)|x|^{\frac{p}{q}}$ improves the convergence toward the equilibrium and leads to finite-time convergence. As illustrated in Fig. 22 it can be observed that when x is at a threshold distance away from the equilibrium, system (4.1) does not prevail over its linear counterpart (setting $p = q$), since the term $sgn(x)|x|^{\frac{p}{q}}$ tends to reduce the magnitude of convergence rate before reaching the threshold distance from origin. One immediate solution is to introduce

$$\dot{x} = -\alpha x - \beta sgn(x)|x|^{\frac{p}{q}}, \;\; \alpha, \; \beta > 0. \tag{4.7}$$

When x is far away from the equilibrium zero, system (4.7) can be approximated with $\dot{x} = -\alpha x$, whose exponential convergence when far away from zero is well understood. When close to the origin, the dominant dynamics turns into $\dot{x} = -\beta sgn(x)|x|^{\frac{p}{q}}$, which has finite-time settling robustness as discussed above.

More precisely, one can solve (4.7) analytically. The exact time to reach origin, T, is determined by

$$T(x) = t_0 + \frac{q}{\alpha(q-p)} \ln \frac{\alpha x(t_0)^{\frac{q-p}{q}} + \beta}{\beta}. \tag{4.8}$$

Hence, the appealing finite-time convergence characteristic features of this class of nonlinear systems (4.7) are incorporated into the formation control design under uncertainties to enable reference tracking with the requirement that tracking errors be zero by the end of each time horizon over which a segment of reference trajectory is generated.

Based on the analysis in [55], the following lemma is used for the subsequent exponential finite-time stability analysis.

Lemma A.1. *Suppose there exists a continuous function $W(x(t), t)$ on an open connected set, namely, $W(x(t), t) : \mathcal{D} \in \mathbb{R}^2 \to Y \in \mathbb{R}$. Assume that given an initial value $x(t_0) = x_0$, the scalar equation*

$$\dot{x}(t) = W(x(t), t)$$

has a unique solution $x(x_0, t)$ on $t \in [t_0,\ t_1)$. Continuous function $V(t)$ is a solution to the according differential inequality

$$\dot{V}(t) = W(V(t), t), \quad V(t_0) = V_0$$

for $t \in [t_0\ t_1)$. If $V_0 \leqslant x_0$, then $V(t) \leqslant x(t)$ for all $t \in [t_0\ t_1)$.

It is well-known that the classical Lyapunov stability theory is only applicable to a system whose solution from any initial condition is unique. A sufficient condition for the existence of a unique solution to the nonlinear differential equation $\dot{x} = f(x)$ is that the function $f(x)$ is locally *Lipschitz* continuous. Such a nonlinear system can at best have asymptotic convergence behavior. Based on the above discussion, we present the following theorem that states the sufficient conditions for exponential finite-time stability.

Theorem A.2. *Suppose there exist $\mathcal{C}^1$ positive definite Lyapunov function $V : \mathcal{D} \to \mathbb{R} \geqslant 0$, real constants $\alpha,\ \beta > 0$ and $\gamma \in [0\ 1]$, and an open neighborhood $\mathcal{V} \subseteq \mathcal{D}$ of origin, such that for all $t \geqslant t_0$*

$$\dot{V}(x(t)) \leqslant -\alpha V(x(t)) - \beta V^{\gamma}(x(t)),\ \ x(t) \in \mathcal{V}\backslash\{0\}. \tag{4.9}$$

Then it is said that system (4.3) is exponentially finite-time stable at origin. If $\mathcal{N}$ is defined as in Definition 1 and T is the settling-time function, then

$$T(x) = t_0 + \frac{1}{\alpha(1-\gamma)} \ln \frac{\alpha V(x(t_0))^{1-\gamma} + \beta}{\beta},\ \ x(t) \in \mathcal{N}\backslash\{0\}. \tag{4.10}$$

Proof. Consider the following ordinary differential equation with $\alpha, \beta > 0$ and γ satisfying (4.2)

$$\dot{x}(t) = -\alpha x(t) - \beta x^{\gamma}(t),\ \ x(t_0) \triangleq V(t_0).$$

Although it does not satisfy the global *Lipschitz* condition, the unique solution to this equation can be found as shown in the following.

$$x(t) = \begin{cases} sgn(x(t_0))\big\{\frac{1}{\alpha}[(\alpha x(t_0)^{1-\gamma} \\ \quad +\beta)e^{-\alpha(1-\gamma)(t-t_0)} - \beta]\big\}^{\frac{1}{1-\gamma}} & \text{if } t_0 \leqslant t \leqslant t_0 + \frac{1}{\alpha(1-\gamma)} \ln \frac{\alpha x(t_0)^{1-\gamma}+\beta}{\beta}, \\ 0 & \text{if } t > t_0 + \frac{1}{\alpha(1-\gamma)} \ln \frac{\alpha x(t_0)^{1-\gamma}+\beta}{\beta}. \end{cases}$$

According to Lemma A.1 and with (4.9), one obtains $V(t) \leqslant x(t)$. Because as given above $x(t)$ exponentially converges to zero in finite time

$$T = t_0 + \frac{1}{\alpha(1-\gamma)} \ln \frac{\alpha x(t_0)^{1-\gamma} + \beta}{\beta},$$

positive definite $V(t)$ will also exponentially reach origin no later than T. □

Clearly the reaching time T depends on parameters α, β and initial value $x(t_0)$. Given $x(t_0) \neq 0$, one can tune α and β such that T is as small as needed and systems settle down

adequately fast. It is finite-time stable, thus robust.

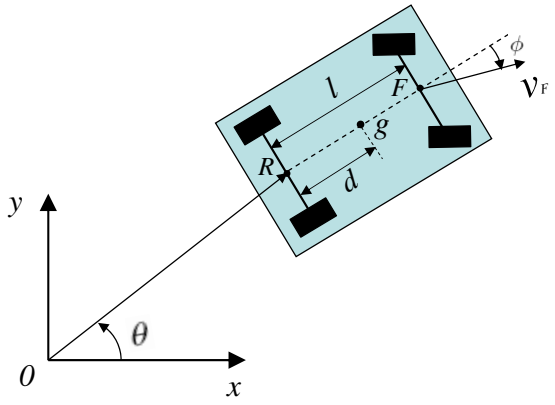

Fig. 23. Sketch of car-like robot platform

B. Finite-time Formation Control

In this section, to design formation tracking controls for multi-robot systems subject to uncertainties, the development in Section A is applied to identify a control law that is exponentially finite-time stable and is suitable for practical implementation.

1. Kinematic Control

Figure 23 is a schematic of a front-wheel drive car-like robot. The kinematic behavior of point R, the center of rear axis, can be described through the well-known unicycle model:

$$\dot{x}_R = v_R cos\theta, \tag{4.11}$$

$$\dot{y}_R = v_R sin\theta, \tag{4.12}$$

$$\dot{\theta} = \omega. \tag{4.13}$$

For the kinematic control design of (v_R, ω), the following nonholonomic system, also called nonholonomic integrator, is first investigated. Namely,

$$\dot{x}_1 = u_1, \tag{4.14}$$

$$\dot{x}_2 = u_2, \tag{4.15}$$

$$\dot{x}_3 = x_1 u_2 - x_2 u_1, \tag{4.16}$$

where states x_1, x_2 and $x_3 \in \mathbb{R}$, and $u_1,\ u_2$ are control inputs. The following stabilization control law is postulated for the above system:

$$u_1 = x_2(\alpha x_3 + \beta sgn(x_3)|x_3|^{\frac{p}{q}}) - \kappa x_1, \tag{4.17}$$

$$u_2 = -x_1(\alpha x_3 + \beta sgn(x_3)|x_3|^{\frac{p}{q}}) - \kappa x_2, \tag{4.18}$$

where α, β and $\kappa \in \mathbb{R}^+$, and p, q are defined as in (4.2).

Proof. Define the following Lyapunov function:

$$V(t) = \frac{1}{2}(x_1^2 + x_2^2).$$

Differentiating it along the trajectories of system (4.14)-(4.16) and substituting u_1 and u_2 with (4.17)-(4.18) yield

$$\begin{aligned}
\dot{V}(t) =& x_1\dot{x}_1 + x_2\dot{x}_2 \\
=& x_1 x_2(\alpha x_3 + \beta sgn(x_3)|x_3|^{\frac{p}{q}}) - \kappa x_1^2 \\
& - x_1 x_2(\alpha x_3 + \beta sgn(x_3)|x_3|^{\frac{p}{q}}) - \kappa x_2^2 \\
=& -\kappa(x_1^2 + x_2^2) < 0.
\end{aligned}$$

Therefore, control law (4.17)-(4.18) stabilizes states x_1 and x_2.

For state x_3, combining (4.16) with (4.17)-(4.18) yields the nonlinear system discussed

above:

$$\begin{aligned}\dot{x}_3 =& x_1u_2 - x_2u_1 \\ =& -x_1^2(\alpha x_3 + \beta sgn(x_3)|x_3|^{\frac{p}{q}}) - \kappa x_1x_2 \\ & -[x_2^2(\alpha x_3 + \beta sgn(x_3)|x_3|^{\frac{p}{q}}) - \kappa x_1x_2] \\ =& -(x_1^2 + x_2^2)(\alpha x_3 + \beta sgn(x_3)|x_3|^{\frac{p}{q}}) \\ =& -2V(\alpha x_3 + \beta sgn(x_3)|x_3|^{\frac{p}{q}}).\end{aligned}$$

Here it is necessary to point out that control parameters α and β need to be tuned large enough to regulate variable x_3 to the origin in finite time before x_1 and x_2 are stabilized, otherwise it will converge to a nonzero constant. Namely, x_3 must converge faster than x_1 and x_2. This completes the proof. □

We know that the problem of trajectory tracking, $x_1 \to x_1^r$, $x_2 \to x_2^r$ and $x_3 \to x_3^r$, is equivalent to stabilizing $\bar{x}_1 \triangleq x_1 - x_1^r$, $\bar{x}_2 \triangleq x_2 - x_2^r$ and $\bar{x}_3 \triangleq x_3 - x_3^r$. Through this new state transformation, one obtains

$$\dot{\bar{x}}_1 = \bar{u}_1, \tag{4.19}$$

$$\dot{\bar{x}}_2 = \bar{u}_2, \tag{4.20}$$

$$\dot{\bar{x}}_3 = \bar{x}_1\bar{u}_2 - \bar{x}_2\bar{u}_1 + \bar{h}, \tag{4.21}$$

where $\bar{h} \triangleq h - \dot{x}_3^r$, and $h \triangleq -x_2^r\dot{x}_1 - (x_2 - x_2^r)\dot{x}_1^r + x_1^r\dot{x}_2 + (x_1 - x_1^r)\dot{x}_2^r$. Likewise, the stabilization control law for the above new system is written as

$$\bar{u}_1 = \bar{x}_2(\alpha\bar{x}_3 + \beta sgn(\bar{x}_3)|\bar{x}_3|^{\frac{p}{q}}) - \kappa\bar{x}_1, \tag{4.22}$$

$$\bar{u}_2 = -\bar{x}_1(\alpha\bar{x}_3 + \beta sgn(\bar{x}_3)|\bar{x}_3|^{\frac{p}{q}}) - \kappa\bar{x}_2, \tag{4.23}$$

where

$$\kappa = \begin{cases} \bar{\kappa} & \text{if } \frac{1}{2}(\bar{x}_1^2 + \bar{x}_2^2) > \epsilon^2, \\ 0 & \text{otherwise}, \end{cases} \tag{4.24}$$

$\bar{\kappa} \in \mathbb{R}^+$, and ϵ can be chosen arbitrarily small and it denotes the neighborhood of desired reference trajectories, *i.e.*,

$$||(x_1^r, x_2^r, x_3^r) - (x_1, x_2, x_3)|| = ||(\bar{x}_1, \bar{x}_2, \bar{x}_3)|| \leqslant \epsilon. \tag{4.25}$$

Then tracking control law for the original nonholonomic system (4.14)-(4.16) is obtained as

$$u_1 = \bar{u}_1 + \dot{x}_1^r, \tag{4.26}$$

$$u_2 = \bar{u}_2 + \dot{x}_2^r. \tag{4.27}$$

Proof. Similarly introduce Lyapunov function $V(t) = \frac{1}{2}(\bar{x}_1^2 + \bar{x}_2^2)$. Then take its derivative along the trajectories of system (4.19)-(4.21) and also with the aid of (4.22) and (4.23), $\dot{V}(t) = -\kappa(\bar{x}_1^2 + \bar{x}_2^2) = -2\kappa V(t)$. Its solution can be solved as

$$V(t) = V(0)e^{-2\kappa t} = \frac{1}{2}(\bar{x}_1^2(0) + \bar{x}_2^2(0))e^{-2\kappa t}. \tag{4.28}$$

Hence, if $\frac{1}{2}(\bar{x}_1^2 + \bar{x}_2^2) = V > \epsilon^2$, then because $\kappa = \bar{\kappa} > 0$, V will decrease until it reaches the ϵ-neighborhood of the origin in $\bar{x}_1, \bar{x}_2$ subspace and the trajectories are confined to this manifold. At this time, as for $\bar{x}_3$, $\dot{\bar{x}}_3 = -2\epsilon^2(\alpha\bar{x}_3 + \beta sgn(\bar{x}_3)|\bar{x}_3|^{\frac{p}{q}}) + \bar{h}$, where α and β are chosen to be large enough such that $\bar{x}_3$ is stabilized no later than

$$T = t_0 + \frac{q}{2\alpha\epsilon^2(q-p)} \ln \frac{\alpha\bar{x}_3(t_0)^{\frac{q-p}{q}} + \beta}{\beta}. \tag{4.29}$$

At this moment and hereafter, $||(\bar{x}_1, \bar{x}_2, \bar{x}_3)|| = ||(\bar{x}_1, \bar{x}_2)||$. Accordingly (4.25) becomes $||(\bar{x}_1, \bar{x}_2, \bar{x}_3)|| = \frac{1}{2}(\bar{x}_1^2 + \bar{x}_2^2) = V \leqslant \epsilon^2$. Then combine with (4.28) and replace t with T

from (4.29),

$$\frac{1}{2}(\bar{x}_1^2(0)+\bar{x}_2^2(0))e^{-2\kappa\{t_0+\frac{q}{2\alpha\epsilon^2(q-p)}\ln\frac{\alpha x_3(t_0)^{\frac{q-p}{q}}+\beta}{\beta}\}}\leqslant\epsilon. \tag{4.30}$$

Namely, to regulate $|(\bar{x}_1,\bar{x}_2,\bar{x}_3)$ into an ϵ-neighborhood of the origin of its according subspace in finite time T, the weighting gains need to further satisfy

$$\big(\frac{\alpha}{\beta}\bar{x}_3(t_0)^{\frac{q-p}{q}}+1\big)^{\frac{q}{2\alpha\epsilon^2(q-p)}}\geqslant\frac{1}{e^{t_0}}\big(\frac{\bar{x}_1^2(0)+\bar{x}_2^2(0)}{2\epsilon}\big)^{\frac{1}{2\kappa}}. \tag{4.31}$$

□

Then, to bring forth kinematic tracking control possessing finite-time settling robustness over each time step, define the state variables and controls of system (4.11)-(4.13) as:

$$x_R\triangleq\frac{1}{2}(2x_1cosx_2+(x_1x_2+x_3)sinx_2), \tag{4.32}$$

$$y_R\triangleq\frac{1}{2}(2x_1sinx_2-(x_1x_2+x_3)cosx_2), \tag{4.33}$$

$$\theta\triangleq x_2, \tag{4.34}$$

and

$$v_R\triangleq u_1+\frac{u_2}{2}(x_1x_2+x_3), \tag{4.35}$$

$$\omega\triangleq u_2, \tag{4.36}$$

then the unicycle model (4.11)-(4.13) can be transformed to the nonholonomic integrator system (4.14)-(4.16).

Substitute (4.26)-(4.27), (4.22)-(4.23) and (4.24) into (4.35)-(4.36), we got the ulti-

mate finite-time tracking control law for the unicycle model:

$$\begin{aligned}\omega =& -(x_1 - x_1^r)[\alpha(x_3 - x_3^r) + \beta sgn(x_3 - x_3^r)|x_3 - x_3^r|^{\frac{p}{q}}] \\ & - \kappa(x_2 - x_2^r) + \dot{x}_2^r, \end{aligned} \tag{4.37}$$

$$\begin{aligned}v_R =& (x_2 - x_2^r)[\alpha(x_3 - x_3^r) + \beta sgn(x_3 - x_3^r)|x_3 - x_3^r|^{\frac{p}{q}}] \\ & - \kappa(x_1 - x_1^r) + \dot{x}_1^r + \frac{\omega}{2}(x_1 x_2 + x_3), \end{aligned} \tag{4.38}$$

where $x_1(x_1^r)$, $x_2(x_2^r)$ and $x_3(x_3^r)$ can be solved through (4.32)-(4.34),

$$x_1 = x_R cos\theta + y_R sin\theta, \tag{4.39}$$

$$x_2 = \theta, \tag{4.40}$$

$$x_3 = x_R(2sin\theta - \theta cos\theta) - y_R(2cos\theta + \theta sin\theta), \tag{4.41}$$

and

$$x_1^r = x_R^r cos\theta^r + y_R^r sin\theta^r, \tag{4.42}$$

$$x_2^r = \theta^r, \tag{4.43}$$

$$x_3^r = x_R^r(2sin\theta^r - \theta^r cos\theta^r) - y_R^r(2cos\theta^r + \theta^r sin\theta^r). \tag{4.44}$$

For continuously differentiable reference trajectories, the continuity of the resulting finite-time kinematic control allows the extension of the robot control at the dynamic level by having the dynamic subsystem outputs track the desired kinematic control inputs of the kinematic subsystem. Accordingly the overall control structure for the car-like robotic systems can be described as in Fig. 24. Thus the finite-time settling robustness at both the kinematic and dynamic levels ensures zero tracking errors by the end of reference trajectory segment computing time interval. The dynamic subsystem and its finite-time dynamic control design in this control structure are summarized as follows.

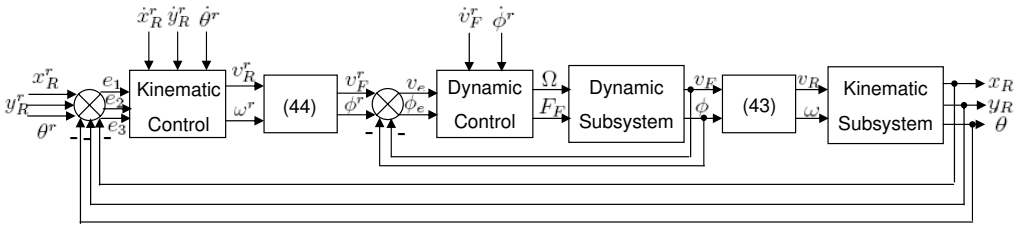

Fig. 24. Control structure for car-like robot platform

2. Dynamic Control

Assuming no lateral skid and no longitudinal slip, using *Lagrangian Principle*, the dynamics of steering at point F, the center of front axis, can be derived as [56]

$$\dot{v}_F = \frac{F_F - sin2\phi(M^* - \frac{I^*}{l^{*2}})v_F\Omega}{M^*cos^2\phi + \frac{I^*}{l^{*2}}sin^2\phi} + w, \quad \dot{\phi} = \Omega, \tag{4.45}$$

where v_F is the velocity at point F, F_F is the component of driving force along the direction of v_F, ϕ is steering angle, M is robot mass, and I is moment of inertial of the robot around the vertical axis passing through R. $(.)^*$ represent unknown constant parameters with w denoting noise signal.

To ultimately achieve zero errors in formation tracking, propose the following control design for the above dynamic subsystem: Control law

$$\begin{aligned} F_F =&(Mcos^2\phi + \frac{I}{l^2}sin^2\phi)(-\mu v_e - \nu sgn(v_e)|v_e|^\gamma + \dot{v}_F^r) \\ &+ sin2\phi(M - \frac{I}{l^2})v_F\Omega, \end{aligned} \tag{4.46}$$

$$\Omega = -\mu\phi_e - \nu sgn(\phi_e)|\phi_e|^\gamma + \dot{\phi}^r, \tag{4.47}$$

where $\mu, \nu > 0$ and γ satisfies (4.2), drives dynamic system (4.45) to exponentially con-

verge to origin in finite time.

Proof. Choose $V = \frac{1}{2}\phi_e^2 + \frac{1}{2}v_e^2 = \frac{1}{2}(\phi - \phi^r)^2 + \frac{1}{2}(v - v^r)^2$. Then its derivative along the trajectories of system (4.45) is derived as

$$\dot{V} = v_e \frac{F_F - sin2\phi(M - \frac{I}{l^2})v_F\Omega}{Mcos^2\phi + \frac{I}{l^2}sin^2\phi} + \phi_e\Omega - v_e\dot{v}_F^r - \phi_e\dot{\phi}^r.$$

Substitute the above dynamic control law (4.46)-(4.47)

$$\begin{aligned}\dot{V} &= -\mu\phi_e^2 - \nu sgn(\phi_e)\phi_e|\phi_e|^\gamma - \mu v_e^2 - \nu sgn(v_e)v_e|v_e|^\gamma \\ &= -2\mu V - \nu(|\phi_e|^{1+\gamma} + |v_e|^{1+\gamma}).\end{aligned}$$

Since for $a > 0$, $b > 0$ and $0 < c < 1$, $(a+b)^c \leqslant a^c + b^c$, one obtains

$$\begin{aligned}\dot{V} &\leqslant -2\mu V - \nu(|\phi_e| + |v_e|)^{1+\gamma} \\ &\leqslant -2\mu V - \nu(|\phi_e|^2 + |v_e|^2)^{\frac{1+\gamma}{2}} \\ &= -2\mu V - \nu 2^{\frac{1+\gamma}{2}} V^{\frac{1+\gamma}{2}},\end{aligned}$$

with $\frac{1+\gamma}{2} \in [0\ 1]$. Then according to Theorem A.2, under control law (4.46)-(4.47), system (4.45) exponentially converges to zero no later than

$$T = t_0 + \frac{1}{\mu(1-\gamma)} \ln \frac{\mu[\frac{1}{2}(\phi_e^2(t_0) + v_e^2(t_0))]^{1-\gamma} + \nu}{\nu}. \tag{4.48}$$

This completes the proof. □

The connection between the kinematic subsystem (4.11)-(4.13) and dynamic subsystem (4.45) can be obtained as

$$v_R = v_F cos\phi, \quad \omega = \frac{v_F}{l} sin\phi, \tag{4.49}$$

or

$$\phi = arctan\frac{\omega l}{v_R}, \quad v_F = \frac{v_R}{cos\phi}. \tag{4.50}$$

Accordingly,

$$\dot{v}_F = \frac{\dot{v}_R cos\phi + v_R\dot{\phi}sin\phi}{cos^2\phi}, \quad \dot{\phi} = \frac{(\dot{\omega}v_R - \omega\dot{v}_R)l}{v_R^2 + (\omega l)^2}, \tag{4.51}$$

where $\dot{v}_R$ can be calculated through taking derivative of

$$v_R = \dot{x}_R cos\theta + \dot{y}_R sin\theta. \tag{4.52}$$

Therefore, the control structure that embeds finite-time settling robust controls guarantees that the settling time of the controlled robotic system is finite and not longer than the preassigned reference trajectory segment computing time interval, while making tracking errors go to zero by the end of the segment. Thus convergence to the desired formation can still be accomplished even if in the presence of parametric uncertainties and noise disturbances as verified in the following section.

C. Case Study

As alluded to previously, the proposed finite-time settling control is integrated into an existing motion planning algorithm to further verify its feasibility and effectiveness. In particular, the real-time algorithm proposed and developed by Maithripala and Jayasuriya [3] that explicitly takes dynamic feasibility into account is used to test out these finite-time settling controllers. The approach to this algorithm is to embed both robot nonholonomic constraints and formation constraints into the generation of reference trajectories to be used simultaneously by the decentralized tracking controllers of individual robots. The algorithms computation time step is chosen as $\delta t = 1$ sec. Then, over each time interval each robot needs to converge to the incrementally generated reference trajectories in less than 1 sec to eliminate the accumulating errors.

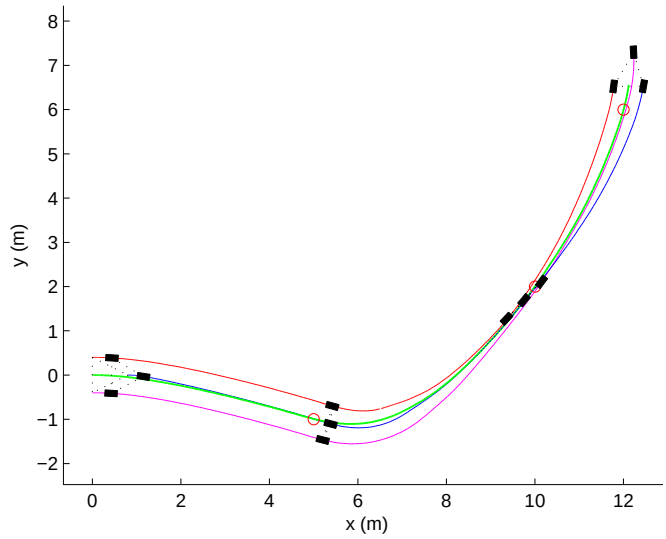

Fig. 25. Formation keeping and formation reconfiguration for three car-like mobile robots

In this case study the above motion planning algorithm generates the following scenario: As illustrated in the form of a series of snapshots of three robots' motion evolution (Fig. 25), a team of three mobile robots are required to move through a given set of waypoints (marked as solid circles) while maintaining and reconfiguring predetermined inter-robot formation patterns. While their center of mass tracks the trajectory generated from the algorithm, they start from a triangular formation, then transition to a column formation, followed by triangle pattern again.

The finite-time settling control structure is implemented in a decentralized manner on each individual robot. In addition to adding random noise, unknown system parameters M^*, I^* and l^* in the dynamic subsystem are bounded by $(.)^* \in [(.)_{min}\ (.)_{max}]$ and $0 < (.)_{min} < (.)_{max} < \infty$, respectively. Figure 26 shows the tracking errors of formation center. By comparing Fig. 26(a) with 26(b), it can be observed that these finite-time settling

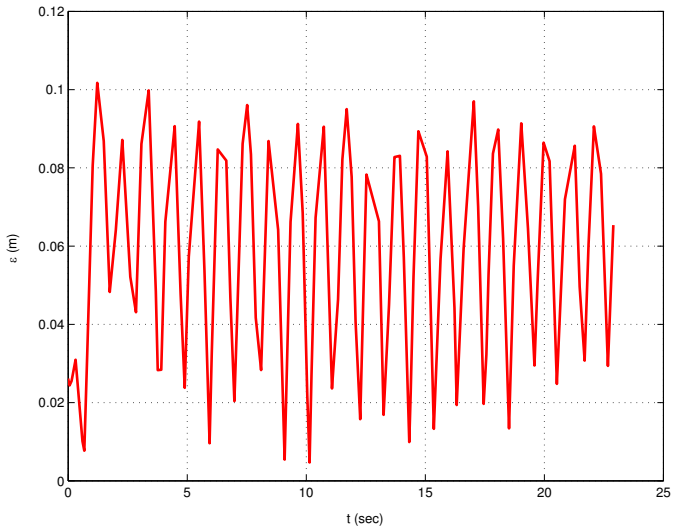

(a)

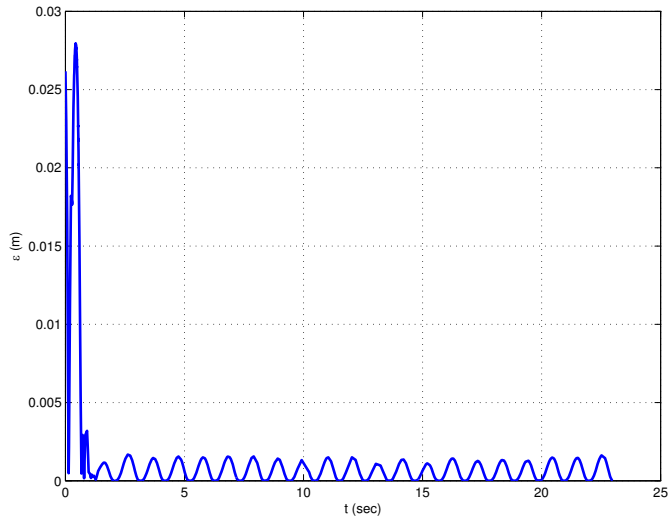

(b)

Fig. 26. A comparison of tracking errors of control design under uncertainties: (a) linear feedback control, and (b) the proposed nonlinear finite-time settling control.

controllers substantially reduce the errors from conventional linear control (setting both β in kinematic control (4.37)-(4.38) and ν in dynamic control (4.46)-(4.47) to zero). Except for the unaligned initial condition for the first time interval, this class of novel finite-time settling controllers effectively suppresses uncertainties and disturbances, keeps ”locking” formation tracking errors to zero, and precisely aligns the reference and actual trajectories by the end of each time step, though at times it diverges from the reference trajectories inside the time step. The minimum, maximum and average time it takes to converge within a time segment are 0.87 sec, 0.96 sec and 0.92 sec, respectively, which are all less than the algorithms preassigned computation time step 1 sec. Thus the ultimate formation control goals can still be guaranteed despite noise disturbances and parametric uncertainties. Moreover it is practically implementable in real time in the sense that simulation time, 14.69 sec, is shorter than the actual time, 23 sec.

CHAPTER V

COMMUNICATION ISSUE IN FORMATION CONTROL OF MULTI-ROBOT SYSTEMS

Inspired from recent development in topology control and through applying graph theory [26, 57, 58], a Local Minimum Spanning Tree (LMST)-based communication algorithm is presented in this chapter to relax the global communication needs in formation control. Namely, no central command is required, and robots individually perceive neighborhood relations. A communication topology is constructed by having each robot independently build its own minimum spanning tree merely based on local information and keep only one-hop on-tree agents as its neighbors. Accordingly, it avoids superfluous information exchange, reduces energy consumption, and improves network efficiency while still preserving network connectivity ensuring convergence into a desired formation.

As an application example, based on graph *Laplacian* and feedback control theory a desired rigid formation acquisition is accomplished by incorporating the developed LMST-based dynamic communication algorithm. Emphasis is placed upon the time-delay influence on the acquired formation in the situation where interconnection time-delays occur in certain information flow channels while robots are communicating with spatially separated neighboring robots. A robust stabilization scheme is presented to improve or even recover from a destroyed formation pattern.

A. LMST-based Dynamic Communication Algorithm

Before discussing this communication algorithm, the following graph theory preliminaries are needed [57, 58].

Definition A.1 (Cycle/Tree)**.** A *cycle* is a close path (that is, a path from vertex v_i to itself),

in which the intermediate edges are all distinct. A connected graph without cycles is defined as a *tree*.

The following two lemmas are fundamental.

Lemma A.1. *Every connected graph contains a spanning tree.*

Lemma A.2. *The number of edges in a tree with n vertices is $n-1$. Conversely, a connected graph with n vertices and $n-1$ edges is a tree.*

Next we define physical neighbors and logical/physical agent degree.

Definition A.2 (Physical Neighbors)**.** For a team of robots $\mathcal{R}$, the physical neighbors for robot R_i are a subset $N_i \subset \mathcal{R}$ defined as $N_i \triangleq \{R_j \in \mathcal{R} | \ ||r_j - r_i|| \leqslant d_i\}$, where $r_{(.)}$ are position vectors for robot $R_{(.)}$ and $d_i > 0$ is the communication range of robot R_i.

Definition A.3 (Logical/Physical Agent Degree)**.** Logical agent degree means the number of logical neighbors, derived from LMST-based topology. However, physical degree of an agent refers to the number of agents within its communication range. A smaller average agent degree usually implies less contention and interference, and better spatial reuse.

Through communication, the robotic team forms an undirected simple graph $G = (V, E)$, where V is the set of robots, and E is the edge set defined by the physical neighbors N_i of each robot R_i, namely, $E = \{(R_i, R_j) | R_j \in N_i\}$. We denote by $G_i = (V_i, E_i)$ the induced subgraph of G such that $V_i = N_i$. A unique *id* is assigned to each robot R_i, for example, $id(R_i) = i$.

The communication algorithm consists of the following two phases: *information collection* and *topology construction*. First, each agent periodically broadcasts a hello message through applying its maximal transmission power to obtain the attention of its physical neighbors N_i. Based on N_i, agent R_i constructs an LMST $T_i = (V(T_i), E(T_i))$ of G_i

which spans all its neighboring agents in N_i. The generation of LMST can be formed by utilizing existing algorithms, such as Prim's algorithm [59]. Here a unique weight function has been defined on the edge of (R_i, R_j) in terms of $||r_i - r_j||$, max$(id(R_i), id(R_j))$ and min$(id(R_i), id(R_j))$ such that the constructed LMST is unique [26]. Then topology derived from LMST has all robots as its agent set V and their individually perceived neighborhood relations. Note that the derived topology is not a simple superposition of all local MSTs.

Definition A.4 (Topology by LMST, G_0)**.** LMST-based topology is a directed graph $G_0 = (V_0, E_0)$, where $V_0 = V$ and $E_0 = \{(R_i, R_j)|R_i \to R_j, \text{where} R_i, R_j \in V(G)\}$.

With generated LMST, a logical neighboring relationship and logical neighbor set can be defined as follows.

Definition A.5 (Logical Neighbors)**.** Robot R_j is a logical neighbor of robot R_i, denoted as $R_i \to R_j$, if and only if $(R_i, R_j) \in E(T_i)$. $R_i \leftrightarrow R_j$ if and only if $R_i \to R_j$ and $R_j \to R_i$. The logical neighbor set LN_i of robot R_i is defined as $LN_i = \{R_j \in V(G_i)|R_i \to R_j\}$.

Connectivity can then be formally defined as follows.

Definition A.6 (Network Connectivity)**.** For any two agents $R_i, R_j \in V(G_0)$, agent R_i is said to be *connected* to agent R_j, denoted as $R_i \Leftrightarrow R_j$, if there exist agents $A_k \in V(G_0)$ where $k = 0, 1, \cdots, m$ forming a path $A_0 = R_i, A_1, \cdots, A_{m-1}, A_m = R_j$ such that $A_j \leftrightarrow A_{j+1}$ where $j = 0, 1, \cdots, m-1$.

The above topology may be further simplified as follows.

Definition A.7 (Topology by LMST with Link Removal, G_0^-)**.** The topology, G_0^-, is a undirected graph $G_0^- = (V_0^-, E_0^-)$, where $V_0^- = V_0$ and $E_0^- = \{(R_i, R_j)|(R_i, R_j) \in E(G_0)$ and $(R_j, R_i) \in E(G_0)\}$.

The main reason for employing LMST-generated topology as the communication algorithm among multi-robot systems is because it possesses the following favorable properties [26].

Proposition 1. *The network topology G_0 under LMST preserves the connectivity of G, i.e., G_0 is connected as long as G is connected.*

Proposition 2. *The degree of any agent in G_0 is bounded by 6, i.e., deg$(R_i) \leqslant 6, \forall R_i \in V(G_0)$.*

Proposition 1 implies that the connectivity of the mobile robotic network is always guaranteed by the LMST topology G_0. This property is extremely important, if not imperative, as explicitly pointed out in [60]: "Shared information is a necessary condition for coordination". It is known that connectivity of the associated information graphs among networked robots is one of the fundamental requirements to ensure convergence of formation control [61].

Proposition 2 says no robot has more than 6 logical neighbors. Compared with utilizing maximum transmission power, this would eliminate a significant number of those redundant topology links and results in more cost-effective and efficient communication.

As a demonstration of the proposed LMST-based communication algorithm, the following scenario is considered here: 100 agents are randomly deployed in a $1000 \times 1000m^2$ region with communication range $d_i = 250m$. Intuitively from Fig. 27 it is observed that the algorithm largely simplifies the much denser topology derived from using maximum transmission power. Furthermore, no agent is isolated or disconnected from the network and connectivity is preserved as well. In addition, Compared with the average logical agent degree of one-to-all communication among neighbor set N_i, 15.06, LMST achieves the much smaller value, 2.08. This is very close to the theoretical bound: It is known that among all the spanning graphs, global spanning tree has the least average logical agent

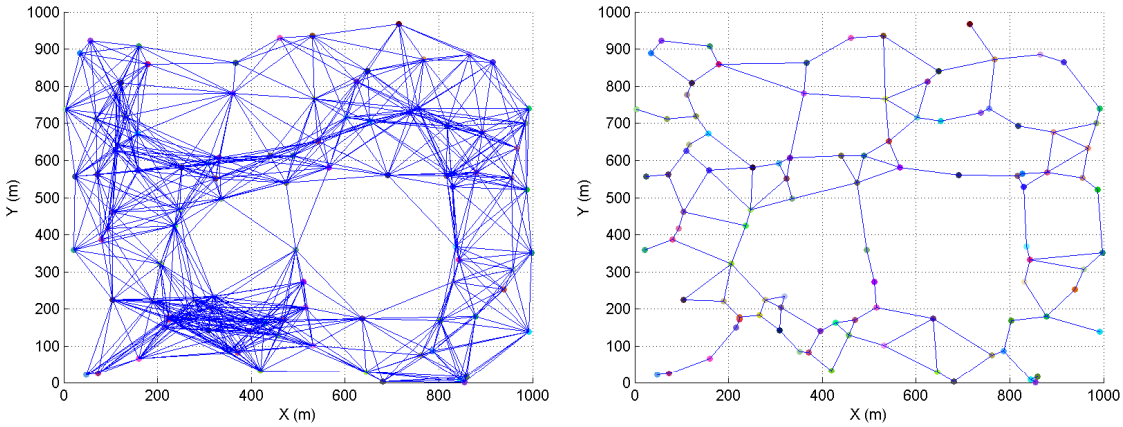

(a) (b)

Fig. 27. Communication topology: (a) by maximal transmission power, and (b) by LMST.

degree: $2-(\frac{2}{n}) \rightarrow 2$, as $n \rightarrow \infty$ [62]. Therefore, the LMST-constructed communication algorithm seems to reduce superfluous information exchange, leading itself to a cost-effective communication strategy.

It should be noted that the topology derived from LMST is not fixed or time-invariant. It evolves dynamically depending on several factors, for instance, time period of broadcasting, current motion conditions of each robot, and its mobility and communication range.

Hence, the LMST-based communication algorithm not only eliminates the global communication requirement, but also favorably guarantees the uninterrupted information propagation among multi-robot systems and greatly improves energy consumption and communication quality, efficiency and capacity. Moreover, the algorithm is localized and distributed, because no central authority is required and each robot dynamically constructs its own local topology solely relying on locally gathered information. So this LMST-based algorithm realistically models less required communication among robots, and is

very amenable to practical implementation on formation control. Hence, in the following section through incorporating the presented LMST-based dynamic communication algorithm, a desired rigid formation pattern is achieved by utilizing graph *Laplacian* and feedback control theory.

B. Laplacian Formation Control

1. Without Interconnection Time-delays

The following model is an idealization of the real world, but the analysis can provide guiding principles for actual implementations of decentralized control laws. The simplest model involves what we call holonomic point robots or point robots for short. Each robot is modeled as a point which undergoes holonomic motion.

For robot i, consider the following dynamic model,

$$\dot{x}_i(t) = Ax_i(t) + Bu_i(t), \tag{5.1}$$

where $x_i(t) \triangleq [P_{ix}\ \dot{P}_{ix}\ P_{iy}\ \dot{P}_{iy}]^T, u_i(t) \triangleq [u_{i1}(t)\ u_{i2}(t)]^T, i = 1, 2, ..., N$, $A \triangleq \begin{bmatrix} 0 & 1 & 0 & 0 \\ 0 & a & 0 & 0 \\ 0 & 0 & 0 & 1 \\ 0 & 0 & 0 & b \end{bmatrix}$, and $B \triangleq \begin{bmatrix} 0 & 1 & 0 & 0 \\ 0 & 0 & 0 & 1 \end{bmatrix}^T$, where $a, b \in R$. Without loss of generality, in this chapter also choose a=b=0 to have typical double integrator model.

The above dynamics is utilized throughout this work for the sake of presenting the main formation control design for multi-robot systems subject to interconnection time-delays rather than getting involved in the technical details of dealing with nonlinear control of nonholonomic mechanical systems, which was studied elsewhere [63, 64].

Then for N robots,

$$\dot{x}(t) = \hat{A}x(t) + \hat{B}u(t), \tag{5.2}$$

where $x(t) \triangleq [x_1(t)\ ...x_i(t)...\ x_N(t)]^T, u(t) \triangleq [u_1(t)\ ...u_i(t)...\ u_N(t)]^T$. $\hat{A} \triangleq I_N \otimes A$, and $\hat{B} \triangleq I_N \otimes B$. Here I_N is an $N \times N$ identity matrix.

Consider the coordination system with dynamics (5.1), assume each robot has access to its own state and exchanges information with some of the neighboring robots, as determined by the constraints of the underlying communication network defined by the *Laplacian* matrix L [65, 66]. This also facilitates considering time-delay issues in the interconnection states. Similar to [66], define the following output function,

$$y(t) = L(x(t) - r(t)), \tag{5.3}$$

where $r(t) \triangleq [r_1(t)\ ...r_i(t)...\ r_N(t)]^T, r_i(t) \triangleq r_i^d(t) \otimes [1\ 0]^T, r_i^d(t) \triangleq [P_{ix}^d(t)\ P_{iy}^d(t)]^T$, and $L \triangleq L_G \otimes I_4$. Here L_G is the *Laplacian* of the corresponding communication topology graph and $r_i^d(t)$ is the desired final position vector for robot i.

To achieve a certain formation configuration, design the following output feedback controller,

$$u(t) = \hat{K}y(t), \tag{5.4}$$

where $\hat{K} \triangleq I_N \otimes K$ and the feedback gain matrix has the format $K \triangleq \begin{bmatrix} k_1 & k_2 & 0 & 0 \\ 0 & 0 & k_1 & k_2 \end{bmatrix}$. Then we have the following closed loop system,

$$\begin{aligned}
\dot{x}(t) =& \hat{A}x(t) + \hat{B}u(t) = \hat{A}x(t) + \hat{B}\hat{K}y(t) = \hat{A}x(t) + \hat{B}\hat{K}L(x(t) - r(t)) \\
=& \hat{A}x(t) + \hat{B}\hat{K}(L_G \otimes I_4)(x(t) - r(t)) = (I_N \otimes A)x(t) + (L_G \otimes (BK))(x(t) - r(t)) \\
\triangleq& \bar{A}x(t) - \bar{B}r(t),
\end{aligned} \tag{5.5}$$

where $\bar{A} \triangleq I_N \otimes A + L_G \otimes (BK)$ and $\bar{B} \triangleq L_G \otimes (BK)$.

Moreover, we know the following statements are equivalent: converge to desired formation $\Longleftrightarrow$ G is a rooted directed tree $\Longleftrightarrow$ L_G has only one zero eigenvalue $\Longleftrightarrow$ $A + \lambda_i BK$ is *Hurwitz* for every nonzero eigenvalue λ_i of L_G. So control gains k_1 and k_2 are chosen such that the above is satisfied.

2. With Interconnection Time-delays

If time-delays come into the system, then the above equation (5.5) becomes

$$\dot{x}(t) = A_0 x(t) + A_\tau x(t-\tau) - \bar{B} r(t), \tag{5.6}$$

with $x(t-\tau) \triangleq x(0)$, when $t \in [0, \tau), \tau \in R^+$ and $\dot{\tau} = 0$.

Illuminated by Razumikhin Theorem, for this time-delay system, state feedback stabilization design is more convenient to increase the delay margin or even make the system stable independent of delay. For the above system, (5.6), as a departure from most of the memoryless state feedback control in the literature, here a Delay Proportional (DP) two-term memory state feedback controller is proposed,

$$u_\tau(t) = G_0 x(t) + G_\tau x(t-\tau), \tag{5.7}$$

where $G_0 \triangleq g_0 A_0^{'}$ and $G_\tau \triangleq g_\tau A_\tau^{'}$.

Note due to the information flow topology constraint for this distributed system (relative to lumped system), $A_0^{'}$ and $A_\tau^{'}$ are analogous to A_0 and A_τ, respectively. In other words, the zero entries in A_0 and A_τ should still remain zero in $A_0^{'}$ and $A_\tau^{'}$. By choosing $A_0^{'} \triangleq A_0$ and $A_\tau^{'} \triangleq A_\tau$, then the new closed loop system has the following format,

$$\begin{aligned} \dot{x}(t) =& A_0 x(t) + A_\tau x(t-\tau) + u_\tau - \bar{B} r(t) \\ =& (1+g_0) A_0 x(t) + (1+g_\tau) A_\tau x(t-\tau) - \bar{B} r(t). \end{aligned} \tag{5.8}$$

C. Case Study

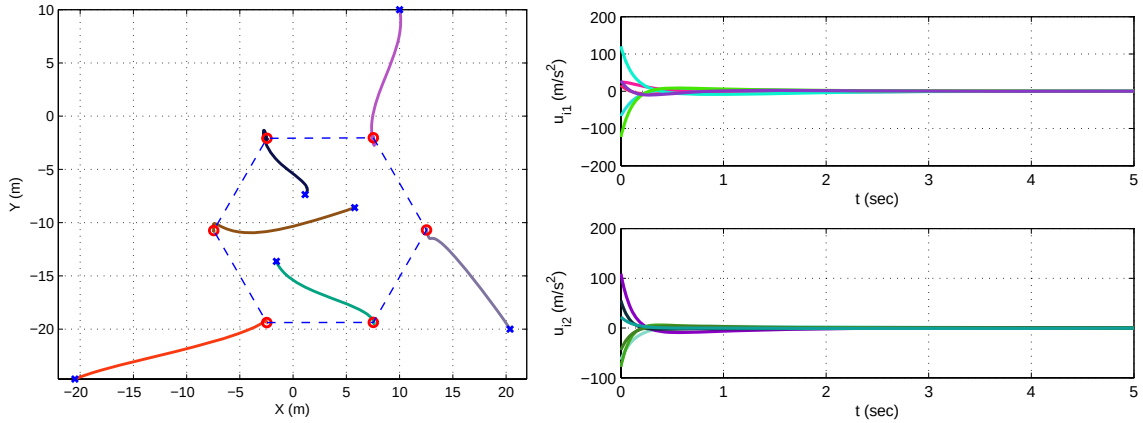

(a) (b)

Fig. 28. Delay-free case: (a) hexagon formation under random initial position conditions, and (b) corresponding controls $[u_{i1}(t)\ u_{i2}(t)]^T$.

In the delay-free case, namely, data propagation delays do not occur when robots are sensing and/or communicating with spatially separated neighbors. Figure 28 shows validating simulation results of hexagon formation acquisition in the case of six robots and validates the Laplacian-based control design (5.4). Here both k_0 and k_1 are chosen as -3.

Then assume robot R_2 for some reason receives delayed data from neighboring robots. That is, delays occur in the unidirectional channels of $E = \{(R_i, R_2)|R_i \in N_2\}$. By comparing with Fig. 29(a) and 29(b), it can be clearly seen that the two-term memory state feedback controller u_τ successfully recovers the hexagon formation acquisition when delays exist in the unidirectional channels of robot R_2 and its neighboring robots. This satisfactory performance demonstrates the effectiveness of the robust control design in the appearance of interconnection time-delays. The parameters are selected as $d_i = 22m, \tau =$

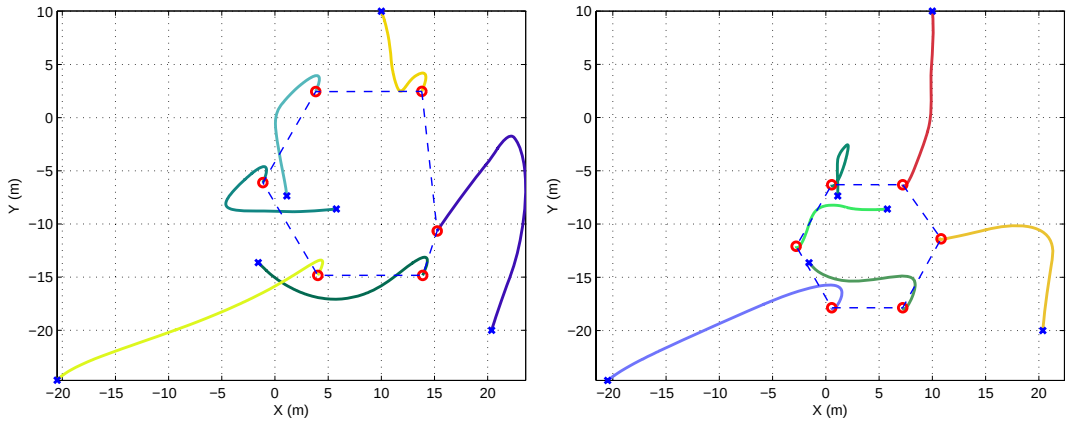

(a) (b)

Fig. 29. Hexagon formation with interconnection time-delays: (a) without robust control u_τ, and (b) with u_τ.

$2sec$, and $g_0 = g_\tau = 0.5$.

Figure 30 shows a few snapshots of the LMST topology of the robot team during the simulation period. These snapshots illustrate that the topology of the LMST dynamically varies with robots' motion. Since the LMSTs are always connected, the convergence results are obtained. These simple simulation results demonstrate the proposed algorithms.

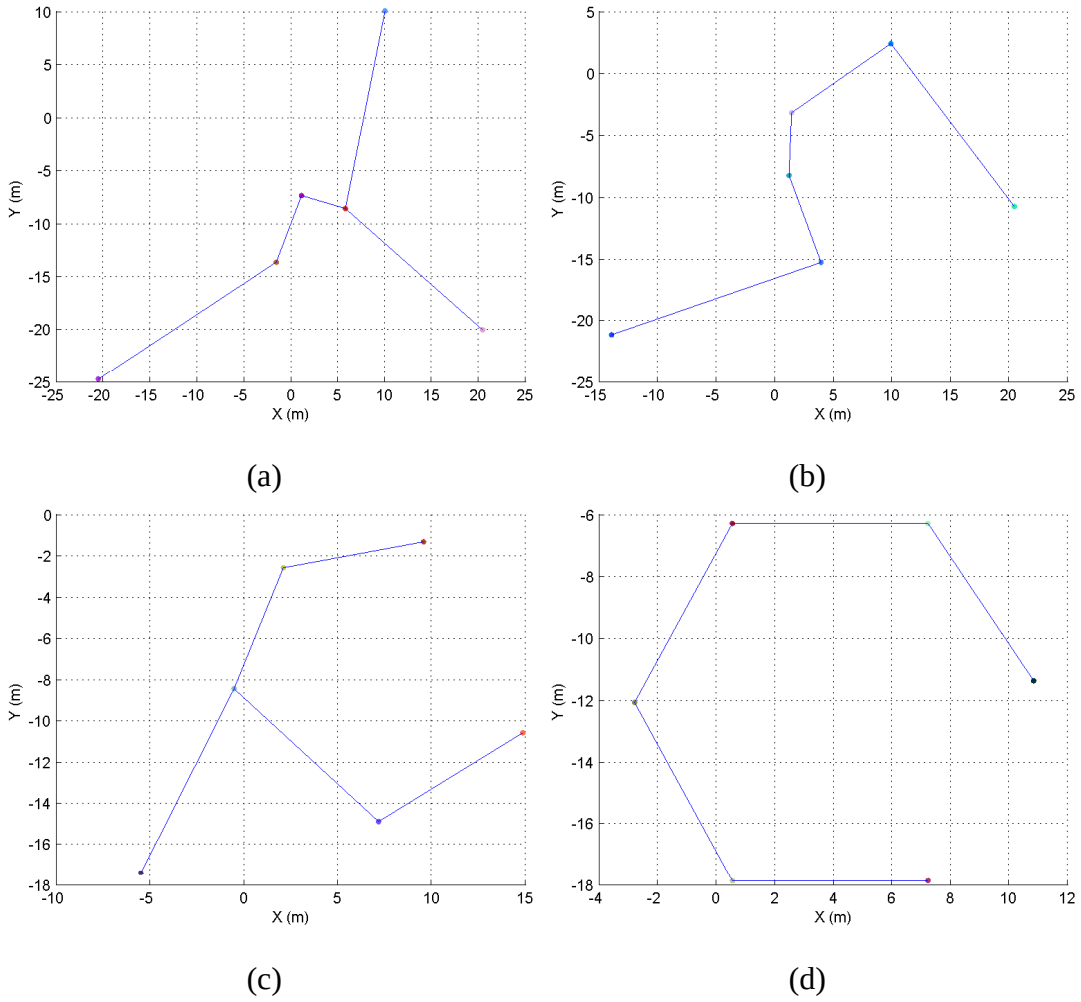

Fig. 30. Snapshots of the LMST topology: (a) $t = 0sec$, (b) $t = 2sec$, (c) $t = 3sec$, and (d) $t = 5sec$.

CHAPTER VI

CONCLUSION AND FUTURE WORK

A. Conclusion

There always exist uncertainties in postulated models of actual physical systems, and it is likely that during each time step of local path following in cooperative motion control, the online incrementally generated reference motion trajectories may not be exactly tracked in real time. If not carefully done tracking errors due to the ever present uncertainties can accumulate over each time segment over which reference trajectories are computed moving the ultimate formation to be significantly different from the desired one. Thus, one goal of this research was to guarantee incrementally calculated online reference motion trajectories are exactly tracked in real time, and tracking errors are not accumulated over each time segment to influence the next piecewise control computation. Thus the desired formation can still be fulfilled despite the presence of uncertainties. By virtue of the finite-time convergence behaviors of a class of nonlinear systems, a provable control methodology to accomplish exponential finite-time stability was presented. It was then employed for decentralized control of car-like mobile robots to enable the robotic systems with the ability to react rapidly enough to ensure time constrained convergence, and provide robustness to parametric uncertainties in the dynamic model. Stability analysis showed guaranteed control precision and a straightforward way to get the control parameters. Simulations verified the satisfactory multi-robot motion evolution and improved formation control performances.

A two-stage framework for multi-task formation control of a class of nonholonomic dynamic systems was also presented. The trajectory planner is at the top layer, while tracking controller sits at the bottom layer. In the trajectory planner, tasks are accounted for by

specifying a series of objective functions along with the desired behaviors in the task space. The motion planner for each robot integrates and prioritizes these tasks of the robot team in a systematic and dynamic fashion by dynamically exchanging information with the rest of the team to generate motion reference for trajectory tracking, whereby the assigned task evolution is ensured by proper local robust dynamic tracking control strategies. The proposed methodology enables a robotic team to intelligently handle multiple tasks for a wide range of complex practical applications as long as these desired behaviors are appropriately described, such as reaching a navigational goal, avoiding hazards and inter-robot collision, while simultaneously maintaining or reconfiguring formations.

B. Summary of Contributions

As discussed in previous chapters, this research addressed some key issues that must be considered in formation control.

(i) We achieved decentralized real-time robust tracking of reference trajectories for satisfactory collective motion of multi-robot systems under indispensable model uncertainties. It is well-known that systems under linear control converge asymptotically and can only settle in infinite time. In this research control strategies with nonlinear features were developed to guarantee high precision and time-constrained convergence by employing a novel class of real-time controllers at both the kinematic and dynamic levels of the robotic systems. This manifested in the settling time of the controlled system being finite and no longer than the predefined reference trajectory segment computing time interval, thus making tracking errors go to zero by the end of the time interval. This led to a guarantee of zero errors in formation over the entire time horizon and ensured desired multi-robot motion evolution in spite of uncertainties.

(ii) To meet the challenge of the increasingly wide range of potential applications of multi-robot systems, we developed a systematic and provable design framework for effective multi-task formation control. The proposed framework endows multi-robot nonholonomic systems with the ability to simultaneously deal with multiple tasks in dynamic environments. The established methodologies fully integrate and effectively organize many possible behaviors in a systematic and dynamic fashion. Including a proposed novel collision prevention scheme, tasks are accounted for by specifying a series of objective functions along with the desired behaviors in the task space. These prioritized tasks are then taken into consideration by each robot through dynamically exchanging information with other robots to generate motion reference for trajectory tracking. The assigned task evolution is ensured by the proper local robust dynamic tracking control strategies. This enables a robotic team to intelligently deal with multiple tasks for a wide range of complex practical applications as long as these desired formation missions are appropriately described, such as reaching a navigational goal, avoiding hazards and inter-robot collision, while simultaneously either maintaining or reconfiguring formations. Although we targeted differentially driven two-wheel mobile robots for this study, through proper modeling and design of appropriate controllers the presented formation control architecture and algorithms are immediately applicable more generally to different mobility platforms, such as Unmanned Air Vehicles (UAVs) and Unmanned Underwater Vehicles (UUVs).

(iii) We studied the inherent time-delay influence on the acquired formation in situations where delayed data propagation occur in certain information flow channels while robots are communicating with spatially separated neighboring robots. A robust stabilization scheme was proposed to improve or even recover the destroyed formation pattern. The formation as a whole still manages to steer itself reasonably well along

sufficiently smooth time-varying spatial reference trajectories, despite the effects of perturbations resulting from interconnection time-delays.

(iv) To facilitate practical implementation, communication at the inner-loop control level was also investigated. An LMST-based distributed communication algorithm was presented to relax the global communication needs among all robots. Instead of transmitting at maximal power, robots can individually perceive neighborhood relations and a communication topology is dynamically constructed. This was done by having each agent independently build its own local topology solely relying on locally gathered information and by keeping only one-hop on-tree agents as its neighbors. Hence, the proposed communication algorithm mitigates superfluous information exchange and unnecessary data propagation. Thus it reduces energy consumption, accordingly, extending battery life, a critical resource in many mobile applications, and also improves communication quality, efficiency and capacity while still maintaining connectivity for ensuring formation control convergence.

C. Future Work

There is still some work yet to be done. A rigorous proof of Theorem A.2 proposed in Chapter IV needs to be studied and also it would be interesting to investigate how the control performances are affected if the fractional power terms in the controllers change in real time. Moreover, it needs pointing out that the trajectory planner of the framework proposed in Chapter II does not embed robot nonholonomic constraints into the generation of reference trajectories. Namely, dynamic infeasibility needs to considered. Also it will be worthwhile to replace the global communication needs among all robots in the framework with the developed LMST-based dynamic communication algorithm to see whether a desired collective motion of multiple robots is still maintained. Additionally, in this study

constant time-delays are assumed. However, it is probable that in practice data transmission between spatially separated agents could be delayed one or more sampling periods, interrupted for extended intervals, or even randomized. In other words, it is likely that time-delays are inconsistent and unknown, which would much more jeopardize both the two important considerations in formation control as summarized in the abstract. Hence, further investigation along this direction is of necessity, for example, design time-advanced nonlinear state predictor to estimate future states for better real-time trajectory generation and also robust tracking. All these issues need to be further addressed before implementing the developed formation control approaches on real robotic systems.

REFERENCES

[1] J. Lawton, R.W. Beard, and F. Hadaegh, ”A coordination architecture for spacecraft formation control,” *IEEE Transactions on Control Systems Technology*, vol. 9, no. 6, pp. 777–790, 2001.

[2] A. Herbert, ”New horizons for combat UAV,” *Air Force Magazine*, vol. 86, no.12, 2003.

[3] D.H.A Maithripala, D.H.S. Maithripala, and S. Jayasuriya, ”Unifying geometric approach to real-time formation control,” *Proceedings of American Control Conference*, pp. 789–794, 2008.

[4] L. Moreau, ”Stability of multiagent systems with time-dependent communication links,” *IEEE Transactions on Automatic Control*, vol. 50, no. 2, pp. 169–182, 2005.

[5] Y.U. Cao, A.S. Fukunaga, and A. Kahng, ”Cooperative mobile robotics: antecedents and directions,” *Autonomous Robots*, vol. 4, no. 1, pp. 7–27, 1997.

[6] L.E. Parker, ”Current state of the art in distributed autonomous mobile robotics,” *Distributed Autonomous Robotic Systems*, vol. 4, pp. 3–12, 2000.

[7] R.M. Murray, ”Recent research in cooperative control of multivehicle systems,” *ASME Journal of Dynamic Systems, Measurement, and Control*, vol. 129, no. 5, pp. 571–583, 2007.

[8] J. Sanchez and R. Fierro, ”Sliding mode control for robot formations,” *IEEE International Symposium on Intelligent Control*, pp. 438–443, 2003.

[9] J. Shao, G. Xie, J. Yu, and L. Wang, ”Leader-following formation control of multiple mobile robots,” *IEEE International Symposium on Intelligent Control, Mediterrean Conference on Control and Automation*, pp. 808–813, 2005.

[10] E. Bicho and S. Monteiro, ”Formation control for multiple mobile robots: a non-linear attractor dynamics approach,” *IEEE/RSJ International Conference on Intelligent Robots and Systems*, vol. 2, pp. 2016–2022, 2003.

[11] W. Kowalczyk and K. Kozlowski, ”Artificial potential based control for a large scale formation of mobile robots,” *4th International Workshop on Robot Motion and Control*, pp. 285–291, 2004.

[12] T. Balch and R.C. Arkin, ”Behavior-based formation control for multirobot teams,” *IEEE Transactions on Robotics and Automation*, vol. 14, no. 6, pp. 926–939, 1998.

[13] I. Suzuki and M. Yamashita, ”Distributed anonymous mobile robots: formation of geometric patterns,” *SIAM Journal on Computing*, vol. 28, no. 4, pp. 1347–1363, 1999.

[14] J.P. Desai, J. Ostrowski, and V. Kumar, ”Controlling formations of multiple mobile robots,” *IEEE International Conference on Robotics and Automation*, vol. 4, 1998.

[15] J.P. Desai, J.P. Ostrowski, and V. Kumar, ”Modeling and control of formations of nonholonomic mobile robots,” *IEEE Transactions on Robotics and Automation*, vol. 17, no. 6, pp. 905–908, 2001.

[16] M. Egerstedt and X. Hu. ”Formation constrained multi-agent control,” *IEEE Transactions on Robotics and Automation*, vol. 17, no. 6, pp. 947–951, 2001.

[17] P. Ogren, M. Egerstedt, and X. Hu, ”A control Lyapunov function approach to multi-agent coordination,” *40th IEEE Conference on Decision and Control*, vol. 2, pp.

1150–1155, 2001.

[18] K.D. Do, ”Formation tracking control of unicycle-type mobile robots with limited sensing ranges,” *IEEE Transanctions On Control Systems Technology*, vol. 16, no. 3, pp. 527, 2008.

[19] R. Olfati-Saber and R.M. Murray, ”Consensus problems in networks of agents with switching topology and time-delays,” *IEEE Transactions on Automatic Control*, vol. 49, no. 9, pp. 1520–1533, 2004.

[20] Z. Qu, J. Wang, R.A. Hull, and J. Martin, ”Cooperative control design and stability analysis for multi-agent systems with communication delays,” *Proceedings of American Control Conference*, pp. 970–975, 2006.

[21] B. Triplett and K. Morgansen, ”Abbreviated zero order hold for formation control in the presence of communication and sensing delays,” *Proceedings of American Control Conference*, pp. 6081–6087, 2006.

[22] L. Wang and F. Xiao, ”Finite-time consensus problems for networks of dynamic agents,” *Arxiv preprint math/0701724*, 2007.

[23] S. Khoo, L. Xie, Z. Yu, and Z. Man, ”Finite-time consensus algorithm of multi-agent networks,” *10th International Conference on Control, Automation, Robotics and Vision*, pp. 916–920, 2008.

[24] S.P. Bhat and D.S. Bernstein, ”Finite-time stability of continuous autonomous systems,” *SIAM Journal on Control and Optimization*, vol. 38, no. 3, pp. 751–766, 2000.

[25] P. Santi, *Topology Control In Wireless Ad Hoc and Sensor Networks*, New York: John Wiley & Sons, 2005.

[26] N. Li, J.C. Hou, and L. Sha, ”Design and analysis of an MST-based topology control algorithm,” *IEEE Transactions on Wireless Communications*, vol. 4, no. 3, pp. 1195–1206, 2005.

[27] D.P. Spanos and R.M. Murray, ”Robust connectivity of networked vehicles,” *43rd IEEE Conference on Decision and Control*, vol. 3, 2004.

[28] G. Notarstefano, K. Savla, F. Bullo, and A. Jadbabaie, ”Maintaining limited-range connectivity among second-order agents,” *Proceedings of American Control Conference*, pp. 2124–2129, 2006.

[29] M. Ji and M. Egerstedt, ”Distributed coordination control of multiagent systems while preserving connectedness,” *IEEE Transactions on Robotics*, vol. 23, no. 4, pp. 693–703, 2007.

[30] M.M. Zavlanos and G.J. Pappas, ”Potential fields for maintaining connectivity of mobile networks,” *IEEE Transactions on Robots*, pp. 812–816, 2007.

[31] B.E. Bishop, ”On the use of redundant manipulator techniques for control of platoons of cooperating robotic vehicles,” *IEEE Transactions on Systems, Man and Cybernetics, Part A*, vol. 33, no. 5, pp. 608–615, 2003.

[32] G. Antonelli and S. Chiaverini, ”Kinematic control of platoons of autonomous vehicles,” *IEEE Transanctions on Robotics*, vol. 22, no. 6, pp. 1285–1292, 2006.

[33] J. Yi and H. Wang and J. Zhang and D. Song and S. Jayasuriya and J. Liu, ”Kinematic modeling and analysis of skid-steered mobile robots with applications to low-cost inertial-measurement-unit-based motion estimation,” *IEEE Transactions on Robots*, vol. 25, no. 5, pp. 1087–1097, 2009.

[34] L.A. Pars, *A Treatise on Analytical Dynamics*, Woodbridge, CT: Ox Bow Press, 1979.

[35] F.M.L. Amirouche, *Computational Methods in Multibody Dynamics,* Englewood Cliffs, NJ: Prentice Hall, 1992.

[36] A.M. Bloch, M. Reyhanoglu, and N.H. McClamroch, ”Control and stabilization of nonholonomic dynamic systems,” *IEEE Transactions on Automatic Control*, vol. 37, no. 11, pp. 1746–1757, 1992.

[37] N. Sarkar, X. Yun, and V. Kumar, ”Control of mechanical systems with rolling constraints: application to dynamic control of mobile robots,” *The International Journal of Robotics Research*, vol. 13, no. 1, pp. 55–69, 1994.

[38] H. Nijmeijer and A. van der Schaft, *Nonlinear Dynamical Control Systems*, Berlin: Springer-Verlag, 1990.

[39] H.K. Khalil, *Nonlinear Systems*, Englewood Cliffs, NJ: Prentice Hall, 3rd edition, 2002.

[40] G. Antonelli, F. Arrichiello, and S. Chiaverini, ”Experiments of formation control with collisions avoidance using the null-space-based behavioral control,” *14th Mediterranean Conference on Control and Automation*, 2006.

[41] D.H.A. Maithripala, S. Woo, and S. Jayasuriya, ”Rigid formation keeping,” *ASME International Mechanical Engineering Congress & Exposition*, 2007.

[42] K.R. Frisch, *The logarithmic potential method of convex programming*, Memorandum, University Institute of Economics, Oslo, 1955.

[43] A.V. Fiacco and G.P. McCormick, ”Nonlinear programming: sequential unconstrained minimization techniques,” *Society for Industrial and Applied Mathematics*, 1987.

[44] A. Forsgren, P.E. Gill, and M.H. Wright, ”Interior methods for nonlinear optimization,” *Society for Industrial and Applied Mathematics Review*, vol. 44, no. 4, pp. 525–597, 2002.

[45] T.L. Liao, L.C. Fu, and C.F. Hsu, ”Output tracking control of nonlinear systems with mismatched uncertainties,” *Systems & Control Letters*, vol. 18, no. 1, pp. 39–47, 1992.

[46] J.C. Doyle, K. Glover, P.P. Khargonekar, and B.A. Francis, ”State-Space Solutions to Standard H_2 and H_∞ Control Problems,” *IEEE Transactions on Automatic Control*, vol. 34, no. 8, pp. 831–847, 1989.

[47] J.K. Hale and S.M.V. Lunel, *Introduction to Functional Differential Equations*, New York: Springer-Verlag, 1993.

[48] C. Edwards, E.F. Colet, and L. Fridman, ”Advances in variable structure and sliding mode control,” *Lecture notes in control and information sciences*, vol. 334, 2006.

[49] V.I. Utkin and H. Lee, ”Chattering problem in sliding mode control systems,” *International Workshop on Variable Structure Systems*, pp. 346–350, 2006.

[50] E. Moulay and W. Perruquetti, ”Finite time stability and stabilization of a class of continuous systems,” *Journal of Mathematical Analysis and Applications*, vol. 323, pp. 1430–1443, 2006.

[51] S.G. Nersesov, W.M. Haddad, and Q. Hui, ”Finite-time stabilization of nonlinear dynamical systems via control vector Lyapunov functions,” *Journal of the Franklin Institute*, vol. 345, no. 7, pp. 819–837, 2008.

[52] S. Jayasuriya and A.R. Diaz, ”Performance enhancement of distributed parameter systems by a class of nonlinear controls,” *Proceedings of 26th IEEE Conference on Decision and Control*, vol. 26, pp. 2125–2126, 1987.

[53] V. Haimo. ”Finite time controllers,” *SIAM Journal on Control and Optimization*, vol. 24, no. 4, pp. 760–770, 1986.

[54] E.P. Ryan, *Optimal relay and saturating control system synthesis*, New York: P. Peregrinus on behalf of the Institution of Electrical Engineers, 1982.

[55] J.K. Hale, *Ordinary Differential Equations*, Dover: 1969 edition, 2009.

[56] G.J. Pappas and K.J. Kyriakopoulos, ”Dynamic modeling and tracking control of nonholonomic wheeled vehicles,” *Proceedings of IFAC World Congress*, pp. 241–244, 1993.

[57] R. Diestel, *Graph Theory*, New York: Springer, 2000.

[58] C.D. Godsil and G. Royle, *Algebraic Graph Theory*, New York: Springer, 2001.

[59] Leiserson C. Cormen, T.H. and R. Rivest, *Introduction to Algorithms*, Cambridge, MA: MIT Press, 2nd edition, 2001.

[60] W. Ren, R.W. Beard, and E.M. Atkins, ”A survey of consensus problems in multiagent coordination,” *Proceedings of American Control Conference*, pp. 1859–1864, 2005.

[61] A. Jadbabaie, J. Lin, and A.S. Morse. ”Coordination of groups of mobile autonomous agents using nearest neighbor rules,” *IEEE Transactions on Automatic Control*, vol. 48, no. 6, pp. 988–1001, 2003.

[62] C. Monma and S. Suri. ”Transitions in geometric minimum spanning trees,” *Discrete and Computational Geometry*, vol. 8, no. 1, pp. 265–293, 1992.

[63] J. Zhang, J. Yi, and S. Jayasuriya, ”A framework for multi-task formation control of nonholonomic robotic systems,” *ASME Dynamic Systems and Control Conference, Oct. 20-22, 2008,Ann Arbor, MI, USA.*

[64] J. Zhang and S. Jayasuriya. ”Cooperative control of multi-robot nonholonomic systems with dynamics uncertainties and control time-delays’” *9th International Symposium on Distributed Autonomous Robotics Systems, Nov. 17-19, 2008, Tsukuba, Ibaraki, Japan.*

[65] F. Xiao and L. Wang. ”Dynamic behavior of discrete-time multiagent systems with general communication structures,” *Physica A: Statistical Mechanics and its Applications*, vol. 370, no. 2, pp. 364–380, 2006.

[66] G. Lafferriere, A. Williams, J. Caughman, and J.J.P. Veerman, ”Decentralized control of vehicle formations,” *Systems & Control Letters*, vol. 54, no. 9, pp. 899–910, 2005.

APPENDIX A

RELATIVE DEGREE OF THE NONLINEAR SYSTEM (2.12)-(2.13)

The nominal system (2.12)-(2.13), is said to have a constant relative degree ρ, if there exists a positive integer $1 \leqslant \rho \leqslant \infty$, such that

$$L_g L_f^i h(x) = 0,\ i = 0, 1, \cdots, \rho - 2$$

and

$$L_g L_f^{\rho-1} h(x) \neq 0$$

for all $x \in R^n$ and $t \in [0, \infty)$.

It is straightforward to calculate

$$L_g L_f^0 h(x) = L_g h(x) = \frac{\partial h}{\partial x} g(x) = [I_{2\times 2}\ O_{2\times 5}] \begin{bmatrix} O_{5\times 2} \\ I_{2\times 2} \end{bmatrix} = 0,$$

and

$$\begin{aligned} L_g L_f h(x) &= L_g \left[\tfrac{\partial h}{\partial x} f(x)\right] = \frac{\partial \left[\tfrac{\partial h}{\partial x} f(x)\right]}{\partial x} g(x) = \frac{\partial (\Xi \vartheta)}{\partial x} g(x) \\ &= \begin{bmatrix} O_{2\times 2} & W_{2\times 1} & O_{2\times 2} & \Xi \end{bmatrix} \begin{bmatrix} O_{5\times 2} \\ I_{2\times 2} \end{bmatrix} = \Xi \neq 0, \end{aligned}$$

where $W_{2\times 1}$ is a certain vector. Then $\rho = 2$ in the region $D_0 \subset \mathbb{R}^7$, that is, the relative degree of the nonlinear system (2.12)-(2.13) is 2.

APPENDIX B

VERIFICATION OF NULL-SPACE METHOD

$$
\begin{aligned}
&(I - \Phi_a^\dagger \Phi_a) V_b^d \cdot V_a^d \\
=&(I - \Phi_a^\dagger \Phi_a) \Phi_b^\dagger (\dot{J}_b^d + \Lambda_b J_{b,e}) \cdot \Phi_a^\dagger (\dot{J}_a^d + \Lambda_a J_{a,e}) \\
=&\Phi_b^\dagger (\dot{J}_b^d + \Lambda_b J_{b,e}) \cdot \Phi_a^\dagger (\dot{J}_a^d + \Lambda_a J_{a,e}) \\
&- \Phi_a^\dagger \Phi_a \Phi_b^\dagger (\dot{J}_b^d + \Lambda_b J_{b,e}) \cdot \Phi_a^\dagger (\dot{J}_a^d + \Lambda_a J_{a,e}) \\
=&\Phi_b^\dagger (\dot{J}_b^d + \Lambda_b J_{b,e}) \cdot \Phi_a^\dagger (\dot{J}_a^d + \Lambda_a J_{a,e}) \\
&- \Phi_a^T (\Phi_a \Phi_a^T)^{-1} \Phi_a \Phi_b^\dagger (\dot{J}_b^d + \Lambda_b J_{b,e}) \cdot \Phi_a^\dagger (\dot{J}_a^d + \Lambda_a J_{a,e}) \\
=&\Phi_b^\dagger (\dot{J}_b^d + \Lambda_b J_{b,e}) \cdot \Phi_a^\dagger (\dot{J}_a^d + \Lambda_a J_{a,e}) \\
&- (\Phi_a^T (\Phi_a^T)^{-1}) (\Phi_a^{-1} \Phi_a) \Phi_b^\dagger (\dot{J}_b^d + \Lambda_b J_{b,e}) \cdot \Phi_a^\dagger (\dot{J}_a^d + \Lambda_a J_{a,e}) \\
=&\Phi_b^\dagger (\dot{J}_b^d + \Lambda_b J_{b,e}) \cdot \Phi_a^\dagger (\dot{J}_a^d + \Lambda_a J_{a,e}) \\
&- I \Phi_b^\dagger (\dot{J}_b^d + \Lambda_b J_{b,e}) \cdot \Phi_a^\dagger (\dot{J}_a^d + \Lambda_a J_{a,e}) \\
=&0.
\end{aligned}
$$

APPENDIX C

PROOF OF THEOREM A.1 IN CHAPTER III

Proof. To investigate the boundedness, define the following Lyapunov function

$$V(e(t),\eta(t)) = V_e(e(t)) + \varsigma V_i(\eta(t)) \triangleq e^T(t)Pe(t) + \varsigma V_i(\eta(t)), \tag{C.1}$$

where P satisfies (3.25) and $\varsigma \in \mathbb{R}^+$. Notice function $V_i(\eta(t))$ is added to ensure the stability of internal dynamics.

Differentiating $V(t)$ along the trajectory of closed system (3.23)-(3.24) yields

$$\begin{aligned}\dot{V} =&\dot{e}^T Pe + eP\dot{e}^T + \varsigma\dot{V}_i \\ =&(A_c e + \bar{B}u_a + \triangle\ \Omega)^T Pe + e^T P(A_c e + \bar{B}u_a + \triangle\ \Omega) \\ &+ \varsigma\frac{V_i}{\eta}\big[p(\zeta,\eta) + \triangle\ \Psi\big].\end{aligned} \tag{C.2}$$

With the aid of (3.25),

$$\begin{aligned}\dot{V} =&e^T(-Q + \gamma P\bar{B}\bar{B}^T P)e + 2e^T P\bar{B}u_a + 2e^T P\ \triangle\ \Omega \\ &+ \varsigma\frac{V_i}{\eta}\big[p(\zeta,\eta) + \triangle\ \Psi\big] \\ =&-e^T Qe + \gamma(1-2\bar{k})||e^T P\bar{B}||^2 + 2e^T P\ \triangle\ \Omega \\ &+ \varsigma\frac{V_i}{\eta}\big[p(0,\eta) + p(\zeta,\eta) - p(0,\eta) + \triangle\ \Psi\big].\end{aligned} \tag{C.3}$$

Under (3.27), it follows that

$$\begin{aligned}\dot{V} \leqslant &-e^T Qe + 2e^T P\ \triangle\ \Omega + \varsigma\frac{V_i}{\eta}\big[p(0,\eta) + p(\zeta,\eta) \\ &- p(0,\eta) + \triangle\ \Psi\big].\end{aligned} \tag{C.4}$$

Based on Rayleigh Principle*, (C2) and (C3),

$$\begin{aligned}\dot{V} \leqslant & -\lambda_{min}(Q)||e||^2 + ||e||(\kappa_1||\zeta|| + \kappa_2||\eta|| + \kappa_3) - \varsigma\chi_3||\eta||^2 \\ & + \varsigma\chi_4 L||\eta||||\zeta(t)|| + \varsigma\chi_4||\eta||(\epsilon_1||\zeta|| + \epsilon_2||\eta|| + \epsilon_3). \end{aligned} \tag{C.5}$$

Under the constraint of external dynamics (3.28), (C.5) can be further formulated into

$$\begin{aligned}\dot{V} \leqslant & (\kappa_1 - \lambda_{min}(Q))||e||^2 + (\kappa_1 B_r + \kappa_3)||e|| + \big[\kappa_2 + \varsigma\chi_4(\epsilon_1 + L)\big] \\ & \times ||e||||\eta|| + \varsigma(\epsilon_2\chi_4 - \chi_3)||\eta||^2 + \varsigma\chi_4\big[\epsilon_3 + B_r(\epsilon_1 + L)\big]||\eta||. \end{aligned} \tag{C.6}$$

Since

$$\begin{aligned}&(\kappa_1 B_r + \kappa_3)||e|| \leqslant \frac{1}{4}||e||^2 + (\kappa_1 B_r + \kappa_3)^2 \\ &\big[\kappa_2 + \varsigma\chi_4(\epsilon_1 + L)\big]||e||||\eta|| \leqslant \frac{1}{4}||e||^2 + \big[\kappa_2 + \varsigma\chi_4(\epsilon_1 + L)\big]^2||\eta||^2 \\ &\varsigma\chi_4\big[\epsilon_3 + B_r(\epsilon_1 + L)\big]||\eta|| \leqslant \varsigma\Big\{\frac{\chi_3||\eta||^2}{4} + \frac{\chi_4^2\big[\epsilon_3 + B_r(\epsilon_1 + L)\big]^2}{\chi_3}\Big\}, \end{aligned}$$

$$\begin{aligned}\dot{V} \leqslant & -(\lambda_{min}(Q) - \kappa_1 - \frac{1}{2})||e||^2 - ||\eta||^2\Big\{\varsigma(\frac{3}{4}\chi_3 - \chi_4\epsilon_2) \\ & - \big[\kappa_2 + \varsigma\chi_4(\epsilon_1 + L)\big]^2\Big\} + (\kappa_1 B_r + \kappa_3)^2 + \frac{\varsigma\chi_4^2\big[\epsilon_3 + B_r(\epsilon_1 + L)\big]^2}{\chi_3}. \end{aligned} \tag{C.7}$$

Let $\varsigma^* \triangleq \frac{\chi_3}{12\big[1+\chi_4(\epsilon_1+L)\big]^2}$ and $\epsilon_2^* \triangleq \frac{\chi_3}{\chi_4}$, then the hypotheses of the Theorem A.1 imply

$$\begin{aligned}\dot{V} \leqslant & -\frac{\lambda_{min}(Q)}{2}||e||^2 - \frac{\varsigma^*\chi_3}{2}||\eta||^2 + d_0, \\ & \text{where } d_0 \triangleq (\kappa_1 B_r + \kappa_3)^2 + \frac{\varsigma\chi_4^2\big[\epsilon_3 + B_r(\epsilon_1 + L)\big]^2}{\chi_3}. \end{aligned} \tag{C.8}$$

If $k_0 \triangleq min(\frac{\lambda_{min}(Q)}{2}, \frac{\varsigma^*\chi_3}{2})$, then $\dot{V} \leqslant -k_0(||e||^2 + ||\eta||^2) + d_0$, which says for sufficiently large $||e(t)||$ or $||\eta(t)||$, the states of closed system (3.23)-(3.24) are uniformly bounded for

*$\lambda_{min}(Q)||e||^2 \leqslant e^TQe \leqslant \lambda_{max}(Q)||e||^2$

all $t \leqslant 0$.

To investigate the ultimate bound of tracking error, inequality (C.7) yields:

$$\dot{V}_e \leqslant -(\lambda_{min}(Q) - \kappa_1 - \frac{1}{2})||e||^2 + \kappa_2||\eta||^2 + (\kappa_1 B_r + \kappa_3)^2. \tag{C.9}$$

Suppose internal dynamics are constrained as $\exists\ B_i \in \mathbb{R}^+$, such that $||\eta|| \leqslant B_i$,then

$$\begin{aligned}\dot{V}_e &\leqslant -\frac{(\lambda_{min}(Q) - \kappa_1 - \frac{1}{2})}{\lambda_{max}(P)}V + (\kappa_2 B_i)^2 + (\kappa_1 B_r + \kappa_3)^2 \\ &\leqslant -k_e V + b_e,\end{aligned} \tag{C.10}$$

which implies $V_e(e(t)) \leqslant V_e(e(t_0))e^{(-k_e t)} + (1 - e^{(-k_e t)})k_e^{-1} b_e$.

Hence, the output tracking error $e(t)$ will eventually converge to the residual set Γ_e,

$$\Gamma_e \triangleq \{e(t) \in \mathbb{R}^{m\rho} | V(e(t)) \leqslant k_e^{-1} b_e\}.$$

Clearly, the size of the compact set relies on the system uncertainties and design parameters.

This completes the proof. □

APPENDIX D

DERIVATION OF ρ

Applying Rayleigh Principle to this particular problem, $\lambda_{min}(P)||(\cdot)||^2 \leqslant (\cdot)^T P(\cdot) \leqslant \lambda_{max}(P)||(\cdot)||^2$, and defining $W(\cdot) \triangleq (\cdot)^T P(\cdot)$, it can be directly obtained that

$$W(x_j(t)) \leqslant \lambda_{max}(P)||x_j(t)||^2$$

and

$$\lambda_{min}(P)||x_j(t-\tau_{ij})||^2 \leqslant W(x_j(t-\tau_{ij})).$$

Combining with the following equation from (C1)

$$W(x_j(t-\tau_{ij}(t))) < q^2 W(x_j(t))$$

yields

$$\begin{aligned}\lambda_{min}(P)||x_j(t-\tau_{ij})||^2 &\leqslant W(x_j(t-\tau_{ij})) < q^2 W(x_j(t)) \\ &\leqslant q^2 \lambda_{max}(P)||x_j(t)||^2.\end{aligned}$$

Hence,

$$||x_j(t-\tau_{ij})|| < q\rho||x_j(t)||,$$

where $\rho \triangleq \sqrt{\frac{\lambda_{max}(P)}{\lambda_{min}(P)}}$.

VITA

Junjie Zhang was born in Dalian, China. He received a B.S. degree in mechanical engineering and a B.A. degree in Japanese in 2003 both from Dalian University of Technology, Dalian, China and a M.S. degree in mechanical engineering in 2005 from the University of Michigan, Ann Arbor, USA. He received his Ph.D. in Mechanical Engineering from Texas A&M University, College Station, USA in 2010. He may be contacted through Dr. Suhada Jayasuriya at the Department of Mechanical Engineering, Texas A&M University, College Station, TX 77843-3123 USA.